A Chemiresistor Sensor Array for Insect Infestation Detection

by

Kanchana Anuruddika Kumari Weerakoon

A dissertation submitted to the Graduate Faculty of
Auburn University
in partial fulfillment of the
requirements for the Degree of
Doctor of Philosophy

Auburn, Alabama
May 7th , 2012

Key words: Polythiophene sensor Polyaniline sensor, Polymer/carbon composite sensor, Sensor array, insect infestation, Thin film sensor array

Copyright 2012 by Kanchana Anuruddika Kumari Weerakoon

Approved by

Bryan A. Chin, Chair, Professor of Materials Engineering
Minseo Park, Associate Professor of Physics
Dong Joo (Daniel) Kim, Associate Professor of Materials Engineering
Zhong Yang Cheng, Associate Professor of Materials Engineering

Abstract

Plants emit volatile organic compounds as a defensive mechanism to protect themselves from insects and pathogens. These volatile organic chemicals, also known as phytochemicals, are given off during the early stages of insect infestation and may be detected using a chemical sensor array. The chemiresistor sensor array, investigated in this study, consists of a silicon substrate, electroactive polymer based active layer and microelectronically fabricated interdigitated electrodes. The sensor array is inexpensive, easy to fabricate, and could be used for onsite detection of insect infestation. Compared to traditional methods of detecting insect infestation such as leaf inspection and insect traps, this method is quick, inexpensive and would not require trained personal.

The sensor array investigated in this dissertation uses three types of polymers as active sensing layers; polythiophene, carbon/polymer and polyaniline. The polymer coatings were deposited onto the sensor platforms via drop casting and spin coating methods. The sensor array was exposed and found to be sensitive to a variety of phytochemicals including γ-terpinene, α-pinene, p-cymene, farnesene, limonene, and cis-hexenyl acetate. The sensor array created a unique fingerprint pattern for each of the different volatile gases. These fingerprints were further analyzed using principle component analysis. To optimize the uniqueness of the fingerprint, sensors that operated with different mechanisms were used. Incorporating sensors with multiple mechanisms into a single array system can be difficult, especially if different film responses are

measured. Therefore, the same film response, relative resistance, was measured as a function of exposure time to the specific volatile gases.

Polythiophene sensors in this study had a sensor detection mechanism that involved physical interactions between the volatile organic vapor and the sensor. The polyaniline sensor had a sensor mechanism which was redox reactions based. The polymer/carbon composite sensors, which consisted of a polymer matrix and carbon particles, operated through a mechanism involving the percolation point.

Acknowledgments

I would like to thank my advisor Dr. Bryan A. Chin for his guidance in doing this research, helping me to develop and complete my dissertation and funding my education at Auburn University. I would also like to thank Dr. Dong-Joo Kim, Dr. Zhong-Yang Cheng and Dr. Minseo Park for agreeing to be a part of my dissertation committee. I would also like to thank Dr. Maria Auad for agreeing to be my university reader.

I would like to thank my lab mates for all their support. I would like to thank past members of our group Dr. Helen Yang for helping me start this research work and guiding me in the right direction. I would also like to thank Dr. John Shu for all his help with test cell design, data acquisition setup and testing methodology. I would like to thank Yating Chai for all her help. I would also like to thank Shin Horikawa for all the help and useful discussions. I would also like to thank Tom Carrington in the chemistry department for helping me with Gas Chromatography and Dr Maria Auad for helping me with Atomic Force Microscopy.

Last but not least I would like to thank my family. My husband Pathum Mendis for helping me and being there for me always. My daughter Saneli Mendis for being a good baby specially while writing my dissertation. My Parents and Parents in laws Menik Weerakoon, Gamini Weerakoon, Premila Mendis and Pemsiri Mendis for all their help, love and encouragement. I would also like to thank my brothers, brother in law and sisters in laws for all their love and support.

Table of Contents

List of Tables

List of Figures

Chapter 1

Introduction

1.1. Back ground

1.1.1. Insect Infestation and Global Economy

Nearly 30 % of world's annual crop production is destroyed due to insect and pathogen infestation. This loss is proportionally higher in Africa and other developing countries due to harsh environmental conditions which are favorable for pests and insects, but not so favorable for plants. Table 1.1 below summarizes losses in eight principal food and cash crops due to pathogens and animal pests, worldwide. Losses are shown as percentages. Table 1.2 summarizes the damage/costs for various food and cash crops in the United States by specific insect pathogens [1-5].

1.1.2. Current Methods of Insect Infestation Detection

Much of the loss due to insect infestation could be avoided if there was a method of detecting the early stages of insect/pathogen infestation. Current methods of detection include traditional methods such as regular inspection, traps, barriers and environmental control, as well as more recent detection methods such as gas chromatography analysis and acoustic sensor control [6-13]. Details of each of these methods are discussed below.

Table 1.1. Crop losses (as a % of total produced) due to pathogens and pests [1].

Crop	Pathogens	Animal pests	Total
Rice	15.1	20.7	35.8
Wheat	12.4	9.3	21.7
Maize	10.8	14.5	25.3
Potatoes	16.4	16.1	32.5
Soybeans	9.0	10.4	19.4
Cotton	10.5	15.4	25.9

Table 1.2. Examples of damages ($) done by insects in the United States in various years [2-4].

Type of Crop	Types of Insects	Damage per Year	Year
Potato	Green peach aphid Colorado Potato Beetle Potato Leafhopper	100 million	2003
Soy bean	Soybean looper Velvet bean caterpillar Bean leaf beetle	250 million	2003
Cotton	Bold worm Spider mite Beet Army Worm	1.021 billion	2006
Tobacco	Horn worm Bud worm Flea beetles	5.5 million	1997
Oak	Gypsy moth Oak ambrosia beetle	30 million	1980-1996
Berries	Aphids Spider mites Leaf trollers	5 million	2001
Pine trees	Southern pine beetle Bark beetle	1.5 billion	1998

1.1.2.1. Conventional Methods

1.1.2.1.1. Regular Inspection

Regular inspection is the traditional method of pest control. This method involves trained personal inspecting for infested plant parts, and taking necessary measures to prevent further infestation. Although this method is accurate, it is time consuming, especially if the field is large and many crops are involved. It also requires trained personnel and commitment [13].

1.1.2.1.2. Traps

Traps have been used to monitor and survey insect populations over the years. Traps have been used not only to reduce pest population but also to develop spatial and temporal patterns of various pest insects. However in order for the traps to be effective, the traps must be systematically observed. Therefore using traps is time consuming and requires trained personal. Traps come in various styles including flat traps, bucket traps, wing traps, delta traps, triangular traps, cylindrical traps, cone traps and bag traps. Most of these traps include various baits to maximize insect attraction to the traps. Many mathematical models show that baits or lures in traps enhance trap effectiveness. Examples include baited electrical traps used to capture tobacco worms, baited light traps and sticky traps and oil traps with pheromones used to suppress pink bollworm populations. Mass trapping using pheromones and other baits has not been feasible in the United States because of high costs (both material and labor costs). Other types of traps include bands which are made of various materials such as hay rope, wrapping paper, building paper, flannel cloth, canvas and burlap. These traps are wrapped around the scraped trunks and barks of trees. Livestock insect traps, color traps which use color as an attractant, plant material traps and fermentation traps are other examples [6-7, 13].

1.1.2.1.3. Barriers

Barriers stop insects from entering feeding and reproduction sites. Common kinds of barriers include: screens, row covers, mulches, trenches, various particles, bags, shields and packaging. In many green houses, or warehouses growing tobacco, screens are used to exclude any insects or pests from entering, and prevent infestation. Typical screens consist of a mesh, strainer and a sheet to capture insects. However the efficacy of these screens is controlled by having the perfect hole size to prevent and capture each insect species, and this is not practical when many insect species are present. The use of creosote furrow barriers was standardized in the US in the 1930's and has been used to control many infestation types since. However this method is ineffective when there are strong winds present and insects are blown over the creosote barriers. The barriers were also ineffective in certain soil types, which make digging the furrow difficult. The method was improved over time, using paper strips soaked in creosote. Plastic lined trenches with fine soil particles have been used to effectively control many insect species, specially the colorado potato beetles. Many barriers made of different material including earth, metal, tar paper, or corrugated paper are used today. Usually some sort of repellant such as kerosene is used to increase the efficiency of the barrier. Other types of barriers include sand, granite, glass splinter or fossilized coral, specially used to control termite infestation and dust barriers made of silica sand, kaolin, wood ash, specifically to protect grains from insect infestation. Bags made of different material including cheese cloth, paper and mosquito net have been used specially over branches of various fruit trees such as peaches and oranges [13].

1.1.2.1.4. Physical Disturbances

Physical disturbances have been used in many crops. This type of control was more popular in the past. Types of physical disturbances include "shaking," where branches of trees were shaken, and insects were dislodged onto sheets placed beneath. "Jarring" is another method where trees or branches were cut down from time to time and are examined for insects. Another method would be mechanical disturbances where grain types are moved using shaking, jarring and centrifugal forces to detect any infestations present. Physical disturbances such as sound, a simple idea, however are not practical in large fields [13].

1.1.2.2. Modern Methods

1.1.2.2.1. Irradiation

High frequency radiations could be used in many agricultural crops to control insect infestation. Examples include microradiation where microwaves similar to those generated in ovens are used to treat post harvest grain types to destroy any pupae present. However, this method cannot be used for early detection of insect infestation. Highly reactive gamma rays which damage organisms by breaking chemical bonds could be used to control insects. This method is often used to control the population of insects by sterilizing the male insect species. Using infrared radiation is another method used to control infestation. In this method, heat from infrared lamps is used to attract various insect types. The lamp is then heated to a higher temperature to kill these insects [13].

1.1.2.2.2. Temperature Control

Insects thrive within only a limited specific temperature range, and raising or lowering the temperature to outside this range will cause the insects to die. These methods are more effectively used during storage of foods. However, they could also be used in various fruit orchards, specifically mangoes, oranges and grapefruits by exposing hot forced air, for short periods to kill pest populations. Vapor heat (steam) is also effective in killing insects in smaller type crops such as potatoes. Heat produced by burning hay or wheat stubble is also used to control infestation in certain crops. Heat which is generated by radio waves in biological materials could be used to control specific insect types, especially by killing its larvae. Insect infestation control by cold temperatures is mainly applied to post harvest produce [13].

1.1.2.2.3. Gas Chromatography Analysis

Gas chromatography systems have been developed to identify insect infestations. These gas chromatography systems detect phytochemicals emitted by the plants. Plants emit these compounds when attacked by herbivores, as a defensive mechanism. The gas chromatography systems are capable of monitoring kinetic and other aspects of phytochemical production. Detecting insect infestations with gas chromatography could be accurate, if samples are carefully collected. However, this method requires samples to be collected in the field, and later analyzed in the lab. This method has not yet been implemented in actual agricultural fields or farms. However, many investigations have been reported and published in the literature [9-10].

1.1.2.2.4. Acoustic Wave Sensor Control

Acoustic sensor systems have been reported to successfully detect infestations. Examples include a sensor array for detecting larvae of the rice weevil and grain borers in grain crops. The sensor array system was computer based, and was able to quantify infestation of internally feeding larvae in grains. This acoustic sensor system was able to detect feeding noises created by the larvae. The computer system connected to the sensor array was able to successfully correlate the obtained data to the locations of the sound sources. The feeding times of the insects were obtained through differential distortion induced by sound propagation through the non uniform medium to the different sensors. This was accomplished by obtaining outputs of all sensors and cross correlating adjacent sensor pairs with the largest signal, through cluster analysis. Although this sensor works in various weather conditions, the sensor is sensitive to other sounds produced and hence field tests have not been successful to date [6, 24].

1.1.3. Plant Defense Mechanisms

Plants constantly face challenges in nature caused by pathogens, insects and environmental stress. To overcome these challenges, they show different physical and biochemical responses [15-23, 25-27]. Three of such common responses are the hyper sensitive response, compatible disease response and the induced plant response [25]. All of these three responses lead to phytochemical production in plants. "Phytochemicals" is a generic term for all types of chemical compounds that occur naturally in plants, which affect the health of plants but are not established essential nutrients. The phytochemicals emitted as a plant defense mechanism are essentially caused by a change in the plant's secondary metabolism [25]. It should be noted that terminology used in plant defense literature is often confusing. Although "induced plant

response" is the term often used for phytochemical production during defense mechanisms, in some texts, this may include a complex set of responses. It should also be noted that induced plant response could be a result of the hyper sensitive response and compatible disease response. Each of these responses are discussed below [26].

a) **Hypersensitive Response:** This is a response of plants to bacterial, fungal and viral pathogens as well as herbivores. In this particular defensive mechanism, when a plant is attacked by pathogens, a disorganization and granulation occurs at the site of attack. Once the hypersensitive response occurs, it will trigger various resistance mechanisms such as phytochemical production due to changes in plant secondary metabolism [27]. Examples include phytoalexin production in wheat in response to Pseudomonas *syringae pv.syringae.* Hypersensitive responses also trigger formation of necrotic responses common when attack is by herbivores. When herbivores attacks and lays eggs, the hypersensitive response triggers the formation of a necrotic area around the eggs, ultimately killing them. The formation of these necrotic areas will change the secondary metabolism, which may encourage phytochemical emission. When attacked by insects and pathogens, some plants have a tendency to form galls. These galls may take different shapes and sizes as shown in figure 1.1 These galls usually contain eggs, larvae or even adult insects. It should be noted that the formation of some galls may be a survival mechanism in some plants, where the galls host some beneficial symbiotes. However when the symbiotes are destructive to the host plant, galls would cause the hypersensitive response. The hypersensitive response would then cause necrosis around the gall area, killing any insects or pathogens present. Hypersensitive response is also present when there are atmospheric pollutants such as the presence of ozone

in the environment. The hypersensitive response would also trigger phytochemical emission as mentioned earlier. Some galls are also reported to encourage phytochemical excretion namely, phenolic compounds [27].

b) **Compatible disease response:** Compatible disease responses such as necrotic lesions caused by leaf spotting due to insect and pathogen infestation in plants, do not severely affect the plants. They induce other resistance mechanisms similar to hypersensitive mechanisms which will result in emitting phytochemicals due to changes in plant secondary metabolism. The emission of these chemicals or other elicited resistance mechanisms may not be specific to the insect attacked. An example would be the increased emission of peroxidases in velvet leaf when attacked by *C.coccodes* or phytoalexin emission in sickle pod due to *A. cassiae* infestation [27].

c) **Induced responses:** Induced responses in plants are defined as the enhancement of resistance in plants in response to extrinsic stimuli which are biotic or abiotic in nature. Biotic examples include insects, pathogens or humans, while abiotic examples include mechanical wounding caused by wind or other chemicals that may be present. Induced resistance in plants may be localized at the site of attack, or systemic. Systemic induced resistance is also known as systemic acquired or activated resistance. Induced responses could be incidental and could range from shifts in water content, leaf toughness, nitrogen uptake, changes in secondary chemistry/metabolism, trichrome density (trichromes being the bristle like out growth from the epidermis of a plant), and increase in traits attractive to predaceous arthropods [29]. These responses successfully reduce the performance of attacking herbivores. They may also increase the levels of plant fitness as pointed out in some studies. However induced plant responses may not be always be beneficiary. In some

cases, it may cause slow growth of larvae, which may cause increased consumption of plant tissue. In this research, we are interested in the changes of secondary chemistry/metabolism of plants during herbivore and pathogen attack, which are responsible for the emission of phytochemicals [29].

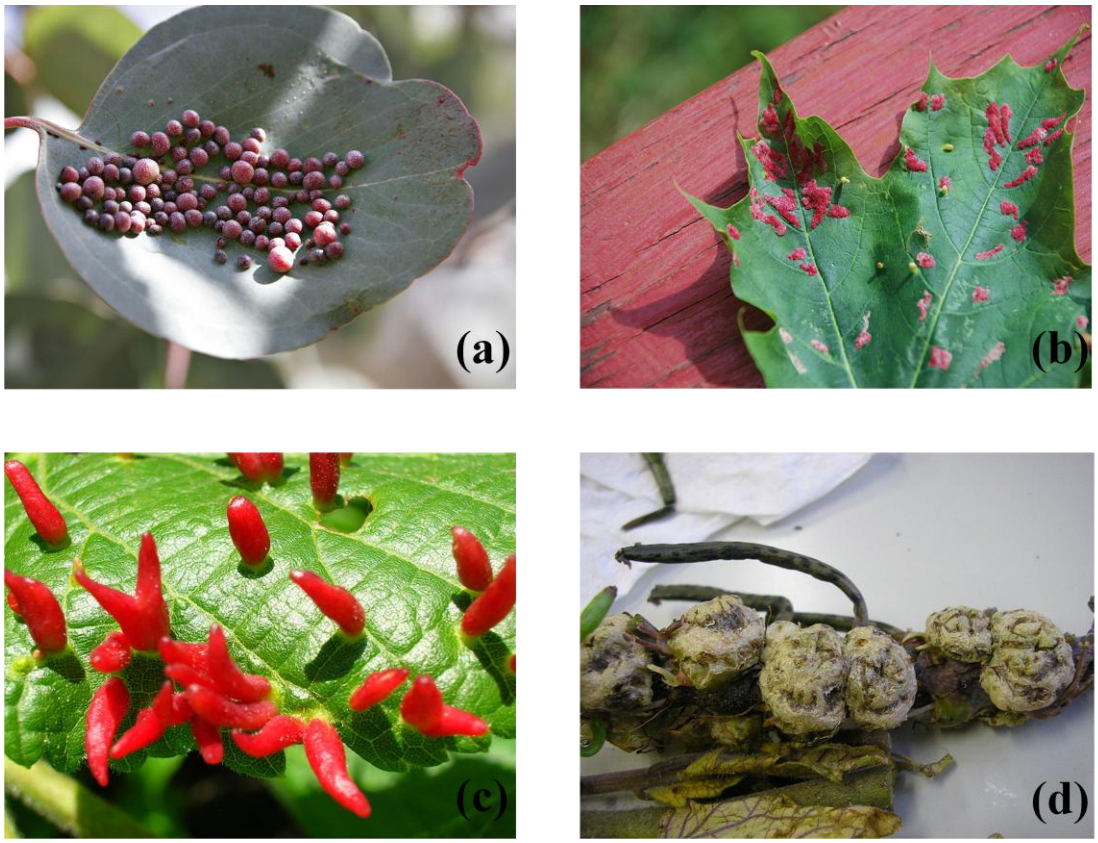

Figure 1.1. Gall responses in some plants due to insect and pathogen infestation: (a) galls in eucalyptus leaf; (b) galls in a maple leaf; (c) nail galls in lime leaf; and (d) Kalanchoe crown galls due to *agrobacterium tumefaciens* infestation [28].

Secondary metabolites in plants are defined as metabolites which are not directly involved in primary processes of basic growth and development. These chemicals play an important part in the interactions between plants and other biological species including herbivores and pathogens. Secondary metabolites are responsible for the flavor and taste in plants which may attract beneficial herbivores, especially for plant dispersal. The secondary metabolism system acts similar to the endocrine system in animals, producing five major kinds of plant hormones, abscusic acid, auxins, cytokinins, ethylene and gibberellins. These hormones are transported within the plant by either cytoplasmic streaming within cells, or by use of vascular tissues, sieve tubes or xylem [25-27].

Most secondary metabolites are found in epidermal vacuoles, cell walls, oil glands, or on leaf waxes. In most plants, the leaf surface of the plants hosts waxes and sugars which contain alkanes, alkanols, alkanoic acids and specific amino acids. In plant families such as solanceae, labiatae, and composites, trichromes or glandular hairs host different mono, sesqui and diterpinenes. Mixtures of terpenoids are found in almost all essential oil plants. Plants may also store semiochemicals in different parts of its body. A semiochemical is a chemical emitted by a plant or an animal that evokes a behavioral or physiological response in another organism. A semiochemical which affects an individual of the same species is known as a pheromone while a semiochemical which affects a different species is known as an allelochemical [26]. Examples of common semiochemicals include phenylpropenes, furanocumarins and polyaceytlenes. Secondary metabolites are synthesized in many different routes, as shown in figure 1.2. The starting ingredient of all pathways is carbohydrates [25].

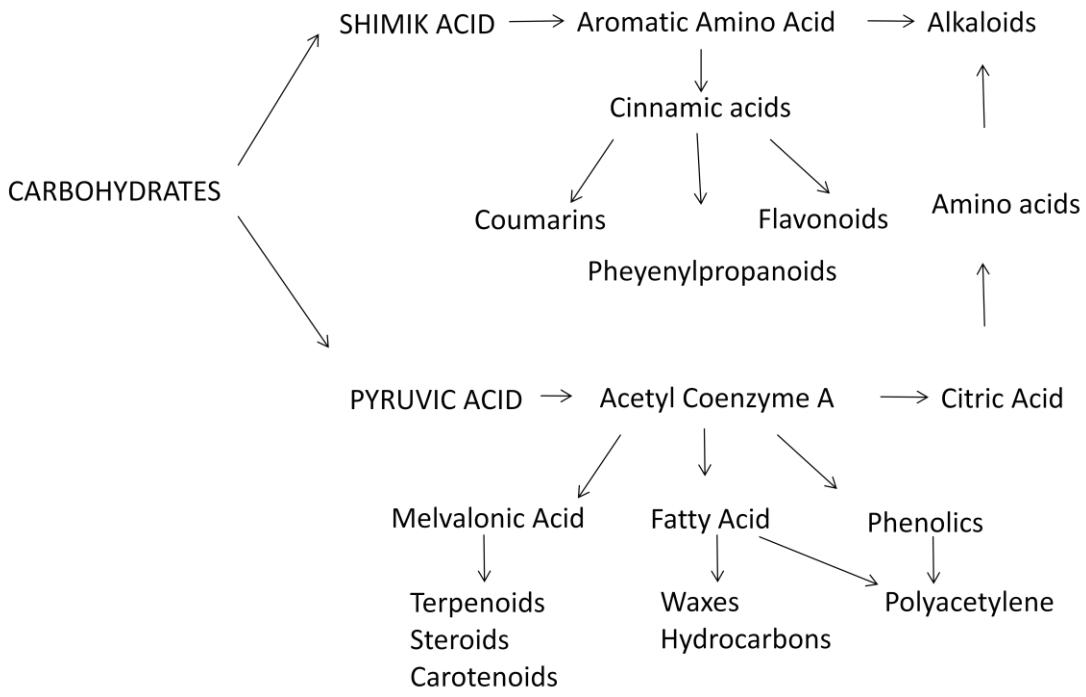

Figure 1.2. Pathways of secondary metabolism in plants: many different pathways are involved in the synthesis of plant volatile compounds, where all of them initiate from carbohydrates [25].

At the time of attack, the secondary metabolism of plants is changed through the hypersensitive response, compatible disease response or induced plant response. There are two ways in which the secondary metabolism could be changed. It could be changed by raising the level of various metabolites. An example would be the increased levels of allelochemicals, which attracts enemies of herbivores and pathogens. The second method in which the secondary metabolism is changed is when already existing metabolites are changed into toxic compounds harmful to herbivores and pathogens. The increased levels of metabolites or the harmful toxic chemicals produced are emitted as phytochemicals, which are all volatile organic compounds. Each species of plants has its own blend of phytochemicals emitted at the time of danger. Table 1.3 below shows different types of anti-insect, secondary chemicals produced by the cotton plant, when attacked by insects in general. It does not show chemicals emitted due to a particular insect. However the blends from each plant are specific to a particular insect. Table 1.4 shows the various blends of chemicals emitted from various plants when attacked by a particular insect. The average concentration for each of the chemicals emitted is 100 ppm [15-23, 25-26]. For example cotton will emit the phytochemicals illustrated in table 1.3 when attacked by insects. Table 1.4 shows the various blends of chemicals emitted from various plants when attacked by a particular insect, which are produced in various secondary metabolic pathways. Besides leaf age, plant genotype is the major factor that affects the quality and the quantity of the chemicals produced. The quality of the defensive mechanism is reflected by how adaptable the herbivores and pathogens become to the phytochemicals [15-23, 25].

Table 1.3. Anti insect phytochemicals from the cotton plant [25].

Phenolic Acids	**Terpenes**
Benzoic Acids	***Monoterpenes***
Gentisic, Salicylic, Vannilic	Limonene, Myrcene, Ocimene
Cinnamonics	***Seqiuterpenes***
Caffeic, Chlorogenic, Ferulic, Sinapic	Caryophyllene, Bisabolene
Flavanoids	***Terpenoid Aldehydes***
Gossypetin, Kaempferol, Quercetin	Gossypol, Hermigossypol
Apigenin, Cyanidin, Delphinidin,	***Fatty Acids***
Catechin	Malvalic acids, Sterculic acid

Table 1.4. Blends emitted by certain plants when attacked by particular insects [12-23].

Plant	Insect	α-pinene	β-ocemene	Linalool	3-hexynyl acetate	Indole	Farnesene	Sabinene	Limonene	Myrcene	γ-terpinene	p-cymene	β –pinene	Nerolidol
Cotton	Beet Army Worm	**X**	**X**	**X**	**X**	**X**	**X**		**X**	**X**			**x**	**X**
Corn	Spider Mite			**X**	**X**	**X**	**X**							**X**
Carrot Leaf	Carrot Psyllid	**X**	**X**					**x**	**X**	**X**			**x**	
Pine Trees	Bark Beetle	**X**							**X**	**X**	**X**	**X**	**x**	
Oil Seed Rape	Pollen Beetle		**X**			**X**		**x**	**X**	**X**				
Maize	Parastatic wasp			**X**	**X**		**X**							
Tobbaco	Parastatic wasp			**X**	**X**		**X**							
Tomato	Spider Mite		**X**	**X**	**X**	**X**			**X**	**X**		**X**		**X**

1.1.4. Using the Defensive Mechanisms of Plants to Detect Insect Infestation

Monitoring for the appearance of volatile phytochemicals which correspond to the time of first insect attack can be used to detect the early stages of insect infestation. A small chemical resistor sensor array system could be fabricated to detect these volatile organic compounds. For actual application in the field, certain distributed plants could be selected and insect sensors appropriately positioned to monitor for the first appearance of volatile organic compounds emission from the plants. A hand held RFID (radio frequency identification device) could be used to measure the response of the sensors. The recorded data could then be transmitted to a remote location where data could be analyzed using statistical methods. The results could then be used to determine whether there was a herbivore infestation of the plants in the field. An illustration of how this might work is shown in figure 1.3 below.

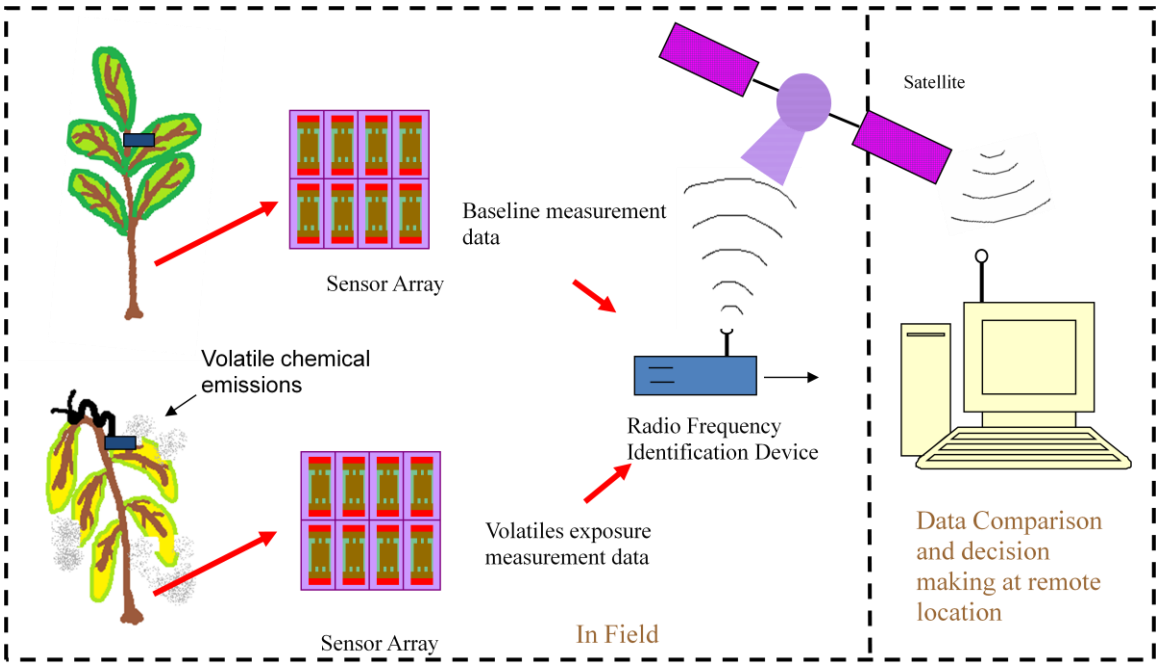

Figure 1.3. Detecting insect infestation using plant defensive mechanisms monitored remotely.

1.2. Sensors for Volatile Organic Compound Detection

Chemical sensors can be broadly classified into four major categories; namely, electronic, photometric, acoustical/mechanical and calorimetric. These sensor technologies are summarized in Table 1.5 below.

Many of these sensor types can be used detect green house gases such as O_2, N_2O, CO_2 and CH_4, but only a few can be used to detect organic compounds. Some of these sensor technologies used to detect volatile organic compounds include: metal oxide sensors, piezoelectric sensors, optical sensors, conductive electro-active and polymer sensors. A brief introduction to each of these sensor technologies is presented below. Advantages and disadvantages of each of these sensor technologies are discussed in Table 1.6 at the end of this section.

1.2.1. Metal Oxide Sensors

Metal oxide gas sensors, because of their high sensitivity, are readily available in the market, as single sensors or as a sensor array. One of its most common uses is the detection of volatile organic compounds. The most common type of metal used in volatile organic metal oxide sensors is SnO_2, doped with catalytic palladium or platinum. These sensors are very versatile because they can be used for different applications simply by varying their operating condition or choice of catalyst. Some of the commercially available tin oxide sensors to detect various organic compounds are listed in table 1.6 [24, 31-32].

Table 1.5. Classification of chemical sensors [24, 32].

Sensor Technology	Output Change	Examples
Electronic		
Amperometric	Current	Polymer, enzyme, whole cell
Resistance	Resistance	and antibody electrodes,
Potentiometric	Voltage	chemical resistor sensors,
Capacitance/impedance	Impedance	field effect transistors, conductometers
Photometric		
Light absorption and scattering refractive index	Light intensity, color or emission	Ellipsometry, internal reflectrometry, laser light scattering, surface plasmon
Fluorescence or luminescence	Fluorescence or	resonance, fiber optic wave
Activation	Chemiluminiscence	guides
Acoustical/Mechanical		
Acoustical	Amplitude, phase or	Saw devices
Mass/density	frequency weight	Piezoelectric devices
Calorimetric		
Thermistor	Temperature	Enzyme and immuno-enzyme Reactors

Table 1.6. Commercially available tin Oxide sensors used for various applications [24].

Model	Category	Measured	Range (ppm)
TGS 550	Odor	Sulfur Compounds	0.1-10
TGS 800	Air Quality	Cigarette smoke	<10
TGS 815	Combustible Gases	Methane	500-10000
TGS 821	Combustible Gases	Hydrogen	50-1000
TGS 822	Organic Solvents	Alcohol, Toluene	50-500
TGS 824	Toxic Gases	Ammonia	30-300
TGS 825	Toxic Gases	Hydrogen Sulfide	5-100

All metal oxide sensors consist of a ceramic support tube containing a platinum heater coil, which is coated with tin oxide on the outside, with catalytic additives. This is illustrated in Figure 1.4 This type of configuration is known as "Figaro" which is named after the company that manufactures them in Japan. The Figaro company literature cites that this type of sensor is sensitive to humidity and each sensor will have individual variations in sensitivity. Therefore these sensors require calibration and sometimes the sensor may be subjected to poisoning unless stored in airtight clean containers [24, 32].

The mechanism by which metal oxide sensors operate (in air and at elevated temperatures: 300^{o}C - 550 $^{\circ}$C) is explained by the concentration of oxygen at the semiconductor surface. When exposed to air, the surface of the sensor (the semiconductor solid) reacts with oxygen to form oxygen ions. Therefore the charge carrier density is reduced which results in a potential barrier that slows the oxygen conversion rate. This affects the electron movement, and the conductivity of the semiconductor material. For n-type semiconductors, the reactive gas combines with absorbed oxygen reducing the height of the potential barrier, while the opposite is true for a p-type semiconductor. For example if the reactive gas is CO, and an n-type semiconductor is used the following gas reactions occur. An illustration of the mechanism for this case is illustrated in figure 1.5 [24, 32].

$$\text{Adsorption of oxygen: } (SnO_2 + e^-) + \tfrac{1}{2}\, O_2 \leftrightarrow SnO_2\,(O^-)_{ad}$$

$$\text{Reduction of Reactive Gas: } SnO_2\,(O^-)_{ad} + CO \rightarrow (SnO_2 + e^-) + CO_2$$

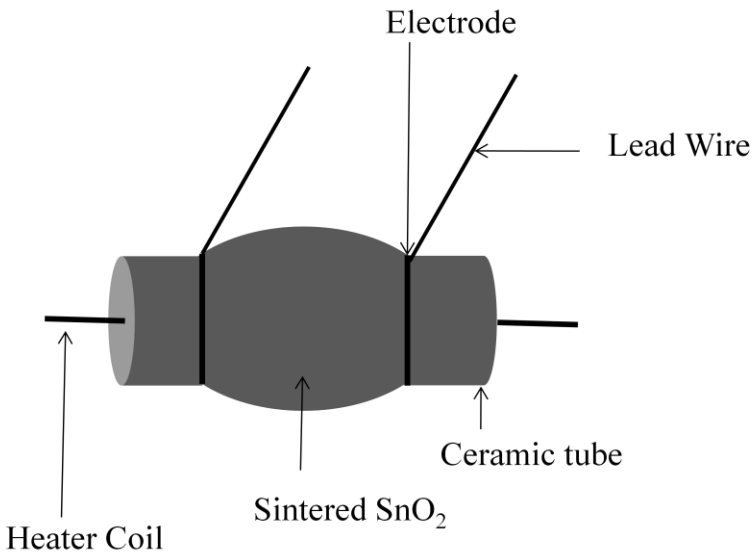

Figure 1.4. Structure of a Figaro type SnO_2 sensor [24, 32].

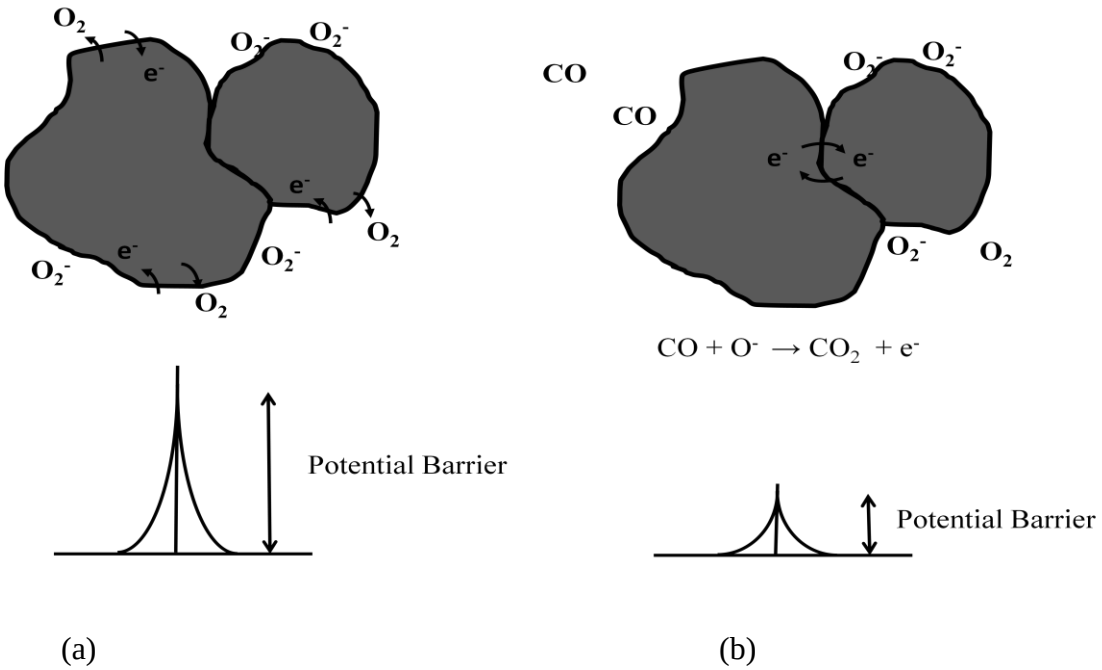

Figure 1.5. (a) Charge exchange of oxygen at the surface of an n-type semiconductor, with chemosorption of oxygen (b) Charge exchange associated with reducing gas and the effect on potential barrier for each case.

Although small and convenient, the power consumption of metal oxide sensors is high, due to the required elevated operating temperature (typically 350 °C-550 °C). More recently there have been metal oxide sensors developed other than SnO_2 including ZnO, TiO_2, WO_3 and perovskites. These sensors are often incorporated into one sensor array to detect volatile organic compounds. Although sensitivity of the array may be high, the selectivity is low. This is because metal oxides have similar reactions with many volatile organics especially if they have similar structures, and thus similar responses. Component analysis is often required to distinguish between similar organic compounds in this case [24, 32].

1.2.2. Acoustic Gas Sensors

Acoustic sensors operate by detecting the change in propagation of acoustic waves with the sorption of analyte molecules. There are two main types of devices based on surface acoustic waves (SAW) and bulk acoustic waves (BAW). Both of these types of sensors consist of a piezoelectric substrate such as quartz, lithium niobate and zinc coated with a sorption layer. When the analyte molecule is absorbed to the sorption layer, the associated acoustic wave will change its velocity, amplitude and frequency. These waves are typically in the range of 1-500 MHz. In the presence of an electric field, the piezoelectric material undergoes a change in its mechanical properties. Therefore an electric field could be used to oscillate the piezoelectric material at its resonance frequency as in a BAW sensor, or produce a surface wave as in the SAW sensor. The sorption layer in the sensor is usually a soft rubbery polymer material, such as polysiloxane which is usually the same coating found in gas chromatography systems. Monolayer films and surface attached molecules are also used. Selectivity is enhanced in these sensors by selecting sorption coatings which absorb specific analytes only. Usually non-covalent

bonds such as Vanderwall, dipole-dipole, dipole-induced dipole and hydrogen interactions are formed between the polymer layer and the sorption molecules. The mechanism and structure of BAW and SAW devices are discussed below [24, 32].

Bulk acoustic wave sensors (BAW) more commonly known as quartz crystal microbalance (QCM) or thickness shear mode (TSM) sensors, are very simple sensors. They are constructed from a single crystal quartz and two electrodes (typically gold). When an alternating current voltage is applied, the device is made to oscillate at its resonance frequency. Here the particle displacement of the sensor surface is normal to the propagation of the wave. This is illustrated in figure 1.6 below.

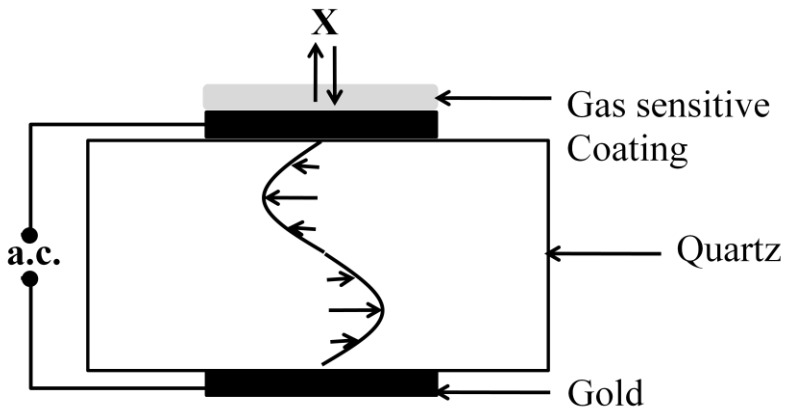

Figure 1.6. The structure and operation of a BAW sensor, where X is particle displacement.

The change in resonant frequency (Δf) when sorption of an analyte molecule occurs is given by the Sauerbrey equation (equation 1.1 below), where f_o is the resonant frequency, ρ_q is the density, μ_q is the shear modulus and m_f is the mass of the film.

$$\Delta f = -\frac{2f_o^2}{A\sqrt{\rho_q \mu_q}} m_f \quad \text{Equation 1.1}$$

If the sorption layer is polymeric, which is the common case for BAW sensors detecting volatile organic compounds, the imaginary and real components of the visco-elasticity should be taken into consideration. BAW sensors can be used to detect a variety of volatile organic compounds, and could be made very selective simply by changing the sorption polymer layer. However, this sensor is very sensitive to changes in temperature, humidity and flow conditions [24, 32].

SAW sensors consist of a relatively thick plate of piezoelectric material with interdigitated electrodes with sorption film. When a voltage is applied to the interdigitated electrodes, the deformation of the crystal forms a surface wave. The waves propagate in both directions from interdigitated electrodes, where the wave fronts are parallel to the fingers of the electrode. The distance between the electrodes is half the wave length. There are two types of SAW configurations: delay line and resonator. In the delay line configuration, a second pair of electrodes is used to receive the signal launched from the transmitter electrode pair. In the resonator configuration, the same electrode pair acts as the transmitter and receiver. In this case, the SAW is reflected by a groove formed on the crystal surface. These two types are illustrated in figure 1.7 below. The frequency change (Δf) of the SAW with the absorption of the vapor is given by equation 1.2 For a simple mass loading effect, the change of frequency of the SAW with sorption of vapor Δf_v and Δf_p is the change of frequency in the polymer film, K_p is the

partition coefficient, ρ_p is the density of the polymer and C_v is the concentration of vapor in gas phase. [24, 32].

$$\Delta f_v = \Delta f_p c_v \frac{K_p}{\rho_p} \quad \text{Equation 1.2}$$

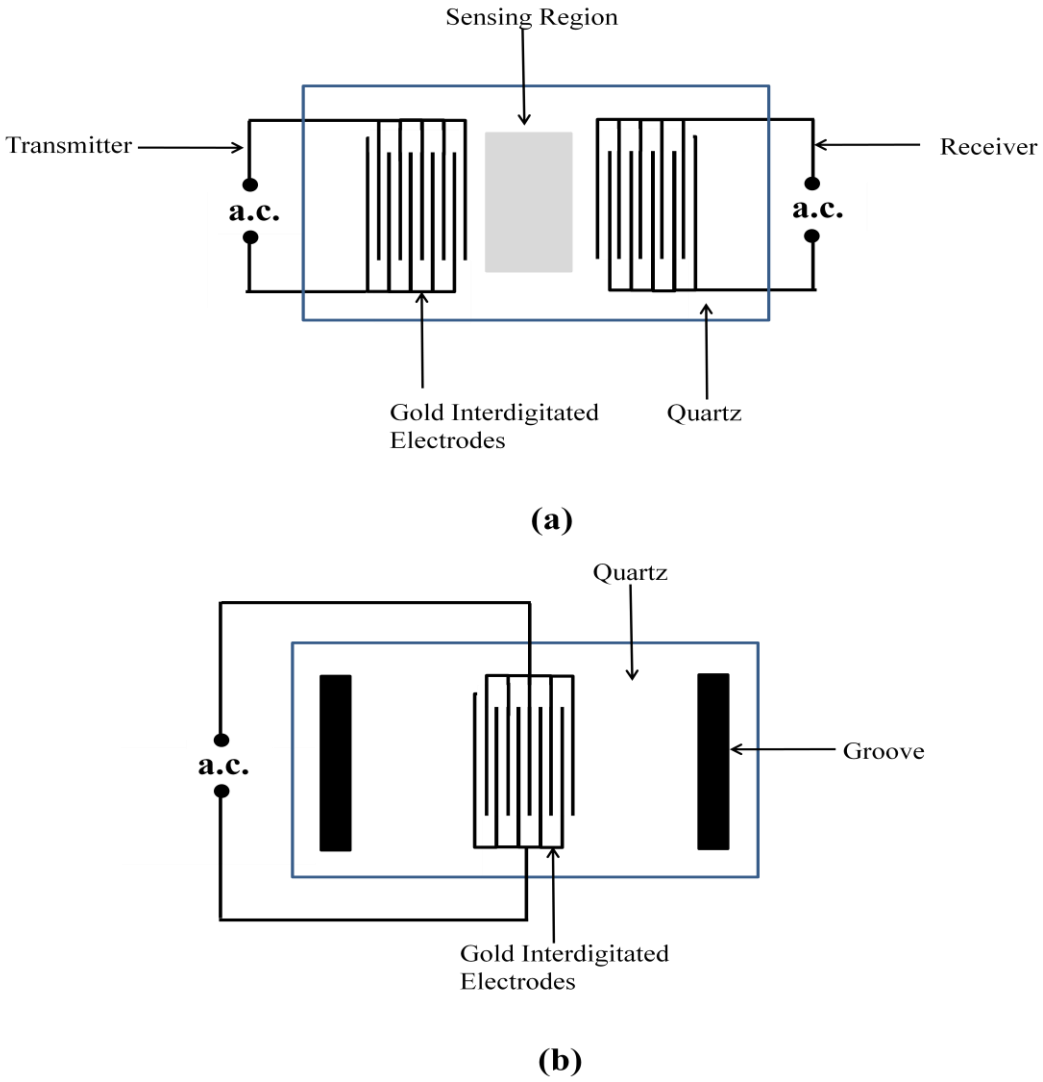

Figure 1.7. Two types of SAW devices (a) delay line (b) resonator.

SAW sensor arrays with soft rubbery polymer coatings have been used to detect various toxic and odorous volatile organic compounds. Similar to BAW devices, SAW devices are also very sensitive and selective, but may be sensitive to humidity and other environmental conditions [24, 32].

1.2.3. Optical Sensors

The most popular optical sensors used to detect volatile organic compounds are fiber optic sensors. The mechanism of these sensors is very simple. The optical fiber in the sensor guides the light from the light source to the chemically sensitive active layer and returns light back to the sensor. This type of sensor is small and versatile. They can be used to monitor volatile organic compounds from remote locations, because light travels over several kilometers. The basic structure of an optical sensor is shown in figure 1.8 below.

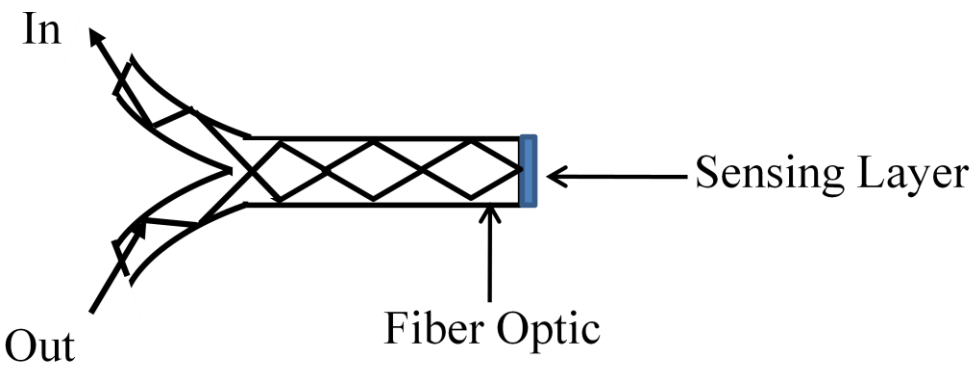

Figure 1.8. Fiber Optic Sensor for volatile organic vapor detection.

Dikinson et. al. have reported on a fiber optic sensor array for detecting volatile organic compounds. In the experiment, the sensing layers were coated with various polymers containing a dye. The color spectra of the dye was heavily dependent on the solvation properties of the polymer. The solvation properties changed uniquely depending on what the polymer layer absorbed. Therefore, it would emit different colors depending on what the polymer layer absorbed. Although this method is highly selective it is not reported to be very sensitive. The reproducibility, stability and the lifetime of these sensors are debatable [24, 32].

1.2.4. Conductive Electro-active Polymer Sensors

Electro-active polymers including intrinsically conducting polymers and polymer/carbon composites are widely used in volatile vapor detection. They are versatile and a wide range of polymers can be synthesized. They also respond to a large number of organic vapors. They operate at room temperature, and in most cases, are stable at ambient conditions. In this section two types of electro-active polymers will be discussed: (1) intrinsically conducting polymers and (2) polymer/carbon composites [24, 30-32].

1.2.4.1. Intrinsically Conducting Polymers for Sensing Volatile Organic Compounds

The most commonly used intrinsically conducting polymers in gas sensors include polypyrrole, polyaniline and polythiophene. Derivatives of these polymers are being used as well. These conducting polymers are popular for several reasons. They are easily synthesized through chemical and electrochemical processes, and their molecular structure can be readily modified for chemical diversity and their chain structure can be modified by copolymerization. They have good mechanical properties which enable them to be conveniently used for sensor

fabrication. Structures of some commonly used intrinsically used conducting polymers are shown in figure 1.9 below [24, 30-33].

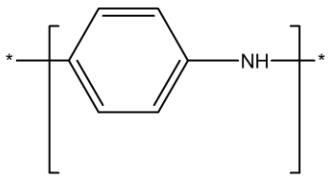

Polyaniline (PANI)

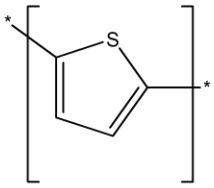

Polythiophene (PTH)

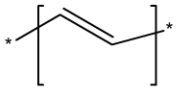

Polyacetylene(PA)

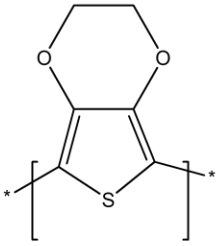

Poly(3,4ethylenedioxythiophene)(PEDOT)

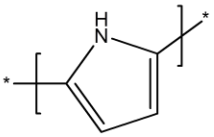

Polypyrolle (PPy)

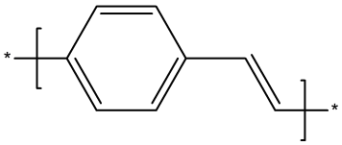

Polyphenyl vinlene (PPV)

Figure 1.9. Some commonly used intrinsically conducting polymers for detecting volatile organic compounds.

Conducting polymers are synthesized for sensor materials usually through electrochemical or chemical oxidation of monomers. This process involves mixing the corresponding monomer with a suitable oxidant in solution. Common oxidants used include ammonium persulfate, ferrum chloride, hydrogen peroxide, potassium dichromate and cerium sulfate. The electrochemical synthesis is done either using galvanostatic, potentiostatic or cyclic voltammetry. Potentiodynamic methods could also be used. The methods require a three electrode system which includes a working electrode, counter electrode and a reference electrode. The working electrode is usually made of platinum, stainless steel or gold indium oxide (ITO) glass. The polymers deposited can be peeled off and directly used for sensor applications. Other polymerization methods such as the Wittig reaction, Heck reaction and Gilch reaction could also be used. Coupling reactions are sometimes used to synthesize polythiophene and its derivatives. Once the polymer is synthesized, it is usually dissolved in a suitable solvent and deposited as an active layer onto the sensor platform using one of the following techniques [24, 32, 33].

a) **Electrochemical deposition:** A convenient method of deposition where the polymer is directly deposited onto the sensor platform using an electrochemical cell. The thickness of the film can be controlled by the charge passed through the cell. Deposition is done on a conducting substrate. This method is widely used for making chemiresistor type sensors.
b) **Dip coating:** The platform is directly dipped in a polymer solution so that the polymer is deposited on the sensor substrate surface. The thickness of the sensor can be controlled by dipping time and the concentration of the solution. Dip coating can also be done by dipping the substrate into the monomer and then oxidizing the solvent. The monomer will then be polymerized on the sensor surface.

c) **Spin coating:** In this method, the conducting polymer solution is deposited onto the surface by using a spin coater. The thickness of the film deposited is controlled by spin speed, time and the concentration of the polymer solution.

d) **Langimuir-Blodgett technique:** This method is used where a very thin film is needed to be deposited onto the sensor surface. The polymer can be directly deposited using this technique, or the monomer can be deposited followed by polymerization.

e) **Layer by layer self assembly:** This method can be useful to produce coupled conducting polymers. In this technique, the substrate is dipped first in the polymeric anion solution and then in the cation solution, which allows layer by layer deposition. The number of steps done (times altered) controls the thickness of the film produced.

f) **Thermal evaporation:** In this technique, the conducting polymer is heated under a vacuum. The polymer evaporates, and is deposited onto the sensor platform. The evaporation time determines the thickness of the film produced.

g) **Drop coating:** Drops of polymer solution are deposited using a syringe or pipette. The solvent slowly evaporates to leave the polymer film behind. This technique is simple, although the thickness is hard to control, and the resulting films are not uniform.

h) **Vapor deposition polymerization:** An oxidant film is first deposited onto the sensor platform. The monomer vapor is then evaporated onto this film. This technique can be used to produce composite films as well as pure polymer films.

Other methods of deposition include electric field induced electrochemical polymerization, packing pellets of conducting polymer onto sensor substrates and inkjet printing [33].

Conducting polymer sensors are used in different types of sensor platforms or configurations including chemiresistors, transistors, diodes, optical devices, piezoelectric crystals and amperometric sensors. Each of these different configurations is discussed below.

a) Chemiresistors: The chemiresistor is the most commonly used configuration with conducting polymers. They are usually produced through cheap and convenient micro-fabrication techniques. A chemiresistor sensor coated with an intrinsic polymer would change its resistance when the polymer absorbs and changes its electrical properties. These resistance changes can be recorded with a data acquisition system. For better performance, the electrodes are interdigitated. The structure and components of a chemiresistor sensor is shown in figure 1.10 [24, 32-33]. The overall resistance of the film depends on the conductivity contributed by intermolecular interactions, σ_c, intramolecular hopping conductivity, σ_h and ionic conductivity, σ_i. The intermolecular conductivity of the polymer is changed by the doping levels of the polymer and redox reactions. Intramolecular hopping conductivity is adjusted by swelling the polymer, changing its crystallinity or by a change in other physical interactions such as hydrogen binding. Ionic conductivity is controlled by the effect of counter ions [24, 32-33]. Chemiresistor sensors are versatile, easily fabricated and operated at room temperature and can be used in a variety of applications. However the resistance of the sensor could be affected by the contact resistance of the electrodes with the polymer film.

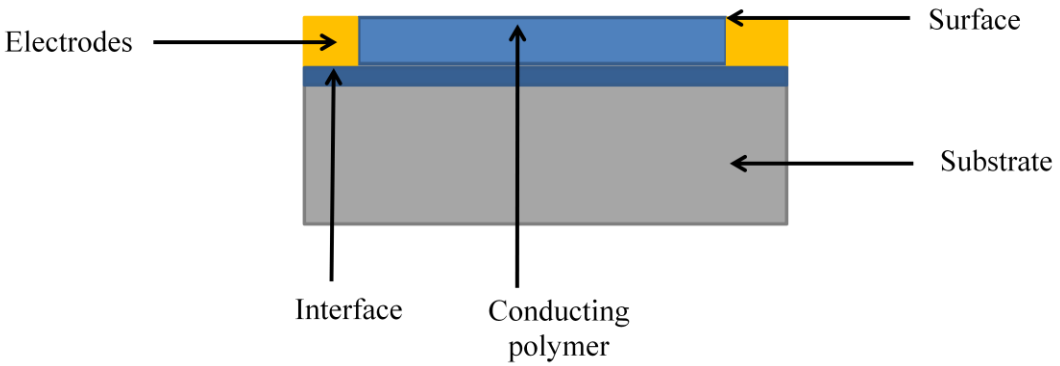

Figure 1.10. Configuration and components of a chemiresistor sensor.

b) Transistors and diodes: Thin film transistors for detecting volatile organic compounds, also known as organic thin film transistors (OTFT) are used in a variety of applications as recorded in literature. These sensors consist of a semiconductor active layer, such as an intrinsically conducting polymer with two electrodes, the source and drain, and a third electrode the gate. The gate is actually the conducting polymer thin film. A source gate voltage can be applied and the current between these two electrodes measured. The gate (active layer) can be used to modulate the current between the two other electrodes. Therefore, when an analyte gas is present, the absorbance would change the electrical properties of the film, which would change the current between the source and the drain. There are two kinds of OTFTs. In the first kind, the current flows through the conducting polymer. In the second kind which is insulated gate field effect transistors (IGFT), the gate which modulates the current between source and drain is separated from the active polymer layer by a insulating layer. These two configurations are illustrated in figure 1.11 below [24, 32-33].

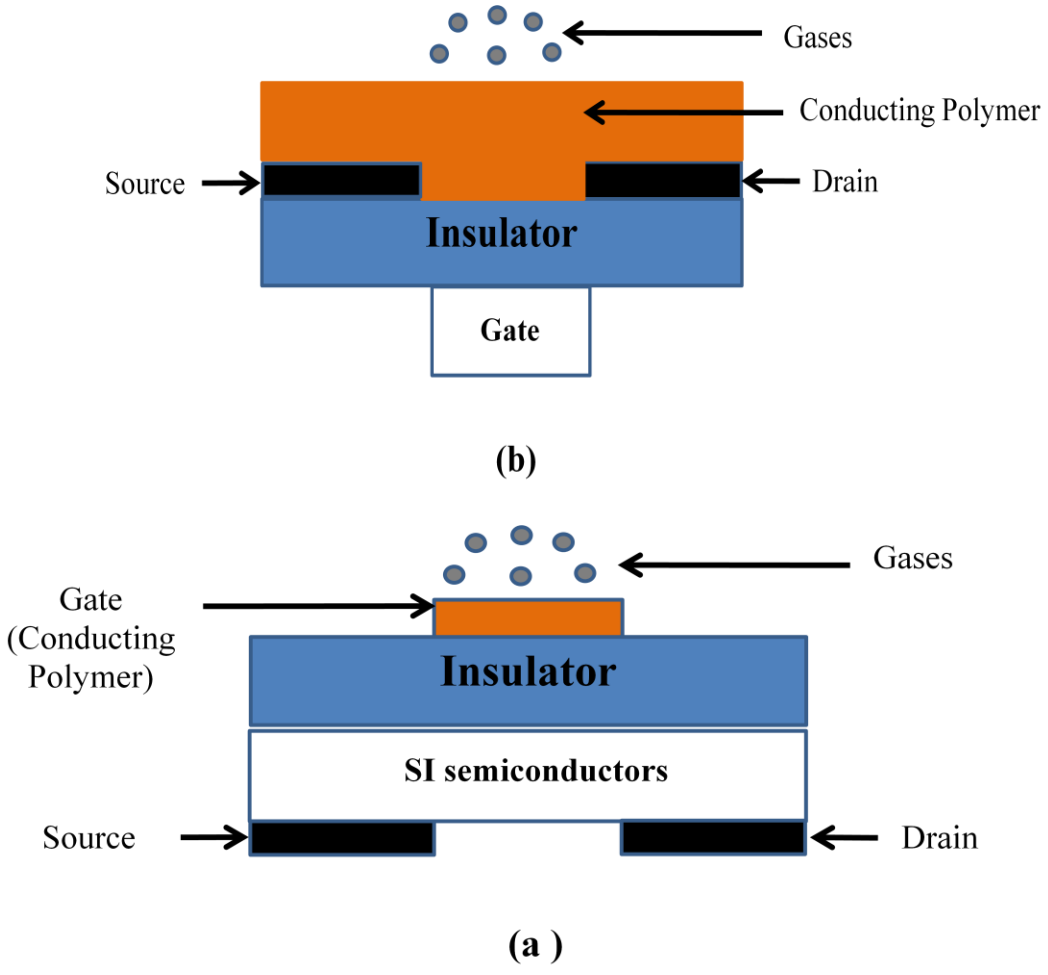

Figure 1.11. Two configurations of organic thin film transistors (OTFTs): (a) Thin film transistors (TFTs) (b) Insulated gate field effect transistors IGFET.

c) **Diode devices:** This is a simple device, where the conducting polymer is deposited onto a metal semiconductor surface. The conducting polymer is p-type. When the polymer comes in contact with a n-type semiconductor, a hetorojunction is created at the interface. The polymer film forms a Schottky barrier with the metal or semiconductor interface. When exposed to gas, several electrical properties of the diode changes, including its current density and rectification ratio. When compared to a chemiresistor, diodes give more information about the sensing activity and the films, which enables different types of measurements. However, the fabrication of a diode is more tedious than a chemiresistor or a transistor [24, 32-33]. The structure of a diode is shown in figure 1.12 below.

d) **Optical sensor devices:** Conducting polymers that change their absorbance of light upon interaction with the target analyte gas can be used as optical sensor devices. When the polymer comes in contact with the analyte gas, it will often form polarons and bipolarons, which will change the band structure and change the film's light absorbance properties. The following methods could be used to measure the change in light absorbance. The components of this sensor are simple. Often this device consists of just a glass slide covered with the polymer [24, 32-33].

UV-vis and NIR spectrometer: A UV-vis or NIR spectrometer could be used to measure the change in absorbance. Although the configuration of the sensor is simple, the measurement of absorbance with a spectrometer requires a special vessel or measurement chamber. Collecting and measuring samples during actual events in the field could be inconvenient.

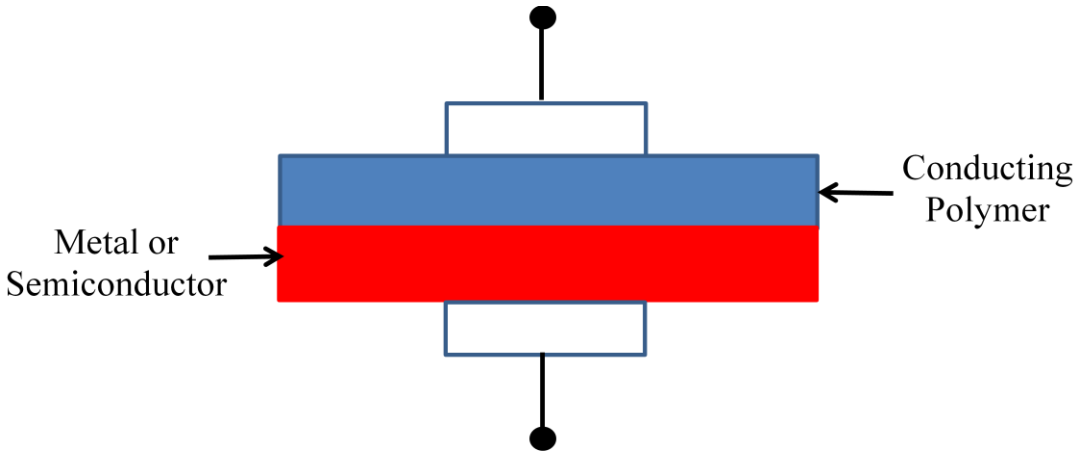

Figure 1.12. The configuration of a polymer based diode sensor.

Optical fibers: Optical fibers could be used to measure the absorbance of the polymer films. There are two methods in which this could be done. In the first method, the polymer film could be placed in the cross section of the optical fiber, and in the second method, a small part of the cladding of the fiber could be replaced with the conducting polymer.

Measuring spectra: The change in spectral properties could be directly measured using colorimetry. This method is a simple concept but actual measuring can be inconvenient, especially in field applications. Special spectrometers are also required.

Surface plasmon resonance: Surface plasma waves are created by free electrons at the boundary of metal and dielectric materials. The corresponding quanta that is created are known as plasmons. Changes in the dielectric layer near the interface will change the excitation of the plasmons. A typical "Kretschmann" type configuration is shown in figure 1.13 Near the resonance angle, small changes in the incident angle cause an acute change in the reflected intensity. When exposed to gas analytes, the change in reflectance curves will shift. This method is very sensitive, although applications in the field can be complicated.

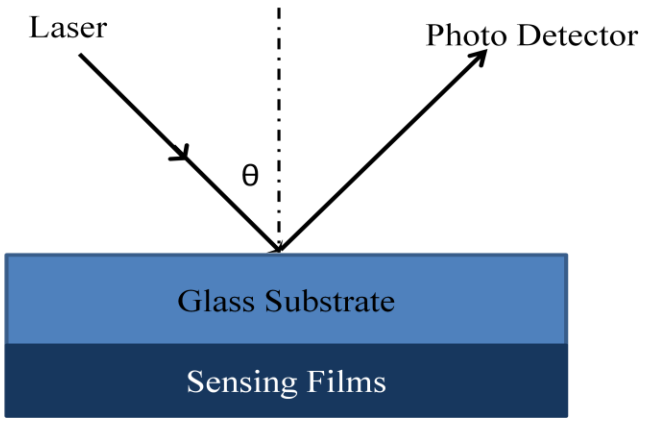

Figure 1.13. Kretschmann type configuration of surface plasmon sensor device.

a) **Piezelectric crystal layers:** SAW devices and quartz crystal microbalances can be used to detect and analyze gases. The active layer is usually a conducting polymer. The advantage of using a conducting polymer is that it reacts with various analytes differently. Selectivity can be increased, by using a non-conducting polymer.

b) **Amperometric sensors:** Amperometric sensors can be used to detect volatile organic compounds, when a conducting polymer sensor is used as the working electrode. An example is the Nafion working electrode. The sensing mechanism is similar to a typical amperometric sensor. A detectable current change is created with the analyte gas oxidizing or reducing at the electrode.

1.2.4.2. Polymer/Carbon Composites for Sensing Volatile Organic Compounds

Another type of electro active polymer sensors are the polymer/carbon composite sensors. The platforms of these sensors are usually chemiresistor based. They are easy to fabricate, and have very high sensitivity. Polymer/carbon composite sensors have been used to detect a variety of organic compounds including polar and non-polar compounds. The mechanism by which polymer/carbon composite film sensors operate is understood and is described in the literature [34-38]. The sensor elements include a film of swellable insulating organic polymer with conductive regions of dispersed carbon particles. The carbon black makes the films conductive. Current travels along continuous pathways of carbon black particles. When sorption happens, swelling of the films occurs, which breaks the continuous pathways increasing the resistance of the composite film. Removal of the analyte species or desorption causes the carbon particles to return to their original places, thus decreasing the resistance of the film. The sensor mechanism is shown in figure 1.14 below. The mechanism by which these sensors operate will be discussed

in greater detail in Chapter 4. Various polymers can be used in the composites, so that the selectivity can be improved. Some of the polymers used in these composites are shown in figure 1.15 [34-38].

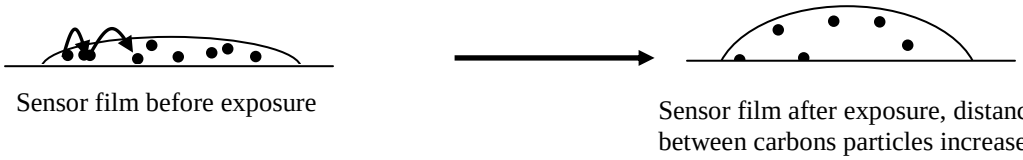

Figure 1.14. Sensing mechanism of polymer/carbon composite sensors.

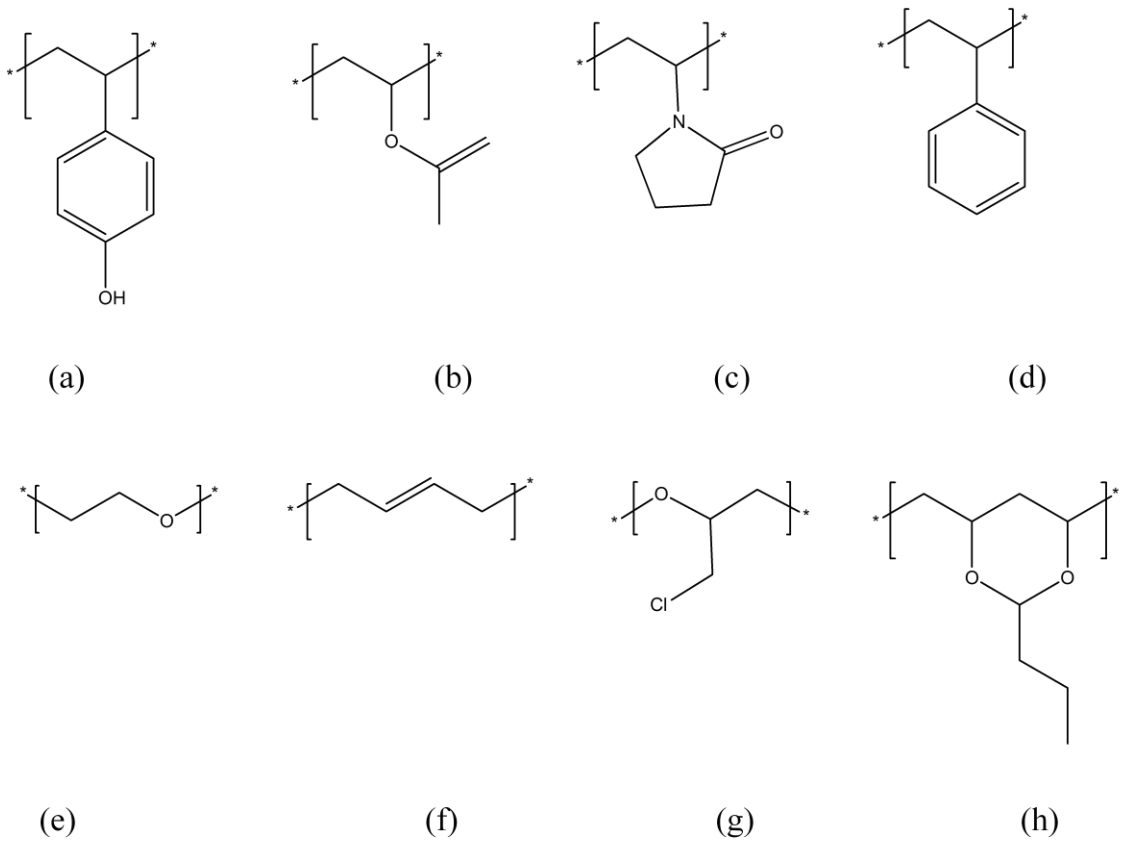

Figure 1.15. Polymers used in various polymer/carbon composites: (a) poly(4-vinylphenol); (b) poly(vinylacetate); (c) poly(N-vinylpyrrolidone); (d) poly(styrene); (e) poly(ethylene oxide); (f) poly(butadiene); (g) poly(butadiene); and (h) poly(vinyl butyral).

The advantages and disadvantages of various sensor technologies is summarized in table 1.7 According this summary, electroactive polymer based sensors are ideal to use as active materials in insect infestation detection sensors, because of their versatile actuator systems, sensitivity and stability under varying environmental conditions.

Table 1.7. Advantages and disadvantages of various sensor technologies [24, 32].

Sensor type	Advantages	Disadvantages
Metal Oxide sensors e.g. zinc oxide, tin oxide etc.	Readily available and cheap; sensitivity range: 5-5000 ppm	Highly sensitive to humidity; poisoning to sulfur compounds; base line shift; usually operated at high temperatures
Acoustic sensors	High selectivity and sensitivity	Sensitive to temperature; poor for true static conditions
Optical sensors	Geometric versatility; low attenuation; good selectivity	Low sensitivity, reproducibility, stability and lifetime questionable.
Conductive electro active polymers	Operation at ambient conditions; high sensitivity 0.1-100 ppm; ease of fabrication; reversibility in analytical signals; fast kinetics	Selectivity marginal, i.e. could be sensitive to a broad range of volatile organic compounds

Various types of sensors for detecting volatile organic compounds were evaluated and their advantages and disadvantages were considered. After careful consideration, it was decided that a chemiresistor sensor array with electroactive polymers would be investigated for the detection of volatile organic compound given off by plants during an insect infestation. For this application it was important that the sensors have high sensitivity, selectivity and stability under environmental conditions experienced in the agricultural field.

1.3. Research Objectives

In this research, a chemiresistor sensor array was designed, fabricated, tested and analyzed. The primary research objectives were to produce a sensor array that will

a) Provide accurate monitoring of volatile organic compounds emitted by plants with a sensitivity of at least 100 ppm;
b) Remain stable under environmental conditions encountered in the agricultural field;
c) Remain insensitive to common gases present in the agricultural field atmosphere;
d) Return to its original resistance so that the sensors need not be replaced after each use
e) Be placed easily in the field, i.e. small in size and minimal power consumption.

These objectives could be achieved by using a sensor array consisting of chemiresistors, that is micro electronically fabricated, small in size, and could be easily attached to plants. In this research, polymer active layers were used to obtain the necessary sensitivities. Various electroactive polymer including poly3-hexylthiophene (spincoated and drop casted), poly3-dodecylthiophene, polyaniline, polystyrene/carbon, polyethyleneoxide/carbon, polyethylene-co-vinylacetate (0% vinylacetate)/carbon, polyethylene-co-vinylacetate (12% vinylacetate)/carbon, polyethylene-co-vinylacetate (18% vinylacetate)/carbon, polyethylene-co-vinylacetate (25%

vinylacetate)/carbon, polyethylene-co-vinylacetate (40% vinylacetate)/carbon and polyisoprene/carbon were used for optimum selectivity. Principle component analysis was used to distinguish between compounds detected.

1.5. References

[1] E. C. Oerke, H. W. Dehne, F. Schönbeck and A. Weber, "Crop Production and Crop Protection: Estimated Losses in Major Food and Cash Crops", 1st ed. , Elsevier, Amsterdam, the Netherlands, 1994.

[2] S. G. Cooper, D. S. Douches, K. Zarka and E. Grafius, "Enhanced Resistance Control Tuber Worm by Combining Engineering Resistance, and Natural Resistance Derived by Solanum Chacens", *Am. J. Potato Res.* , vol. 86, pp. 24-30, 2009.

[3] G. M. Kishore and C. Shewmaker, "Enhancing Human Nutrition in Developing and Developed Worlds", *Proc. Natl. Acad. Sci.* , vol. 96, pp. 5968-5972, 1999.

[4] D. Pimental, H. Acquay, M. Biltonen, P. Rice, M. Silva, J. Nelson, V. Lipner and S. Giordana, "Environmental and Economic Cost of Pesticide Use", *Bioscience.*, vol. 42, pp. 756-760, 1992.

[5] J. E. Losey and M. Vaughan, "The Economic Value of Ecological Services Provided by Insects. *Bioscience*, vol. 56, pp. 311-323, 2006.

[6] R. W. Mankin, J. S. Sun, D. Shuman, D. K. Weaver, "Shielding Against Noise Interfering with Quantitation of Insect Infestations by Acoustic Detection Systems in Grain Elevators", *Applied Acoustics*, vol. 50, pp. 309-323, 1997.

[7] D. Shuman, J. A. Coffelt, K. W. Vick and R. W. Mankin, "Quantitative Acoustical Detection of Larvae Feeding Inside Kernels of Grain", *J. Econ. Entomol.* , vol. 86, pp. 933-938, 1993.

[8] L. L. Zhao and W. Wei, "Chemotaxis of the Pinewood Nematode Bursaphelenchus xylophilus, to Volatiles Associated with Host Pine, Pinus Massoniana, and Its Vector Monochamus Alternatus", *J. Chem. Ecol.* vol. 33, pp. 1207- 1216, 2007.

[9] D. M. Printo and J. D. Blande, "Ozone Degrades Common Herbivore-Induced Plant Volatiles: Does This Affect Herbivore Prey Location by Predators and Parasitoids" *J. Chem. Ecol.* , vol. 33, pp. 683 -694, 2007.

[10] R. E. Shade, E. S. Furgason, L. L. Murdock, "Detection of Hidden Insect Infestations by Feeding Generated Ultrasonic Signals", *Am. Entomol.* , vol. 36, pp. 231-235, 1990.

[11] J. E. Rechcigl and N. A. Rechcigl, "Insect Pest Management: Techniques for Environmental Protection", 1st Ed. , Lewis Publishers, Washinton D. C. , 1999.

[12] J. E. Rechcigl and N. A. Rechcigl, "Biological and Biotechnological Control of Insect Pests", 1st Ed. , Lewis Publishers, Washinton D. C. , 1999.

[13] D. Dent, "Insect Pest Management", 1st Ed. C.A.B. International, Oxon, U. K. 1991.

[14] L. Mattiacci, B. A. Rocca, N. Scascighini, M. D'Allesandro, A. Hern, S. Dorn, "Systematically Induced Plant Volatiles Emitted at Time of Danger", *J. Chem. Ecol.* 27, pp. 2233-2252, 2001.

[15] R. Grote and U. Niinemets, "Modelling Volatile Isoprenoid Emissions – A Story With Split Ends", *Plant Biology*, vol. 10, pp. 8-28, 2008.

[16] J. A. Byers and Q. H. Zhang, "Strategies of a Bark Beetle, Pityogenes Bidentatus, in an Olfactory Landscape" *Naturwissenshaften*, vol. 87, pp. 503- 507, 2000.

[17] M. Jonsson and P. Anderson, "Emission of Oilseed Rape Volatiles After Pollen Beetle Infestation; Behavioural and Electrophysiological Responses in the Parasitoid Pharadis Morionellus" *Chemoecology,* 17, pp. 201- 207.

[18] C. M. De Moraes, W. J. Lewis, P. W. Pare, H. T. Alborn, J. H. Tumlinson, "Herbivore-Infested Plants Selectively Attract Parasoids", *Letters to Nature*. vol. 393, pp. 570-573, 1998.

[19] P. W. Simons, R. C. Lindsay, C. E. Peterson, "Analysis of Carrot Volatiles on Porous Polymer Traps" *J. Agric. Food Chem.*, vol. 28, pp. 549-552, 1980.

[20] T. C. J. Turlings and J. H. Tumlinson, "Systematic Release of Chemical Signals by Herbivore-Injured Corn", *Proc. Natl. Acad. Sci. USA.* vol. 89, pp. 8399-8402, 1992.

[21] E. M. Pettersson and W. Boland, "Potential Parasitoid Attractants, Volatile Composition Throughout a Bark Beetle Attack", *Chemoecology*, vol. 13, pp. 27-37, 2003.

[22] M. R. Kant, K. Ament, M. W. Sabelis, M. A. Harling and R. C. Shuurink, "Differential Timing of Spider Mite-Induced and Indirect Defenses in Tomato Plants", *Plant Physiol*. vol. 135, pp. 4833-495, 2004.

[23] P. W. Paré, W. J. Lewis, J. H. Tumlinsonm, "Induced Plant Volatiles: Biochemistry and Effects on Parasitoids" in *Induced Plant defenses against pathogens and herbivores* 1st ed. A. A. Agrawal, S. Tuzan and E. Bent, APS Press, St. Paul, Minnesota, 2000, pp. 167 - 180.

[24] R. F. Taylor and J. S. Schultz, "Introduction to Chemical and Biological Sensors" in *Handbook of Chemical and Biological Sensors*, Institute of Physics Publishing, R. F. Taylor and J. S. Schultz, (Eds.). Philadelphia, pp. 1-10, 1996.

[25] T. N. Ananthakrishnan, "Insects and Plant Defense Dynamics", Science Publishers inc. , Enfield, USA, 2001.

[26] A. A. Agrawal, S. Tuzun, and E. Bent, "Induced Plant Defenses against Pathogens and Herbivores", APS Press, St. Paul, Minnesota, 2000.

[27] N. K. Zidak, "Implications of Induced Resistance to Pathogens and Herbovores for Biological Weed Control" in *Induced Plant Defenses Against Pathogens and Herbivores* 1st

ed. A. A. Agrawal, S. Tuzan and E. Bent, APS Press, St. Paul, Minnesota, pp. 371 -377, 2000.

[28] http://en.wikipedia.org/wiki/Gall

[29] J. Kroymann, "Natural Diversity and Adaptation in Plant Secondary metobolism", *Current Opinion in Plant Biology*, vol. 14, pp. 246-251, 2011.

[30] J. W. Gardner and P. N. Bartlett, "Electronic Noses: Principles and Applications", Oxford University Press, New york, 1999.

[31] B. R. Eggins, "Chemical Sensors and Biosensors", John Wiley and Sons, Nothern Ireland, UK, 2002.

[32] J. Janata, "Principles of Chemical Sensors", Plenum Press, New York, 1989.

[33] H. Bai and G. Shi, "Gas Sensors Based on Conducting Polymers". *Sensors*, vol. 7, pp. 267-307, 2007.

[34] J. W. Grate and M. H. Abraham, "Solubility Interactions and the Design of Chemically Selective Sorbent Coatings for Chemical Sensors and Arrays", *Sensors and Actuators B.* , vol. 3, pp. 85-111, 1991.

[35] B. C. Sisk and N. S. Lewis, "Vapor Sensing Using Polymer/Carbon Black Composites in the Percolative Conduction Regime", *Langimuir*, vol 22 (18), pp. 7928-7935, 2006

[36] N. Tsubokawa, Y. Shirai, M. Okazaki, K. Maruyama, "A Novel Gas Sensor From Crystalline Polymer-Grafted Carbon Black: Responsibility of Electric Resistance of Composite from Crystalline Polymer-Grafted Carbon Black Against Solvent Vapor",*Polymer Bulletin*, vol. 42, pp. 425-431, 1999.

[37] J. Chen, and N. Tsubokawa, "A Novel Gas Sensor from Polymer-Grafted Carbon Black: Responsiveness of Electric Resistance of Conducting Composite from LDPE and PE-b-PEO Grafted Carbon Black in Various Vapors", *Polymers for Advanced Technologies*, vol. 11, pp. 101-107, 2000.

[38] M. C. Lonergan, E. J. Severin, B. J. Doleman, S. A. Beaber, R. H. Grubbs and N. S. Lewis, "Array- Based Vapor Sensing Using Chemically Sensitive, Carbon Black-Polymer Sensitive, Carbon Black-Polymer Resistors", *Chem. Mater.* , vol. 8, pp. 2298, 1996.

[39] E. J. Severin, B. J. , Doleman, N. S. Lewis, "An Investigation of Concentration Dependance and Response to Analyte Mixtures of Carbon Black/Insulating Organic Polymer Composite Vapor Detectors", *Anal. Chem.*, vol. 72, pp. 658, 2000.

[40] X. M. Dong, R. W. Fu, M. Q. Zhang, and Z. Rhong, "Electrical Resistance Response of Carbon Black Filled Amorphous Polymer Composite Sensors to Organic Vapors at Low Vapor Concentrations", *Carbon*, vol. 42, pp. 2551, 2004.

Chapter 2

Sensor Design and Gas Exposure Test Setup

The sensors consisted of a silicon substrate platform with interdigitated electrodes. The active polymer layers were deposited onto these silicon wafer platforms. Details about the polymer active layer will be discussed in later chapters. This chapter presents the detailed fabrication procedure of the sensor platform.

2.1. Sensor Substrate

Four inch p-type silicon wafers that were 4 inches in diameter and 500 microns in thickness were purchased commercially from Silicon, Inc.. The silicon wafers were used as the substrate for several reasons. First, silicon is an insulator. The resistance of the silicon substrate is much higher than that of the polymer active layer. Silicon also has good adhesion compatibility with the selected electrode structure. The thermal expansion coefficient of silicon is low, and remains stable at various environmental temperatures. The properties of the wafers are summarized in table 2.1.

2.2. Electrode Pattern

The electrode pattern of the sensor was designed so that it would have a larger surface area for better sensitivity. Therefore in this case an interdigitated finger geometry was used. The interdigitated finger geometry also allows the active layer to experience the largest conductivity change in that specific electrode area, which allows the active layer to control the output signal.

Since the resistivity of the active polymer layers are relatively high, it was desirable to use a small spacing between the electrodes. This will limit the driving voltages from becoming too high and hence avoid overheating of the active polymer sensing layer, which may change the electrical properties of the thin polymer films. In this research an electrode pattern with a 15 micron spacing was used.

2.3. Microfabrication Procedure

Common microfabrication procedures such as wafer cleaning, oxidation, photolithography and metal deposition were used in the construction of the sensors. All microfabrication steps were performed at the Alabama Microelectronics Science and Technology Center (AMSTC) at Auburn University. The main microfabrication procedures are explained in the following subsections and are summarized in figure 2.1.

2.3.1. Wafer Cleaning Procedure

A RCA (Radio Corporation of America) cleaning procedure which used a solution of five parts deionized water, one part ammonium hydroxide (NH_4OH), and one part hydrogen peroxide (H_2O_2) was heated in a large beaker on a boiler plate for 55-60 seconds. The wafers were dipped in this solution for 10 minutes, followed by dipping in a deionized bath for 10 more minutes. Finally the wafers were rinsed in a washer system in deionized water, until the resistance of the wash water was greater than a threshold value, and dried with nitrogen in the dryer system. A picture of the washer dryer system is shown in figure 2.2.

Table 2.1. The properties of the wafers used for sensor fabrication procedure.

Property	**Value**
Diameter	100 mm (4 inches)
Dopant	Boron
Orientation	100 ($\pm 0.9^{o}$)
Quality	Virgin Prime
Thickness	475 $\pm$ 50μm
Polish	Single side
Resistivity	0.03-0.05 Ω-cm
SiO_2 Thickness	1000 $\pm$ 50 nm

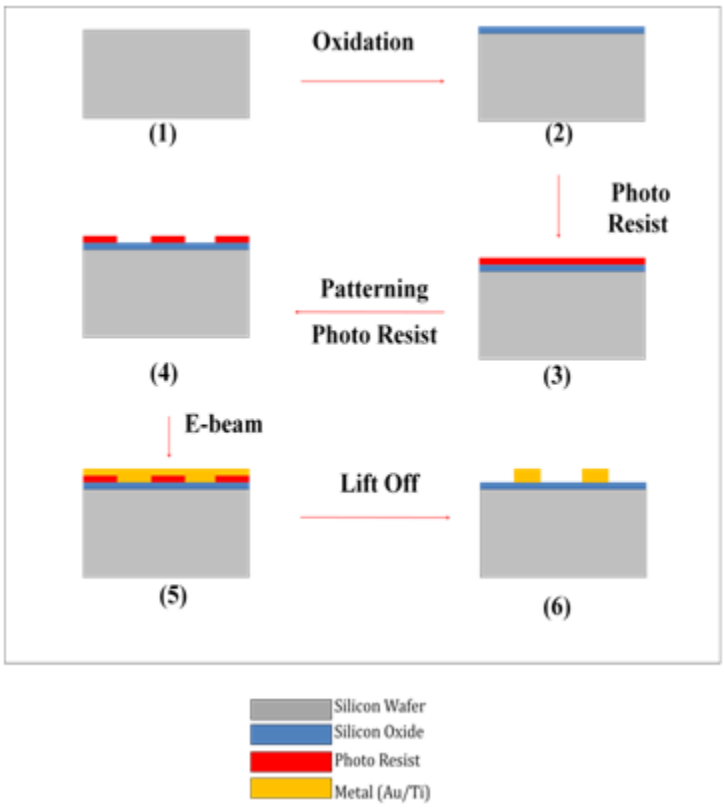

Figure 2.1. A flow chart describing the microfabrication procedures used to produce sensor platforms of the sensor array for detecting insect infestation: (1) 4 inch diameter, single crystal silicon wafer (one side polished). The silicon wafer was initially cleaned using a RCA procedure, prior to oxidation; (2) SiO_2 formed after 1-2 hours of oxidation. Thermal oxidation was performed in a furnace using a wet process, to produce a smooth electrically insulating and chemically inert substrate; (3) photoresist application. Photoresist was spin coated onto the susbstrate at a spin speed of 3000 rpm for 30 seconds; (4) The photoresist film was exposed to UV radiation through a patterned mask, and unwanted areas were dissolved away using solvent to leave the pattern of the electrode on the surface of the oxidized wafer; (5) Metal film deposited on the patterned photoresist layer using Ebeam. Ebeam deposition was performed under a vacuum, with titanium acting as an adhesion layer between silicon dioxide and gold; (6)

The pattern was lifted off with remaining photoresist removed during a cleaning process and the patterned metal film was left on the wafer, completing the sensor fabrication procedure.

Figure 2.2. Washer-Dryer system for wafer cleaning and drying: The washer-dryer system at the AMSTC rinses wafers with deionized water. Then the nitrogen gas is automatically purged through the wash chamber and the wafers were spun until they were dry.

2.3.2. Thermal Oxidation

When exposed to oxygen, silicon forms silicon dioxide which is a high quality electrical insulator. Thermal oxidation is typically done by heating the wafer at a high temperature between 900-1200 °C. Either a dry oxidation procedure which uses pure oxygen or a wet oxidation procedure using water vapor can be used. In this case a wet oxidation procedure was used. The chemical reaction occurring on the surface when using the wet oxidation procedure is as follows:

$$Si+2H_2O = SiO_2 + H_2$$

Using a wet oxidation procedure at 1000 °C, an amorphous layer of silicon oxide that was one micron thick was produced. The oxide thickness was verified with a laser interferometer located at the AMSTC as shown in figure 2.3. The laser interferometer was used to measure the thickness of the wafer at 64 different points, and a mean and standard deviation was computed. Using the interferometer an actual silicon dioxide thickness of 1009.4 was measured with a standard deviation of 0.392%.

2.3.3 Photoresist Deposition

After the silicon dioxide layer was formed, a light sensitive material called the photoresist was deposited onto the silicon dioxide surface. The surface was cleaned and dried to ensure good photoresist adhesion. The wafers were also baked in a furnace in an air atmosphere at 120

°C for 20 minutes to kill any organic residue that may contaminate the wafers. Then the wafers were exposed to hexamethyldisilazane (HDMS) which is a photoresist adhesion promoter, at room temperature for 20 minutes. After the HDMS treatment, AZ5214-EIR photoresist was spin coated onto the wafers. A spin speed of 3000 rpm and spin time of 30 minutes was used to form a thin uniform layer of photoresist. Upon UV exposure the negative AZ5214-EIR photoresist undergoes a photochemical reaction where the exposed regions are dissolved during development. After the photoresist application, a procedure called soft baking or prebaking was used to improve adhesion of photoresist by hardening it and removing residual. The soft baking was done at 110 °C for one minute.

Figure 2.3. Laser interferometer at the AMSTC: The Tencor profilometer runs a sensitive probe across the surface of the wafer and plots the height as a function of position. This generates a surface profile plot. It was calculated that the average electrode height was roughly 230 nm in thickness with a deviation of $\pm$ 20 nm. A total of 33 wafers were measured.

2.3.4. Photoresist Exposure and Pattern Development

The mask used for photoresist exposure was a square glass plate with a patterned metal film which had 360 sensors arranged in a circular 100 mm diameter area. This mask had been produced by a commercial custom shop to our specifications. The mask was designed using CAD software. There were cross hairs marked for dicing the wafers that were later removed after the fabrication procedure.

A Karl Suss BA6/MA6 mask aligner and exposure system which is shown in figure 2.4 was used to expose the pattern into the clean oxidized wafer treated with HDMS. The mask was installed into the mask aligner, and the wafer was exposed for 12 seconds at a distance of 30 microns. The power of the UV light source was 300 W. After pattern exposure, the wafers were developed in a AZ400K developer solution consisting of 1:4 developer to water. The wafers were dipped in the developer solution for about one minute. While developing, the process was closely watched to prevent over development. The exact development time was dependant on how fresh the developer solution was. After pattern development was complete, wafers were immediately immersed and rinsed in deionized water to prevent further development. The wafers were then blow dried with nitrogen and inspected under an optical microscope for any defects.

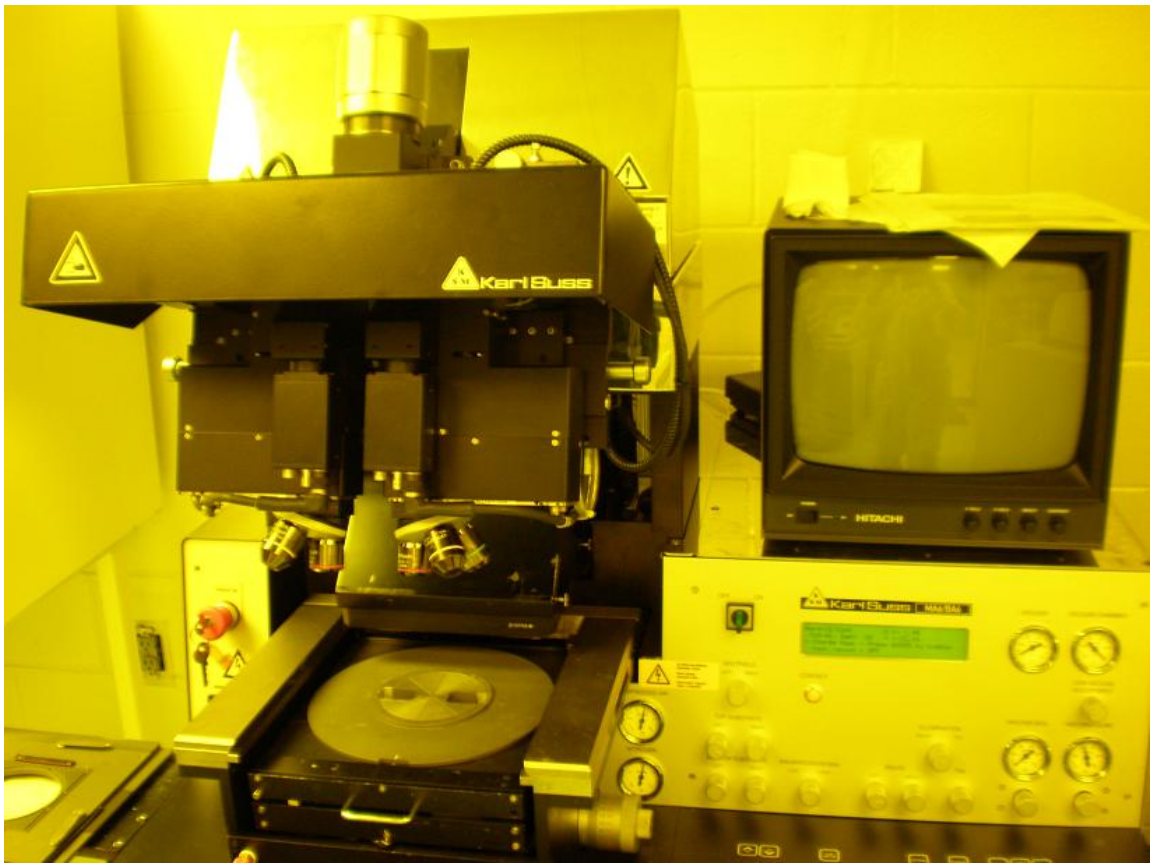

Figure 2.4. Karl Suss BA6/MA6 mask aligner and exposure system: The Karl Suss BA6/MA6 aligner at AMSTC exposed UV radiation onto the wafers coated with photoresist through an electrode mask that was installed in the aligner system.

2.3.5. Electrode Deposition

Before electrode deposition, a dry etch was performed using a matrix plasma etcher, followed by ion cleaning where the plasma etch removed the thin layer of oxide that might have formed during storage and handling. The electrode deposition was done using a Mark 50 E-beam deposition system (figure 2.5) purchased from CHA industries. The deposition unit was able to process 33 wafers per batch. Fifty (50) nm of titanium was deposited followed by a 200 nm gold layer deposition, which resulted in a well adhered electrode pattern, with a height of 250 nm.

2.3.6. Lift off Procedure

After electrode deposition, the wafers were dipped in an acetone bath in an ultra sonicator for 10 minutes. Acetone was then used to wash off the photoresist layer under the electrode pattern leaving the desired electrode pattern only. Wafers were then washed in methanol using a foam brush for 30 seconds, followed by a rinse in deionized water and finally washed and dried in the spin dryer system. The thickness of the deposited electrodes was measured using the profilometer. The average height of the electrodes was 230 nm. To inspect for proper adhesion, kapton tape was placed over the electrodes, and then peeled off. No peeling of the electrode was observed. This ensured that proper adhesion of the electrode to the silicon wafer was obtained.

Figure 2.5. CHA Mark-50 deposition system: The CHA industries Mark 50 E-beam deposition system allows electrode deposition of 33 wafers measuring 100 mm (4") diameter in one run. Fifty nm of titanium was first deposited, followed by 200 nm of gold to form the electrodes.

2.3.7. Wafer Dicing Process

Wafers were diced using a micro automation 1100 dicing machine with a Kulicke and Sofa dicing blade. Each wafer was diced into 360 individual sensors. Manual cutting was preferred over automatic cutting to ensure proper alignment of the blade to the wafers. Table 2.2 illustrates the dicing parameters used. Thirty three silicon wafers were fabricated at a time, where each wafer contains 360 sensors. On average, 8 out of 10 sensors were functional, resulting in an 80% yield. The cost per each sensor is about 2 cents.

2.4. Polymer Film Deposition

To deposit the polymer active films to the sensor platforms, first the polymer solutions were prepared and then the sensor films were either drop casted or spin coated depending on the kind of polymer. In the following subsections, the methods used for solution preparation and how they were applied to the polymer platforms is detailed.

Table 2.2. Dicing parameters used in the wafer dicing procedure.

Parameter	Value
Mode	10 –circular wafer
Dim 1	4000 mils (101.6 mm)
Dim 2	4000 mils (101.6 mm)
Height	5 mils (0.127 mm)
Thickness	40 mils (1.016 mm)
Angle	90 degrees
FWD Cut speed	75
Spindle speed	25000 rpm

2.4.1. Polymer/Carbon Composite Film Sensors

To make the polymer solution, 40 mg of polymer was dissolved in 20 mL of tetrahydrofuran and stirred at 40 °C for 24 hours. After that 1 mg of carbon nano-powder (<50 nm) purchased from Sigma-Aldrich was ultra-sonicated in 20 mL of tetrahydrofuran for 20 minutes. The well dispersed carbon solution was then mixed with appropriate volumes of the polymer solution to obtain a total volume of 5 mL. The carbon to polymer ratio was maintained near the percolation point of each composite. The micro-fabricated sensor platforms were then drop casted with the polymer/carbon solutions. Polymer/carbon composites deposited using this procedure include: polystyrene (PS), polyethylenecovinylacetate (PEVA) 12% vinyl acetate (VA), PEVA 18% VA, PEVA 25% VA, PEVA 40% VA , PEVA 0% VA (Polyethylene), polyethyleneoxide (PEO) and polyisoprene (PISO).

2.4.2. Polythiophene Sensors

Poly3-hexylthiophene/chloroform and poly3-dodecylthiophene solutions were prepared by dissolving 1 mg of polymer in 10 mL of chloroform. The solutions were then stirred overnight, at 45 °C. A KW-4A spin coater from Chemat technology was used to fabricate the P3HT and P3DT spin coated sensors. To fabricate the P3HT drop casted sensors, the P3HT solution was dropped onto the platform, and the solution was allowed to evaporate slowly.

2.4.3. Polyaniline Sensors

To fabricate polyaniline films, 1mg of polymer was dissolved in 10 mL of benzene and was stirred at 40 °C for 24 hours. The micro-fabricated sensor platforms were then drop casted with the polyaniline solution.

2.5. Sensor Fabrication Results

The resulting sensor platform is displayed in figure 3.6 below. An interdigitated fingerprint geometry was used in this case for increased sensitivity. The sensor platform had 25 pairs of electrodes, where each electrode finger was 22 microns wide and 2985 microns long. The spacing between fingers was 15 microns. Thirty three silicon wafers were fabricated at a time, and each wafer had 360 sensors. On average, eight out of the 10 sensors were functional, resulting in a yield of 80%. Since 33 wafers were produced in a batch, the production cost per sensor (including the cost of polymer) was approximately 2 cents. A finished sensor with active layer is shown in figure 2.7 below.

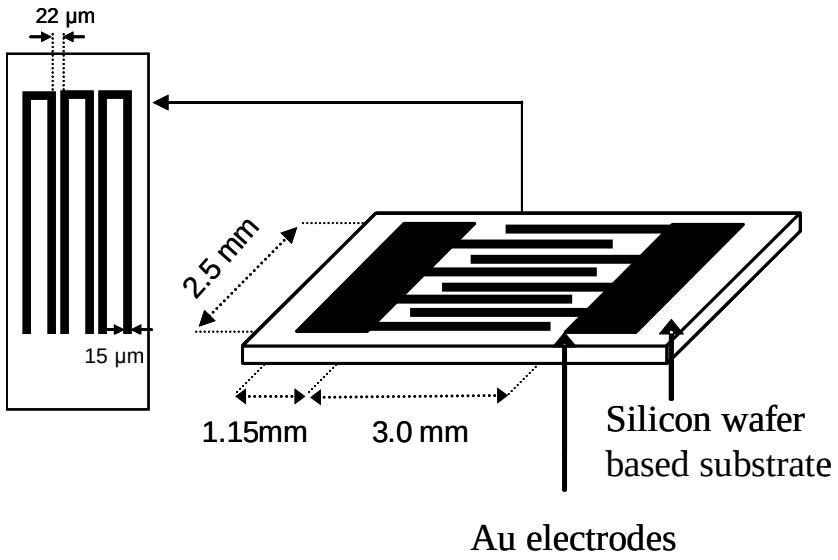

Figure 2.6. Microfabricated silicon wafer platform before active layer deposition: The sensor interdigitated electrode pattern had two main contacts and branched into 25 pairs of parallel electrode fingers. The polymer thin films were deposited above and between the electrodes. The spacing between the electrodes was 15 microns.

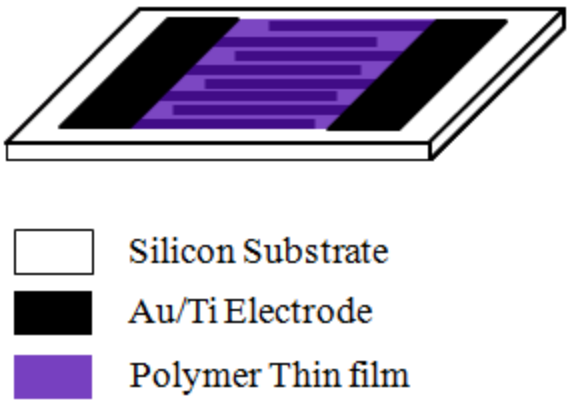

Figure 2.7. Final sensor: The resulting sensor had a silicon substrate sensor platform with Au/Ti Electrodes with a thin polymer film active layer.

2.6. Gas Exposure and Sensor Array Response Measurement

The testing of the sensor was done in a specially fabricated vapor exposure and measurement system shown in figure 2.8. Pure dry nitrogen was used as the carrier gas. The setup consists of a flask that contains the analyte in liquid form, and a chamber that contains the sensor array. Before each test the sensor was exposed to pure nitrogen for 30 minutes to obtain a baseline, by letting the gas flow through regulator "A" only (regulators "B" and "C" were closed at this point). To test the sensor's response to the analyte, nitrogen was allowed to pass through regulators "B" and "C" where the analyte gas was picked up and delivered to the Flask "B" where the sensors were located. In order to adjust the concentration, the flow rate through regulators "B" and "C" was kept constant at 0.2 L/min, while the flow rate through regulator "A" was varied as needed to obtain the desired analyte concentration. The resistance changes of the sensor were measured by an Agilent 34970A data acquisition/switch unit. The gas chamber and the sensor array holder are shown in figure 2.8 below.

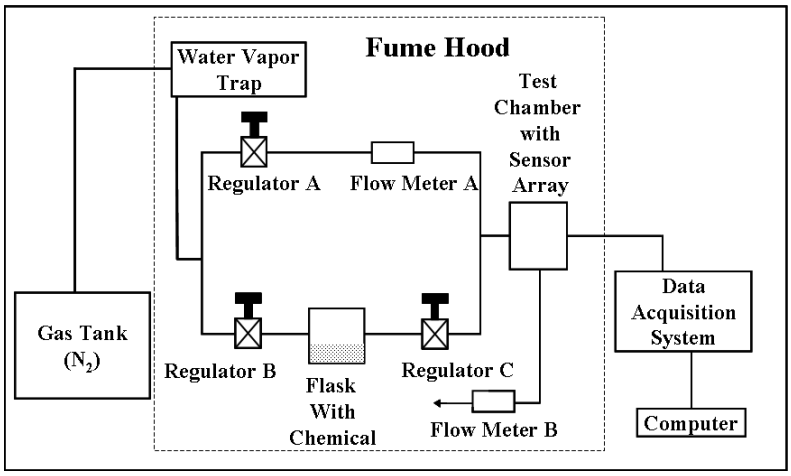

Figure 2.8. Experimental setup to test response of sensor array: The sensor setup consists of a flask filled with the analyte in liquid form and test chamber with sensor array.

2.6.1. Test Cell

A test cell was designed and constructed to hold the sensor array system with multiple sensors. The test cell was made of Teflon PFA (perfluoroalkoxy copolymer resin) or PTFE (polytetrafluoroethylene). Here the tubings, wire coatings and the inside of the sensor were made of PFA or PTFE while the main body of the test cell was made of PFA. The main reason behind choosing this material was because of its inert chemical properties and excellent thermal properties. The sensor array system and the PFA cell is shown in figure 2.9 below.

2.6.2. Carrier and Analyte Gases

High purity nitrogen gas was used as the carrier gas which was commercially purchased from Airgas. All other analytes including γ-terpinene, α-pinene, p-cymene, farnasene, cis-hexyl acetate were acquired from Sigma Aldrich. Some of the gases used to evaluate sensor stability and environmental effects were also purchased from Airgas.

2.6.3. Data Acquisition System

The resistance of the electrodes on each of the sensors was measured by a data acquisition system. The system consisted of a 34970 data acquisition switch connected to a windows PC which runs the Agilent benchlink software. A 20 channel multiplexer module was installed in the data acquisition switch, where 12 of the 20 channels were set to measure two wire resistance, and one switch was set to record temperatures measured from a thermocouple. The rest of the channels were left blank and were not used. Due to the high initial resistance values of polythiophene sensors and the end values of all the sensors in array, 10 MΩ resistors were placed

parallel to each of the sensors. The true resistance of the sensors was determined using equivalent resistance calculations.

Figure 2.9. Gas exposure cell and sensor holder: The sensor exposure cell and sensor holder allows measurement of 12 sensors at a time.

2.6.4. Concentration Calibration and Gas Chromatography Analysis

In order to expose the sensor array system to different concentrations of phytochemicals, the flow rate through Flask A in figure 2.8 was varied so that the chemical vapor entering the gas exposure cell had different concentrations. Here the flowrate through regulators "B" and "C" was kept constant at 0.2 L/min, while only the flow rate through regulator "A" was varied as needed to obtain the desired analyte concentration. To confirm the concentration values for each of the flow rates, first a commercially available volatile vapor trap containing "Super Q" volatile organic absorbent was used to collect the vapor exiting through flow meter B in figure 2.8. The vapor was collected for 2 hours. The collected vapor was then extracted using dichloromethane purchased from Sigma-Aldrich. Gas chromatography was used to analyze the collected vapor. The gas chromatography data was then compared with standard spectra of known concentrations. The concentration values were calculated using flow rate and the time taken to collect the vapor. The concentration values obtained for each of the flow rates are for γ-terpinene shown in figure 2.10.

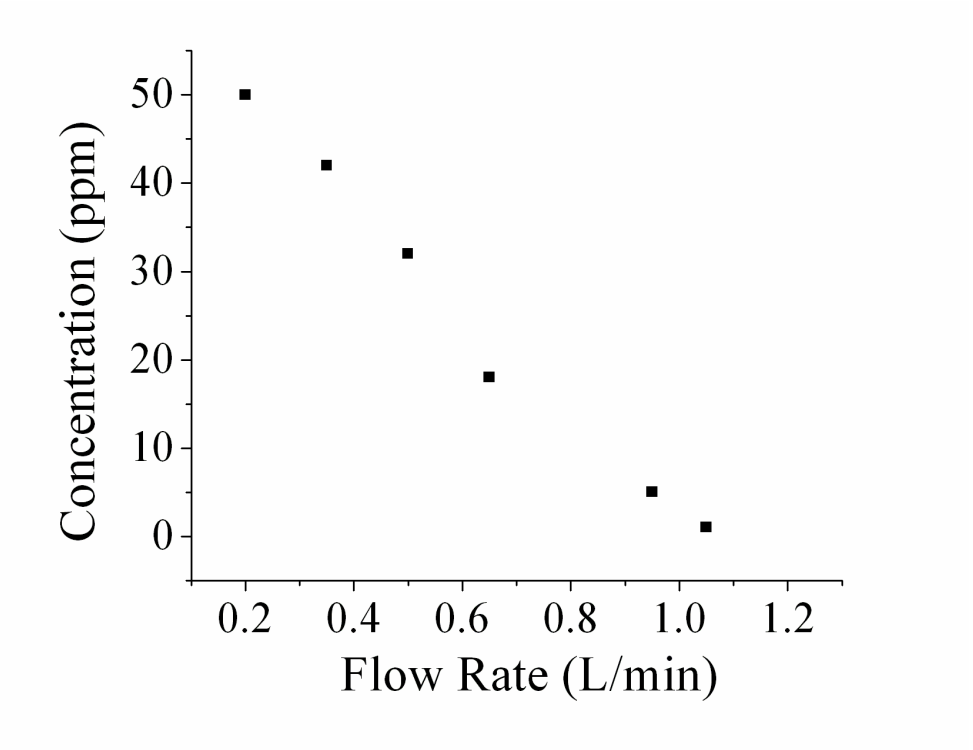

Figure 2.10. Concentration values of γ-terpinene measured for varying flow rates using gas chromatography.

2.6.5. Temperature Chamber and Control System

An Espec ECT temperature chamber was used to vary ambient temperatures to conduct experiments to investigate the effect of temperature on the sensor. The temperature range of the chamber was -70 to 200 °C. A feed through on the left on the side of the chamber was used to carry the gas through tubes to the sensor test chamber and then exit the temperature chamber through a feed through on the right side of the chamber. The analyte gas traveled through coils of the tubing to insure the gas reached equilibrium with the temperature chamber prior to exposure of the sensor. Electrical and thermocouple wires were also routed through the feed throughs.

2.6.6. Humidity Control

In order to measure the effect of humidity on the sensors, the sensors were exposed to nitrogen and the phytochemical γ-terpinene at different humidity conditions. In order to create different humidity conditions, nitrogen or phytochemicals entering the exposure cell was first sent through a flask containing saturated solutions of various salts. The flow rate of the gas was always maintained at 0.2 L/min. Different humidities were created by using alternating kinds of salts. In each experiment, the sensor was first exposed to nitrogen at room condition humidity level, and then exposed to nitrogen at different specific humidities. Then the sensor was exposed to the phytochemical at this desired humidity level. In order to investigate the effect of humidity on the reversibility of the sensor, the sensor array was exposed to nitrogen at the desired humidity conditions.

Chapter 3

Polythiophene Sensor Optimization and Investigation Of Sensor Mechanism

3.1. Polythiophene Thin Films for Volatile Vapor Detection

Thin films made of polythiophene and its derivatives are used as the active material in many organic semiconductor devices. This polymer, because of its high environmental stability, is an excellent choice for detecting volatile organic compounds. Regioregular polythiophene film because of its high ordering exhibits excellent electrical properties, good stability as well as better electro conductivity [1-3]. In this research, two derivatives of polythiophene was used: 1) poly3-hexylthiophene-2,5-diyl; and 2) poly3-dodecylthiophene-2,5-diyl. The structures are shown in figure 3.1. below.

The exact mechanism behind how these conducting polymers detect volatile organic vapors remains unclear. In 1992, Bartlett and Garner proposed five different mechanisms that could be responsible for the changes in the electrical properties of conducting polymer sensors. These five mechanisms happen at five different sites in the material and are demonstrated in figure 3.2 below. In the first mechanism, the organic vapor molecules hinder the charge transfer between the polymer and the gold electrode contact. In the second mechanism, the organic vapor oxidizes or reduces the polymer chain. This mechanism happens mostly when detecting polar, or inorganic analytes. In the third mechanism, the organic vapors interact with the charge carriers, hindering charge mobility. In the fourth mechanism, the analyte vapor interacts with the counter charge carriers along the polymer chain. In the fifth and final mechanism, the organic vapor

physically interferes with the inter-chain charge hopping, changing the conductivity of the polymer film [4].

In a more recent study by Zhang et. al., it was demonstrated that 3-hexythiophene films have nanofibril morphology[5]. The nanofibrils are semicrystalline, with amorphous grain boundaries. In a follow up study by Bo Li and David Lambeth, the microstructure of drop casted films was determined. In this study it was determined that the nanofibrils were arranged in many lamellar sheets. Li and Lambeth were able to determine the exact distance between each lamellar sheet and sheet stacks using x-ray diffraction measurements and atomic force microscopy. The model calculated by Li and Lambeth are shown in figure 3.3 below [6].

Li et al. also described the mechanism of resistance change in P3HT sensors detecting volatile organic compounds. According to this model, the analyte vapor is absorbed between the grain boundaries resulting in a resistance increase. The absorbance of the analyte hinders the charge conduction. This was similar to Bartletts and Gardner's fifth mechanism. Increasing the crystallinity will make it harder for the analyte to increase the resistance of the film. On the other hand, a film with less crystallinity will have a higher resistance to begin with, and analyte absorbance will cause a larger resistance change. This is displayed in figure 3.4 below.

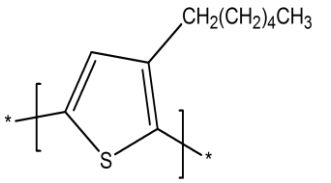

(a)

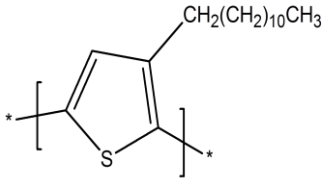

(b)

Figure 3.1. Structures of poly3-hexylthiophene-2,5-diyl and dodecylthiophene-2,5-diyl.

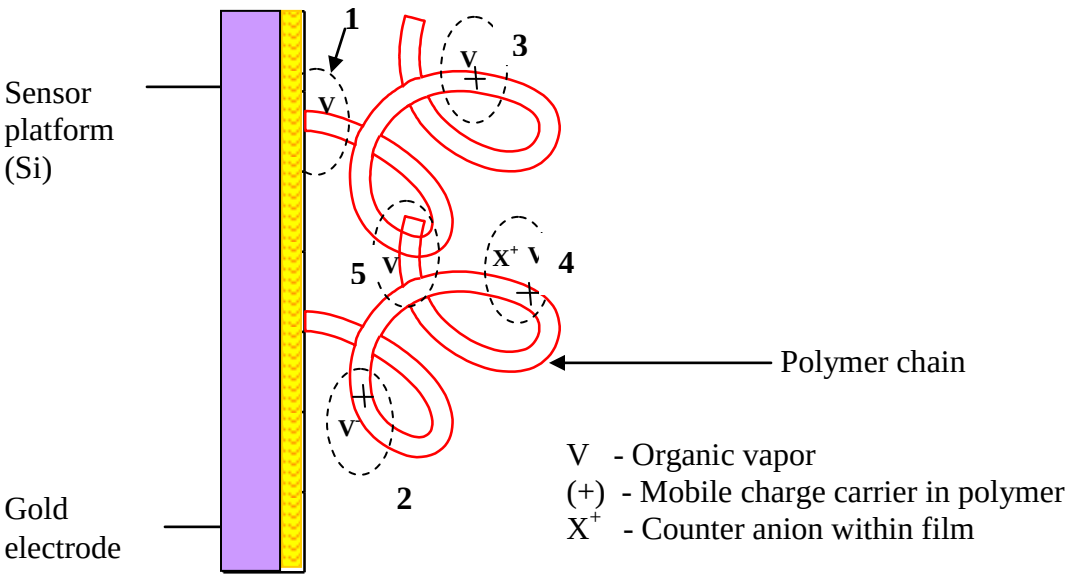

Figure 3.2. Possible interactions of organic vapor molecule in five different sites: These interactions are (1) volatile vapor effecting the charge transfer between electrode and polymer chain (2) the reduction or oxidation of polymer molecule by volatile vapor (3) volatile vapor altering the charge conduction along the polymer chain (4) organic vapor could interacting with counterions (5) organic vapor altering rate of interchain hopping in the material.

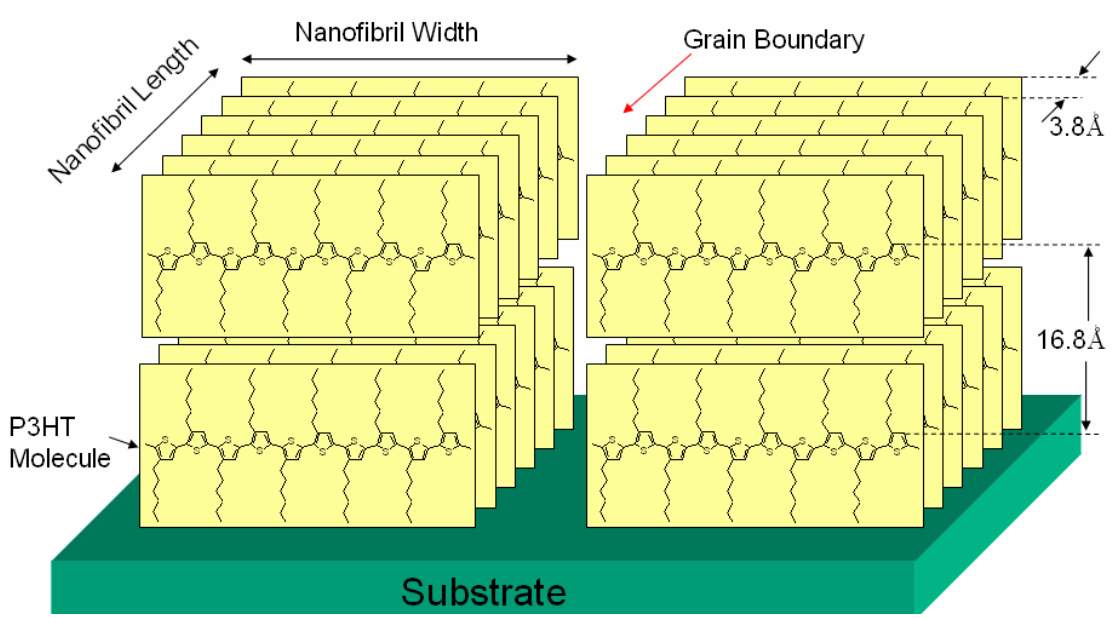

Figure 3.3. Microstructure of drop casted polythiophene films as determined by Li and Lambeth [6].

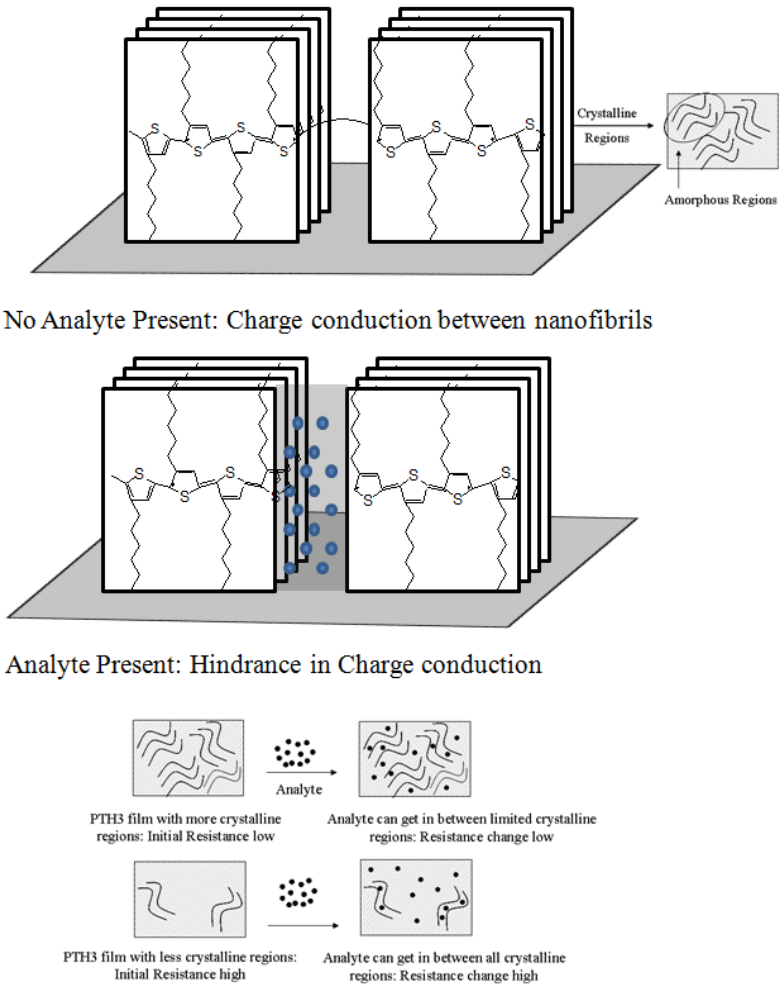

Figure 3.4. The effect of crystallinity on relative resistance change after analyte absorbance: A film with low crystallinity will have a higher relative resistance change.

The crystallinity of a thin film P3HT film can be controlled by molecular weight, regioregularity, deposition methods, solvents and annealing of the polymer film. There are many reports that describe the effect of the P3HT molecular weight [5, 7, 8]. In these studies, it was observed that as the molecular weight increased, connections between the nanorods increased, forming nanofibrils. As the connections between nanorods increased, a highly ordered nanofibril structure was formed. This nanofibril structure consists of lamellar layers of polythiophene chains. The width of the nanofibrils increased with increasing molecular weight. As the molecular weight further increased, the nanofibrils became nodule like structures [5]. Figure 3.5 shows atomic microscope images of thin films of regioregular P3HT of various molecular weights (ranging from 2.4-18.4 kDa) in FET devices prepared by drop casting from toluene.

Studies on regioregularity of P3HT show that regioregular polymers form more crystalline polymers than regiorandom polymers because of their molecular weight. Regioregular polymers consist of only one kind of regioregularity; head to head (HH) or head to tail (HT). Regiorandom polymers have both HH and HT configurations arranged in a random pattern. Generally, regioregular polymers show a preferred orientation where the side chains are perpendicular to the backbone of the polymers. This configuration allows stronger π-π interactions and better stacking of thiophene rings [3-5].

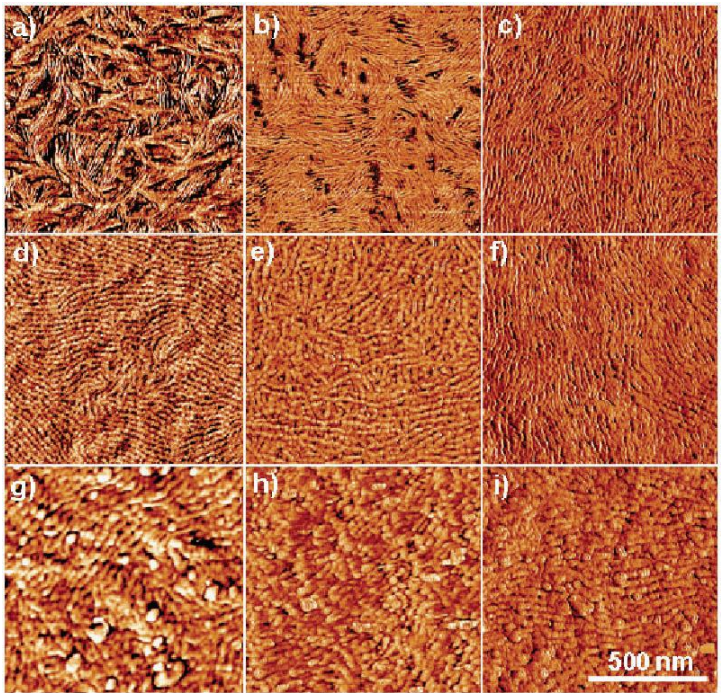

Figure 3.5. Tapping mode AFM images (phase contrast, 1μm x 1μm) of thin films of RR-P3HTs of various molecular weight films: (a-i): 2.4, 4.8, 5.1, 7.0, 7.5, 11.8, 15.7, 17.3 and 18.4 kDa [5].

Studies on P3HT morphology also show that drop casting films have higher crystallinity than spin coated samples [5, 9]. Spin coated samples evaporate faster than drop casted samples, allowing little time to form crystalline regions. On the other hand, with slow evaporation rate, the drop casted samples form films with higher degrees of crystallinity. The choice of solvent is another factor that decides the degree of crystallinity. It is reported in literature that high crystallinity was obtained by solvents like toluene and xylene when compared to solvents such as chloroform. A solvent with higher boiling temperature results in high crystallinity which results in a slower evaporation rate, thus a higher degree of crystallinity. To obtain a higher degree of crystallinity, sensor films should be prepared using a solvent that dissolves the polymer at room temperature and stabilizes in the solid state. Toluene and xylene are examples of such solvents.

The morphology of annealed films when compared to unannealed films has a higher crystallinity [10]. The annealing procedure causes the polymer chains to rearrange so that they have higher crystallinity. As the crystallinity increases, the resistance of the film decreases.

3.2. Optimizing Sensing Properties

In order to acquire maximum sensor performance it is required to optimize the quality of the sensor active layer. In this study, the quality of all sensor active layers that were investigated (polymer/carbon, polythiophene, polyaniline) was optimized for maximum performance. Polythiophene sensors were optimized by investigating effects of annealing, doping and concentration. The performance of polythiophene sensors are also reported to be affected by factors that control the crystallinity of the film such as molecular weight, regioregularity, deposition methods and solvents. Limited resources were available to study the effect of regioregularity and molecular weight, since investigating these factors requires synthesizing

polymers with different molecular weights and regioregularity. Therefore films were optimized by investigating the effect of deposition methods and solvent methods.

3.2.1. Effect of Doping

Doping or oxidizing increases the conductivity of a conducting polymer such as polythiophene. According to the band theory of semiconductors and metals, conducting polymers need to have continuous atomic orbitals in order to conduct electricity. The continuous orbitals must stay close enough to build up delocalized electronic states. Therefore, polymers with a planar or near planar single or double bond chain structure along the backbone can conduct electricity. This intrinsic conductivity is low, due to the small number of charge carriers. In order to increase the conductivity dramatically, these polymers can be oxidized or reduced, by external oxidizing or reducing agents so that the number of charge carriers increases [11-12].

In order to see the effect of doping on polythiophene sensor films for detecting insect infestation, thin polymer film sensors were doped with nitrosonium hexafluorophosphate ($NOPF_6$). $NOPF_6$ was purchased from Alfa Aesar company. The oxidation process is illustrated in figure 3.6 below.

Neutral Chain

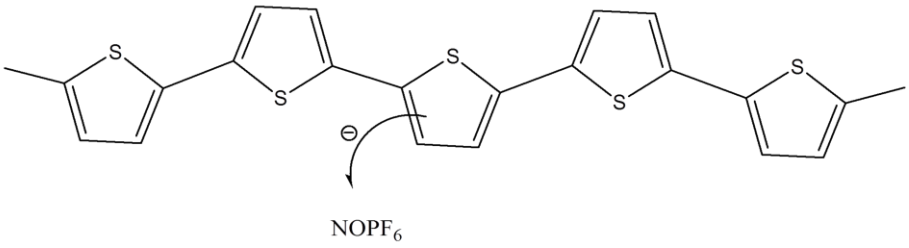

Polaron

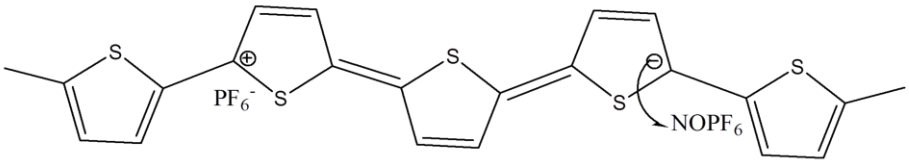

Bipolaron

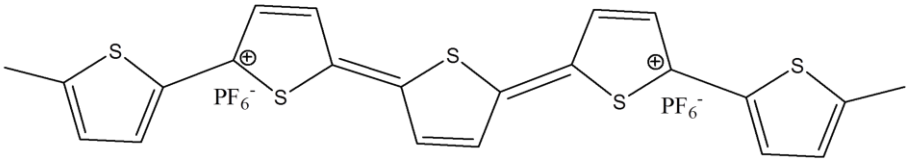

Figure 3.6. Polythiophene oxidation process: The creation of polarons and bipolarons.

During the doping process, an electron is removed from the pi electron system of the polythiophene backbone, and donated to the external acceptor ($NOPF_6$) in this case. This creates a free unpaired electron and a positive charge. To compensate, the denzoid rings in the backbone turn to quinoid like rings. A polaron is created when a free, unpaired electron couples with a positive charge. The polaron creates a new localized electronic state. This new electronic state is located symmetrically in the energy gap, where the lower energy states are occupied by free electrons. Bipolarons will result if the doping process continues. At very high doping levels, the localized bipolarons will merge together to form continuous bipolaron bands. If the lower and upper bipolaron bands overlap, this will make the polymer have metallic like conductivity [13]. The band structure is shown in figure 3.7 below. To investigate whether an increased number of charge carriers created through doping has an effect on the response of P3HT sensors, doped and undoped P3HT sensors were exposed to γ-terpinene and their responses were compared. To dope the sensors, sensors were dipped in a NOPF6/ acetonitrile for 3-5 minutes. Four sensors at a time were then exposed to plant volatiles and tested using the experimental setup described in Chapter 2. The resistance of the undoped layers, which was originally more than $1x10^6$ ohms, decreased to a resistance less than 100 ohms when doped.

Figure 3.8 demonstrates the effect of doping on the sensor response. The sensor had a higher response under undoped conditions, relative to doped conditions. The sensor response is therefore mainly based on physical interactions and not chemical reactions of the analyte gas with the film. Therefore the physical interactions will hinder charge motion, decreasing conductivity of the film. Doping increases the number of charge carriers, which will make it harder for the analyte molecules to hinder charge carrier motion. Therefore, the doped sensors show a smaller response.

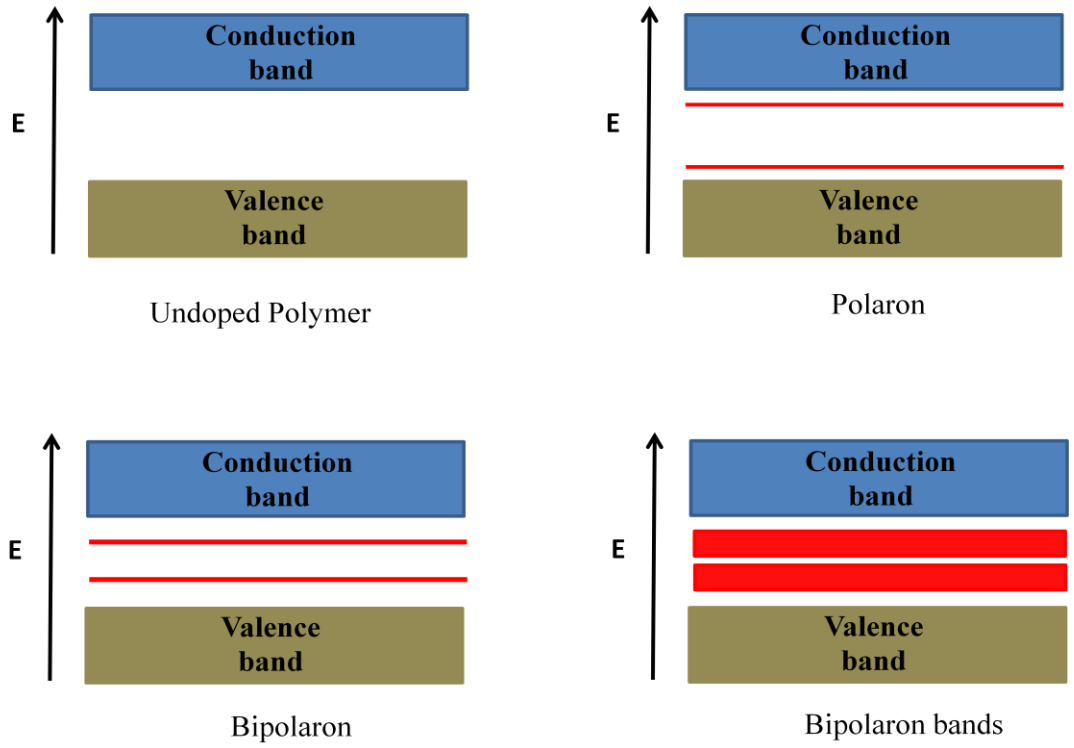

Figure 3.7. Energy levels of undoped polymer, polaron, bipolaron and bipolaron bands: A polaron is formed when a positively charged site is bounded together with a free unpaired electron. As the doping process continues and a free unpaired electron is removed from a polaron, a bipolaron is formed, which connects two positively charged sites with a lattice distortion. At even higher doping levels, localized bipolarons can merge together to form continuous bipolaron bands. When the upper and lower bipolaron bands overlap, it will result in metallic like conductivity.

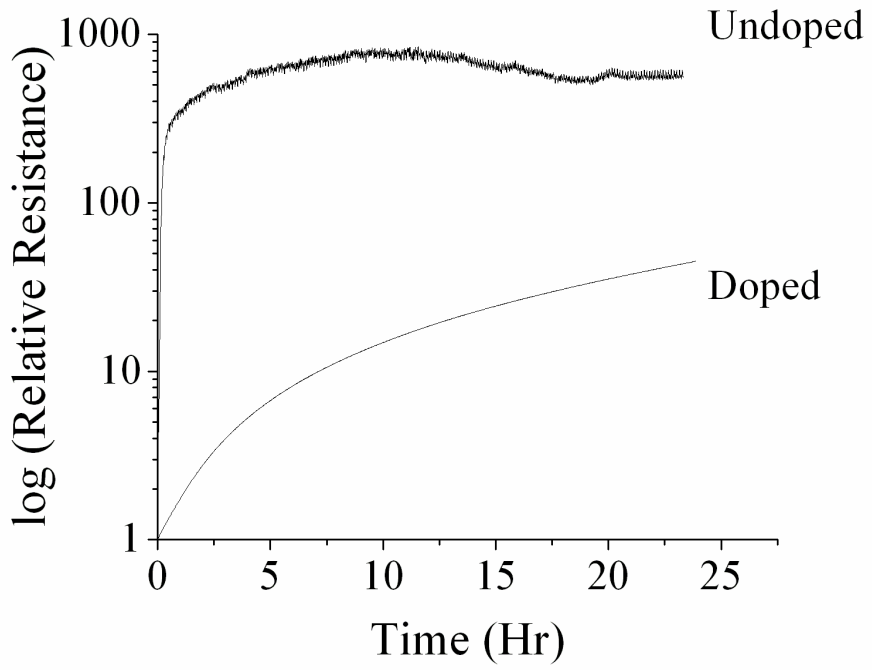

Figure 3.8. Effect of doping on polythiophene sensor performance: undoped sensors had a higher response than doped sensors.

3.2.2. Effect of Film Thickness

In order to measure the effect of film thickness on the sensor response, different concentrations of P3HT chloroform solutions and spin speeds were used to vary the polymer film thickness. Thicknesses of 110, 170, 200, 260 and 300 nm were obtained. The spin time used for all sensors was 30 seconds. The thicknesses of the sensors were measured using an alpha-step 200 profilometer from Tenco Instruments. The sensors were then exposed to γ-terpinene, a volatile organic compound emitted during pine beetle infestation.

Figure 3.9 (a) shows the response of the sensors when coated with different polymer thicknesses. The sensors were exposed to analyte, γ-terpinene, using the carrier gas nitrogen at a flow rate of 0.2 L/min, at room temperature and humidity, under undoped conditions. Figure 3.9 (b) shows the initial response of the sensors for shorter periods of time.

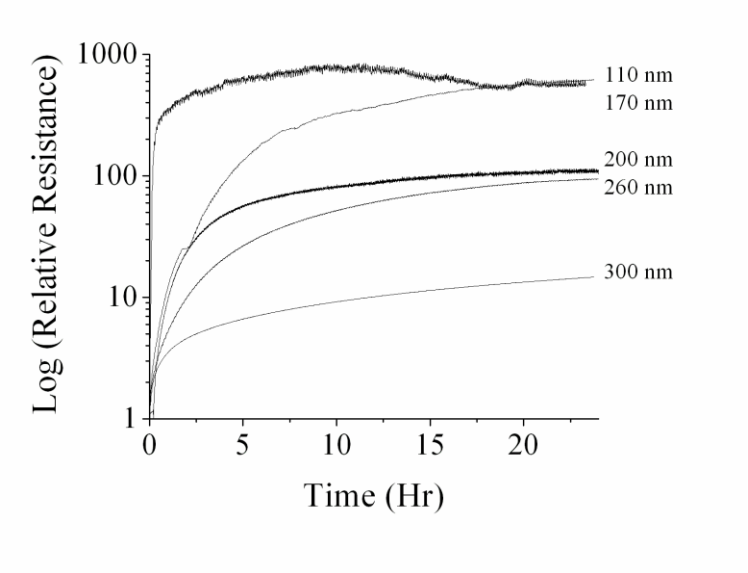

Figure 3.9 (a). Response of P3HT sensors with varying thickness: The response increased with decreasing sensor thickness. The highest response was obtained for sensors with a thickness of 100 nm.

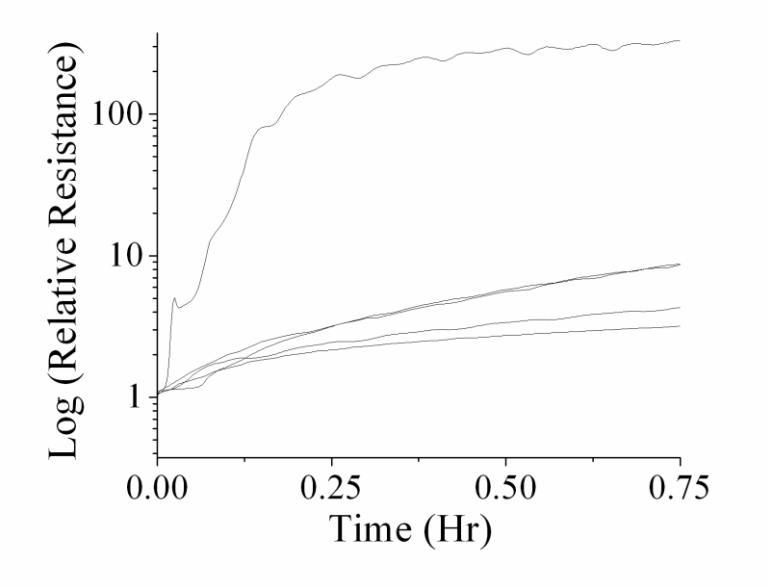

Figure 3.9 (b). Response of P3HT sensors with varying thickness showing the initial stages of response (shorter times).

After exposure for 24 hours, the relative resistance increased more than one order of magnitude for all the sensors. The relative resistance of the film R_r, as shown in equation 3.1 was the resistance of the film at a given time (R) divided by its initial resistance R_o.

$$R_r = \frac{R}{R_0} \quad \text{Equation 3.1}$$

For analysis, each of the sensor responses was divided into two sections; the initial stage and the dynamic stage. In the initial stage, the response is rapid and linear and can be described by equation 3.2.

$$\ln(\frac{R}{R_0}) = St \quad \text{Equation 3.2}$$

Where R is the instantaneous film resistance at time t, R_0 is the initial resistance and S is the sensitivity constant. S is a measurement of sensitivity of the film. The change of the sensitivity constant with thickness is shown in figure 3.10. A linear regression analysis was used to fit the initial stage of the sensor response and the sensitivity constant at each thickness was determined with a correlation co-efficient of 0.99.

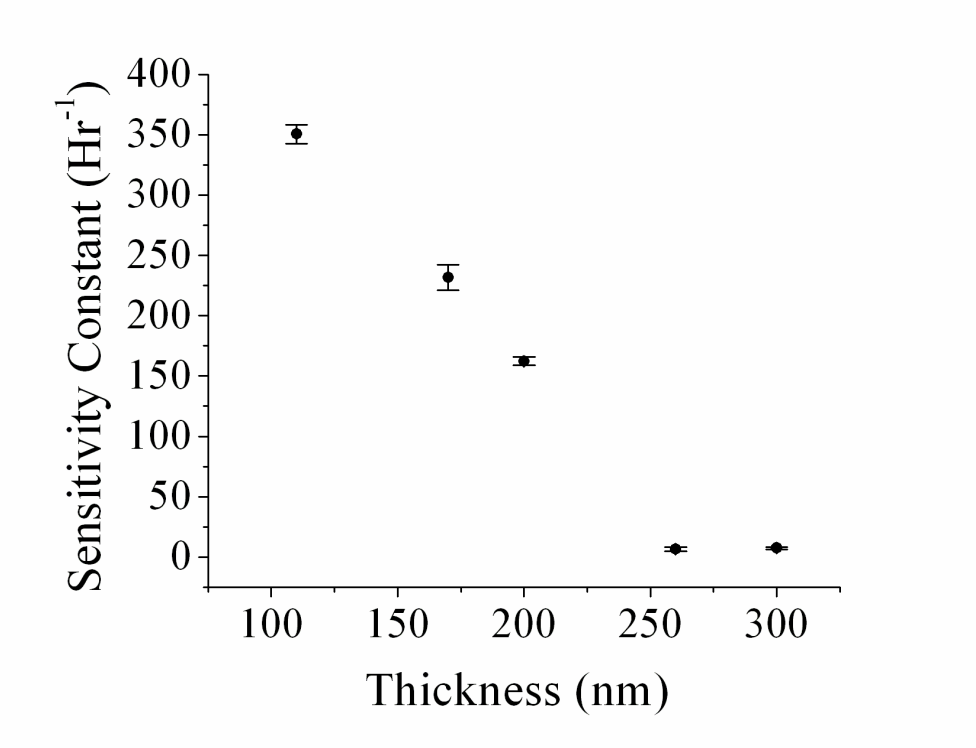

Figure 3.10. Change of sensitivity constant with thickness: The sensitivity constant decreased with increasing thickness.

According to the analysis shown in figure 3.10, the sensitivity constant decreased with increasing thickness of the polymer film. Thin films result in faster diffusion, thus they require less time to show a relative resistance change. Therefore thinner films will result in higher sensitivity constants. The thinnest possible thickness that could be obtained using spin coating techniques is 110 nm. Thinner films may be obtained using chemical vapor deposition or the Langmuir Blodgett technique. However responses of sensors fabricated from extremely thin films are often not stable or repeatable.

3.2.3. Effect of Annealing

The effect of annealing was investigated by exposing annealed and non-annealed sensors to γ-terpinene vapor. The annealing temperature which is between the phase transition and melting temperatures of the P3HT was chosen based on previous studies [15]. As shown in figure 3.11, the non-annealed sensors showed a better response than the annealed sensors. Annealing resulted in increased thermal stability of the film which resulted in a change in crystallinity. Typically the resistance of a crystalline polymer decreases with increasing crystallinity; hence an increase in crystallinity lowered the response of the film [17].

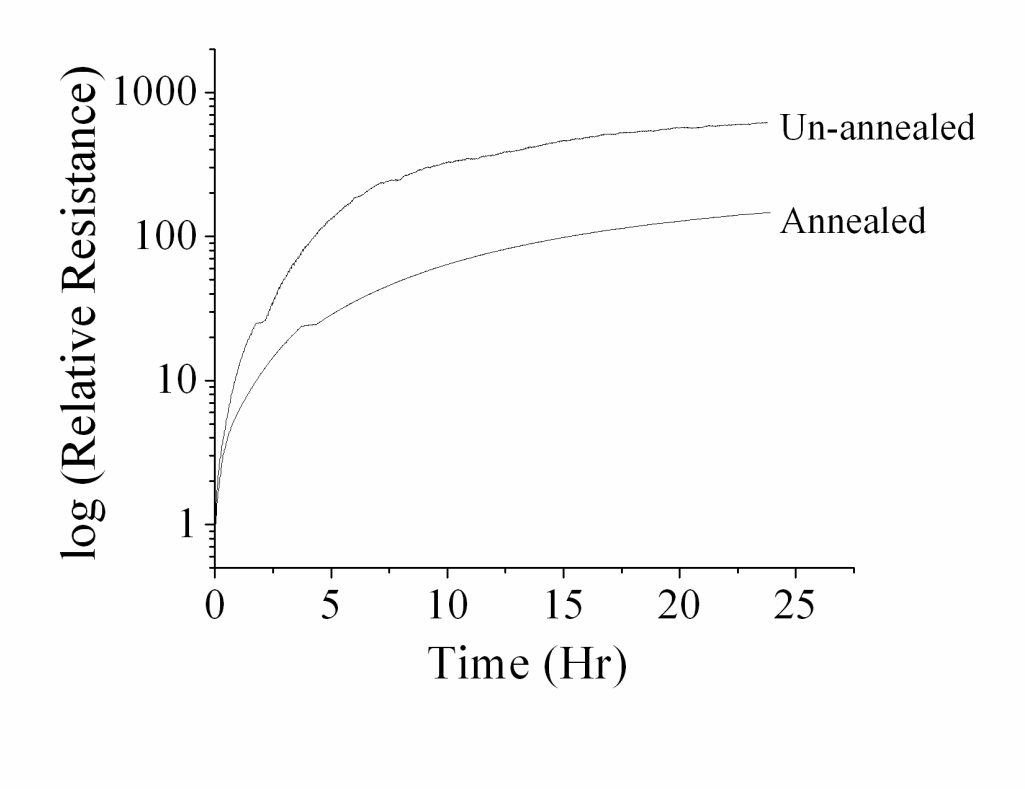

Figure 3.11. Effect of annealing on sensor performance: The un-annealed sensors had a higher response than annealed sensors.

3.2.4. Effect of Sensor Morphology (Solvent and Casting method) on Sensor Performance

The solvent and casting method affects the morphology of the sensor, which affects the conductivity of the sensor. In order to produce different morphologies of the P3HT thin film, two different solvents and two different deposition methods were used. This resulted in a total of four different morphologies of the thin films. The following methods were used: Method 1- spin coating using chloroform as the solvent; Method 2- drop casting using chloroform as the solvent; Method 3- spin coating using toluene as the solvent; and Method 4- drop casting using toluene as the solvent. In each of the methods above five (5) mg of regioregular polythiophene, purchased from Sigma Aldrich, was dissolved in 5mL of chloroform or toluene to make the P3HT solutions for deposition. All solutions were stirred for 24 hours at 40°C prior to use. The active layer poly3-hexylthiophene was then spin coated or drop cast onto the sensor platform and allowed to dry in air for 5 hours. An atomic force microscope (Veeco Instruments Inc., Dimension 3100) in the tapping mode was used to observe the structure and morphology of the films produced by the above four methods. The roughness profiles of each image were obtained using Gwyddion software. Figure 3.12 shows the results of atomic force microscopy tests conducted on samples produced using the four methods detailed in the experimental section above.

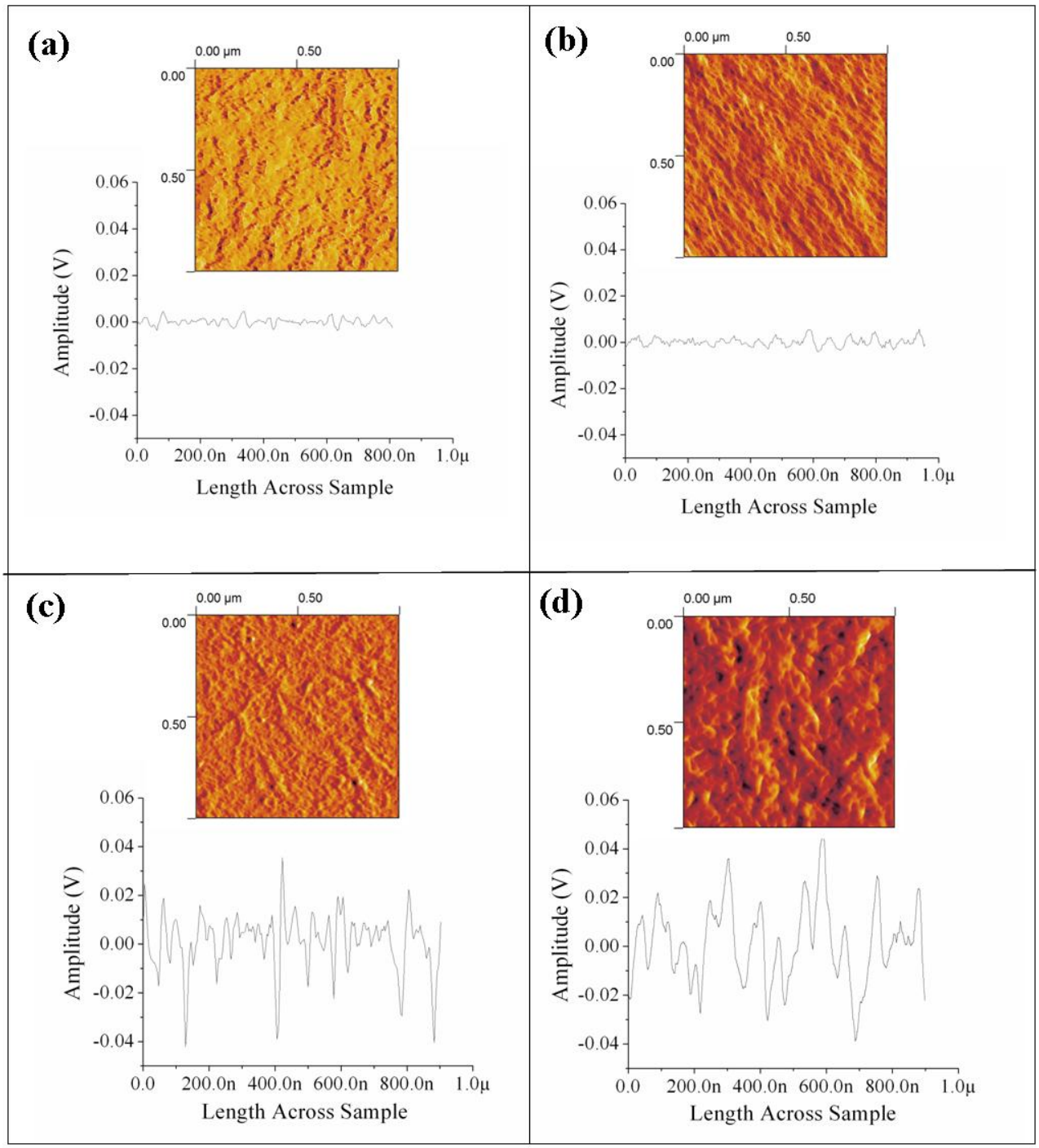

Figure 3.12. AFM images and roughness profiles for P3HT samples fabricated with various methods: (1) Spin coated chloroform; (2) Drop casted chloroform; (3) Spin coated Toluene; and (4) Drop casted toluene.

As explained in many studies, semicrystalline poly3-hexylthiophene films have crystalline domains in an amorphous matrix. The crystalline regions which are also referred to as nanofibrils are a result of π-π interactions between adjacent polymer backbones. These nanofibrils consist of self-organized lamellar layers. Strong interactions between lamellar layers results in high charge mobility between the lamellar layers [6]. The growth, amount and quality of crystalline nanofibrils can be controlled by the casting method, the solvent and the molecular weight of the polymer. Low molecular weight (< 3kDa), low mobility P3HT films have nano-rod like structures, while higher molecular weight polymers make nanofibrils which transform to nodules when the molecular weight is very high [13-16]. In this study RR-polythiophene with a molecular weight of 37 kDa was studied.

As seen in figure 3.12, the nodule like structure was most evident in the sample which was made with toluene via drop coating (method 4). When compared to this sample, the other samples had less features as observed by the AFM images. In order to quantitatively compare the structures, the roughness profiles created through Gwyddion software was compared across the sample for each case. The average height of the features in each of the samples was calculated, by averaging the absolute roughness values. The feature sizes are proportional to the size of the nodules in the samples. The feature sizes calculated for methods 1, 2 3, and 4 were 38.2$\pm$1.7 pm (picometers), 48.4$\pm$1.6 pm, 56$\pm$2.3 pm, and 69.4$\pm$6.6 pm respectively.

When compared to method 4, the feature size of samples prepared by methods 1,2,3 decreased by 45%, 30% and 19% respectively. According to this result, the samples using toluene had more nodule structures than the samples using chloroform. This is because the boiling point of chloroform is lower than the boiling point of toluene, and hence, the chloroform evaporated faster leaving less time for the polymer backbones to form interactions and self-

organize. It can be also observed that the spin coated samples had less nodule like structures when compared to drop casted samples. This is because the drop casted samples had a kinetic advantage, where the polymer backbones had time to form crystalline nodules. However in the spin coated sample, there was no time for self-organized growth, which led to nodule like structures located randomly.

In order to investigate the effect of sensor morphology on sensor performance, the sensors were coated with different films with the 4 methods described above using various solvents and casting methods. The films were then exposed to γ-terpinene, a phytochemical emitted during bark beetle infestation, using the experimental setup described previously. The flow rate was maintained at 0.2 L/min which resulted in a concentration of 50 ppm. The results are shown in figure 3.13 below. The response is shown in figure 3.13 while the sensitivity is shown in figure 3.14. The sensitivity was calculated using equation 3.2 shown in section 3.2.2.

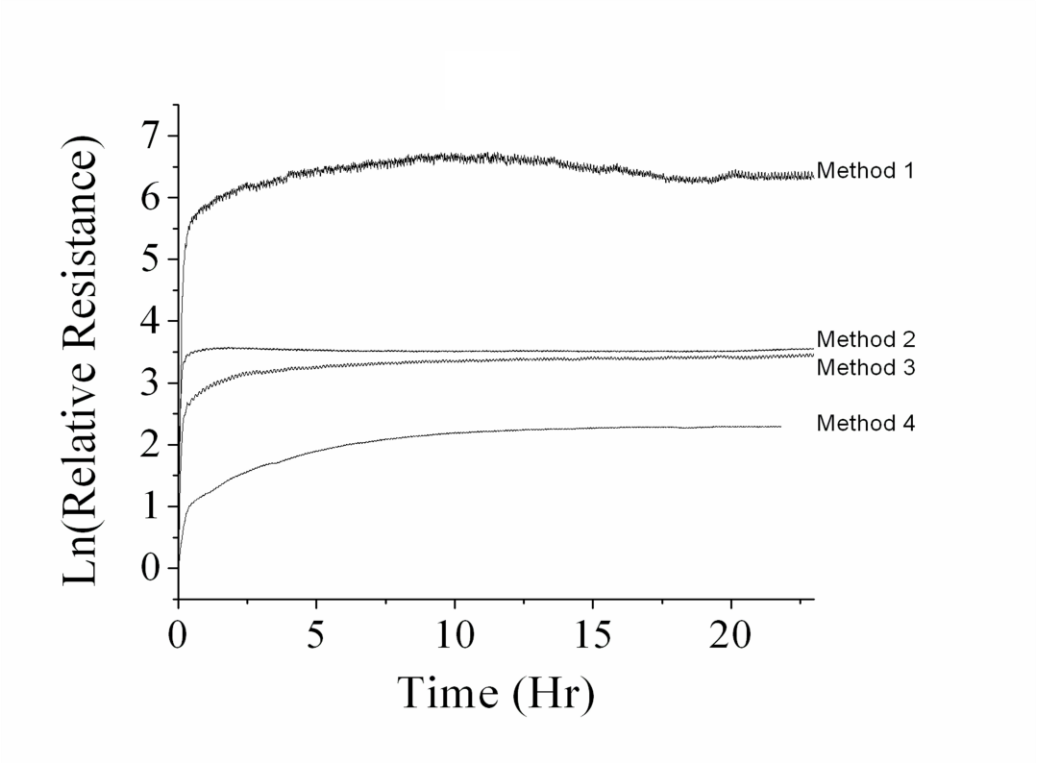

Figure 3.13. Response of sensors coated by various methods: (1) spin coated chloroform; (2) drop casted chloroform; (3) spin coated Toluene; (4) drop casted toluene.

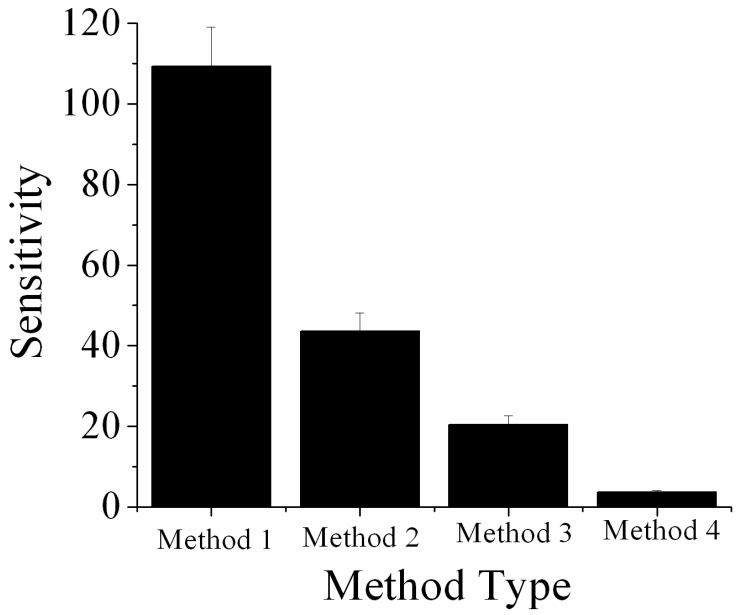

Figure 3.14. Sensitivity of sensors coated by various methods: (1) spin coated chloroform; (2) drop casted chloroform; (3) spin coated Toluene; (4) drop casted toluene.

The results show that the sensor responses can be ordered as follows: drop casted toluene (method 4) < spin coated toluene (method 3) < drop casted chloroform (method 2) < spin coated chloroform (method 1). According to figure 3.12, it was found that the size of the nodular structures, thus the crystallinity of the samples can be ordered as follows: method 4 < method 3 < method 2 < method 1. Typically the resistance of a crystalline polymer decreases with increasing crystallinity [14]. Therefore, it is expected that the resistance change would increase with decreasing crystallinity. Therefore the sample with the highest nodule like structure, and the highest crystallinity had the lowest resistance change. Additionally it was also observed that the change of solvent had a more drastic effect on the sensor performance than change of casting method used, which is consistent with the results explained using figure 3.12.

3.3. Investigation of Sensor Mechanism

To observe the morphology of P3HT sensors before and after exposure to volatile organic compounds, samples coated using each of the four methods explained in the experimental section were exposed to γ-terpinene vapor, and the morphology of the films before and after exposure were investigated using AFM. The samples were exposed to γ-terpinene for 72 hours to make sure the sensor film was fully saturated, so that the maximum change in morphology was obtained. The roughness profiles of the images obtained using Gwyddion Software were also compared. The images are shown in figure 3.15 below.

In each the four methods, the nodule like structures in the film smoothened out when exposed to γ-terpinene vapor. The roughness profiles of each of the samples before and after exposure were used to calculate feature sizes. These results are summarized in table 3.1. below. The feature sizes, thus the nodule sizes and crystallinity of the samples obtained by each of the four

methods decreased when exposed to γ-terpinene vapor. Therefore it is evident that the γ-terpinene vapor absorbed into the amorphous grain boundaries between the nodule like structures separating the crystalline lamellar layers alters the crystallinity of the thin film. The absorbance of the analyte between the amorphous regions hinders the charge mobility between crystalline regions which increased the resistance of the films as shown in figure 3.15. This sensor mechanism also agrees with sensor mechanisms proposed by Li as well as Bartlett and Garner [4-6, 18].

3.4. Stability of Polythiophene Films in the Environment

The stability of the polythiophene sensor in the environment is important when using these sensors to detect plant volatiles. In order to investigate stability, the sensor was tested under various environmental conditions.

3.4.1. Effect of Ambient Gases Present

The stability of the polythiophene sensor in air was investigated by evaluating the sensors resistance change when exposed to air. The response is shown in figure 3.16. According to measurements, the sensor was not sensitive to normal atmospheric gases. Therefore, the sensor is a suitable candidate for insect infestation investigation.

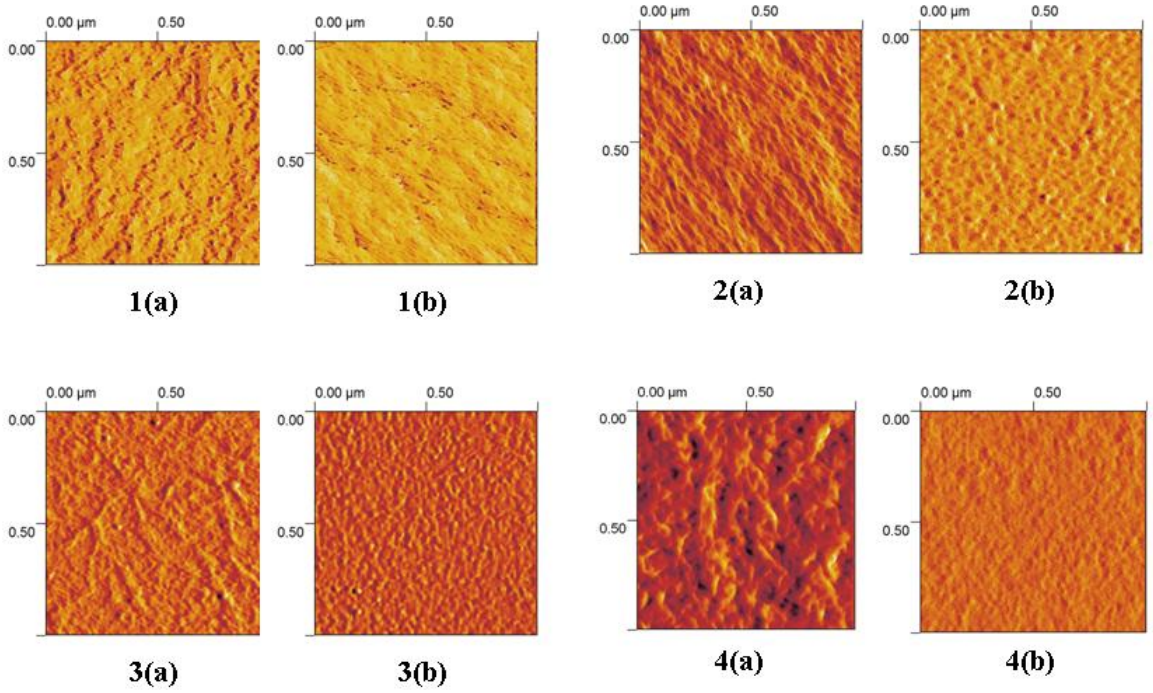

Figure 3.15. The morphology of films (a) before and (b) after exposure to γ-terpinene vapor for each of the film fabrication methods: (1) spin coated chloroform; (2) drop casted chloroform; (3) spin coated Toluene; and (4) drop casted toluene.

Table 3.1. Feature sizes of samples before and exposure to γ-terpinene vapor for each of the film fabrication methods: (1) spin coated chloroform; (2) drop casted chloroform; (3) spin coated toluene; and (4) drop casted toluene.

Method	Feature size (pm)		Change of features (%)
	Before exposure	After Exposure	
1	38.2±1.7	36.9±2.2	3.5
2	48.4±1.6	43.5±2.8	10.2
3	56.0±2.3	47.2±0.8	15.8
4	69.0±6.7	29.7±7.3	57.2

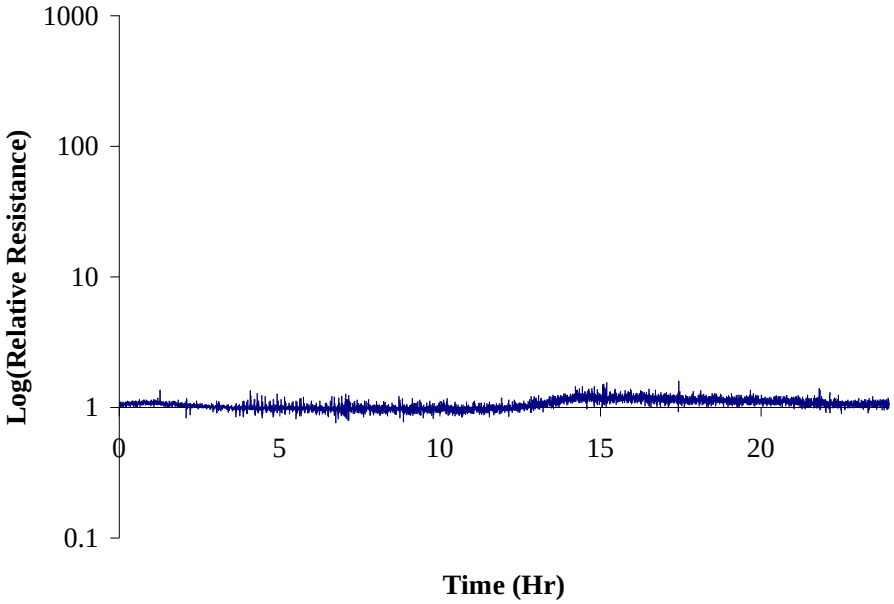

Figure 3.16. The response of polythiophene films to long term exposure in air.

3.4.2. Effect of Temperature

In order to see the effect of temperature, the sensors were first tested under various temperatures without any analyte gas present. In this experiment, the sensors were tested in static air, at temperatures varying from 0, 10, 20, 35, 40, 45 and 50 °C. The results of this experiment are shown in figure 3.17 below. It was observed that at temperatures 0, 10, 20, 35, 40, 45 and 50 °C the resistance of the sensors remained nearly constant. However a slight increase in the relative resistance was seen as the temperature increased. For comparison, the resistance of the polythiophene sensors were tested in a temperature cycle varying from -50 to 80 °C. Figure 3.18 shows the response of the sensor for temperature cycles varying from -50 to 80 °C. The resistance of the sensors stayed almost constant, except for a slight increase of resistance when the temperature increased and a decrease in resistance when the temperature decreased. This agrees with the data illustrated in figure 3.17.

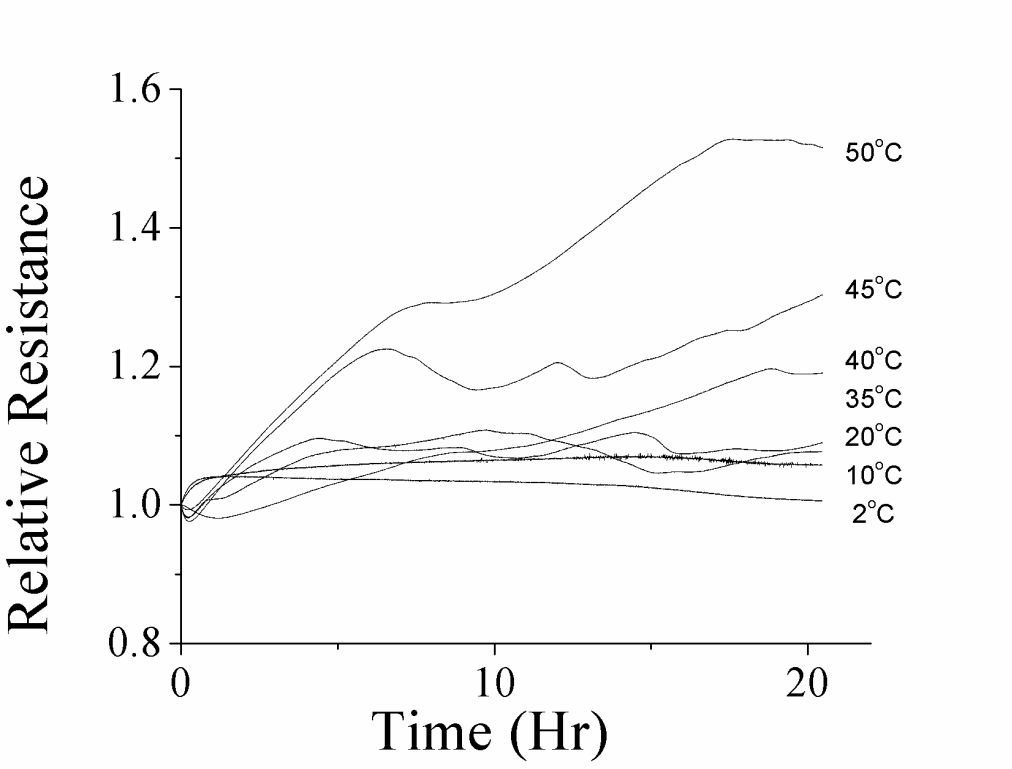

Figure 3.17. The effect of temperature on polythiophene films: The resistance of the films was measured at 0°C, 10°C, 20°C, 30°C, 35°C, 40°C, 45°C, 50°C. The relative resistance change of the film increased as the temperature increased.

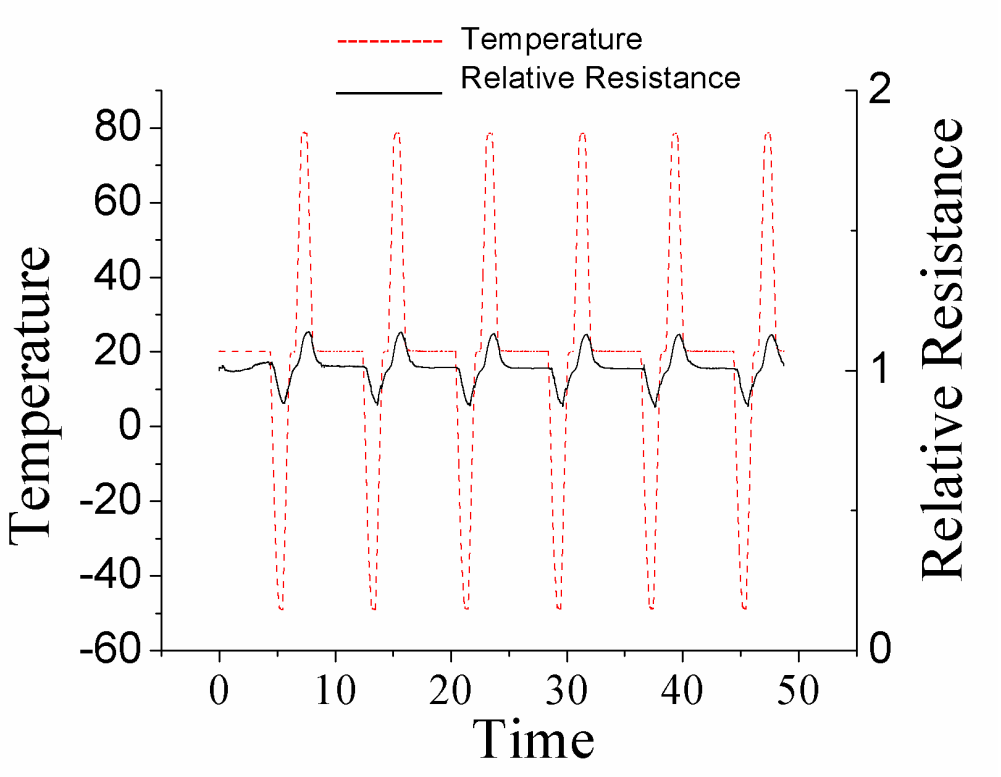

Figure 3.18. The effect of temperature cycling on polythiophene films: The resistance of the films was measured during a temperature cycle varying from -50 °C to 80 °C. The relative resistance of the film increased as the temperature increased. This agrees with the dependency of resistance on temperature illustrated in figure 3.17.

The resistance change of an undoped polythiophene film at different temperatures depends on the mobility of the charge carriers. As the temperature increases, the number of collisions of charged carriers will increase. As a result, the resistance of the film will increase with increasing temperature, and is anticipated to follow the Arrhenius relationship with the activation energy in the form shown by equation 3.3 and 3.4 [19]. Here K is the relative resistance at a certain temperature, Q is the activation energy for the process, T is the absolute temperature, R is the ideal gas constant and A is constant. The sensitivity constant is calculated using equation 3.1 in section 3.2.2.

$$K = Aexp(\frac{-Q}{RT}) \quad \text{Equation 3.3}$$

And

$$lnK = lnA - \frac{Q}{R}(\frac{1}{T}) \quad \text{Equation 3.4}$$

Figures 3.17 and 3.18 above were reanalyzed using equation 3.3. Figure 3.19 and 3.20 shows the ln K vs. ln (1/T) plots for figure 3.17 and 3.18. For figure 3.19, the relative resistance corresponding to part of the temperature cycle varying from -40 ˚C to 80 ˚C was used. In both figure 3.19 and 3.20, the ln (K) is inversely proportional to ln (1/T). For the Arrhenius plot of figure 3.19, two linear lines could be constructed for the values before and after 35˚C. This was due to the conformation changes in the polymer chains at different temperatures. A steeper plot, thus a larger activation energy was observed for the values above 35˚C. As seen in figure 3.20, the temperature cycle showed an arhennius curve with a hysterisis curve. This was again due to

changes in polymer conformation with heating and cooling as reported in literature [20]. The slopes of each graph 3.19 and 3.20 were used to calculate the activation energy. Table 3.2 summarizes the activation energy calculated for each graph as well as some values taken from the literature for undoped poly3-hexylthiophene films. The activation energy value calculated using the resistance changes at various temperature values was more comparable to the literature value than the one calculated using the resistance changes during the temperature cycle [20]. The activation energy calculated for doped Polythiophene films was much higher than the undoped films. Since the number of charge carriers is much higher in doped films, than undoped films, the mechanisms involving the temperature dependence of conductivity of polythiophene films is more complicated, therefore resulting in different activation energies.

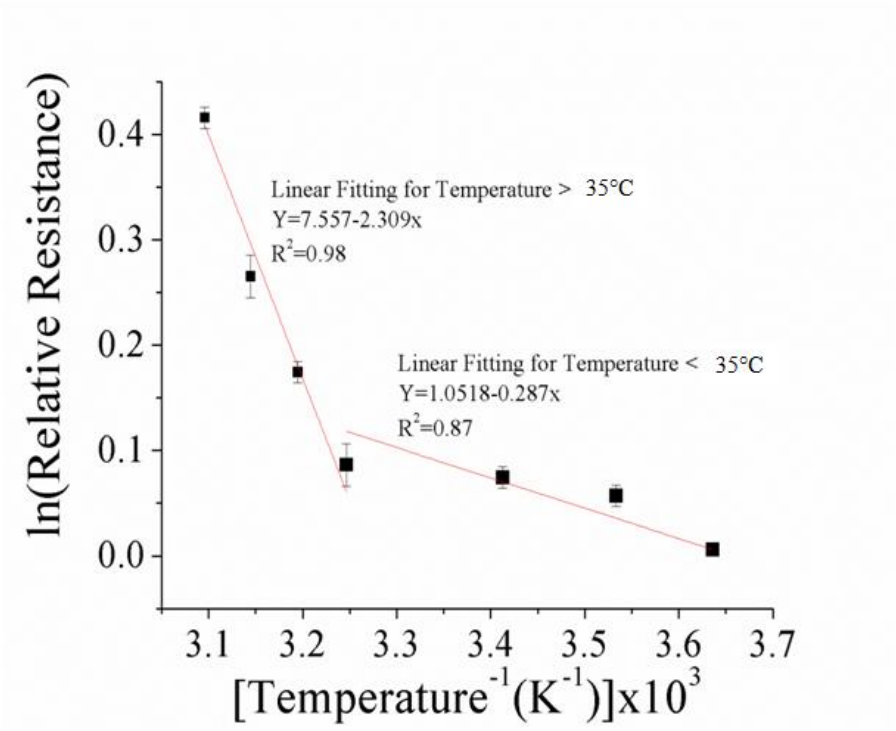

Figure 3.19. Analysis of figure 3.17 using arhennius relationship: Two linear lines were fitted to the temperature dependence values below and above 35˚C with R^2 values of 0.87 and 0.98 respectively. Change in polymer chain conformation was responsible to the change in activation energy. The slopes of the line was used to calcute the activation energy of the polymer film for temperatures below and above 35˚C. The calcuted activation energy values were 19.197 and 2.386 J/mol for temperatures below and above 35˚C.

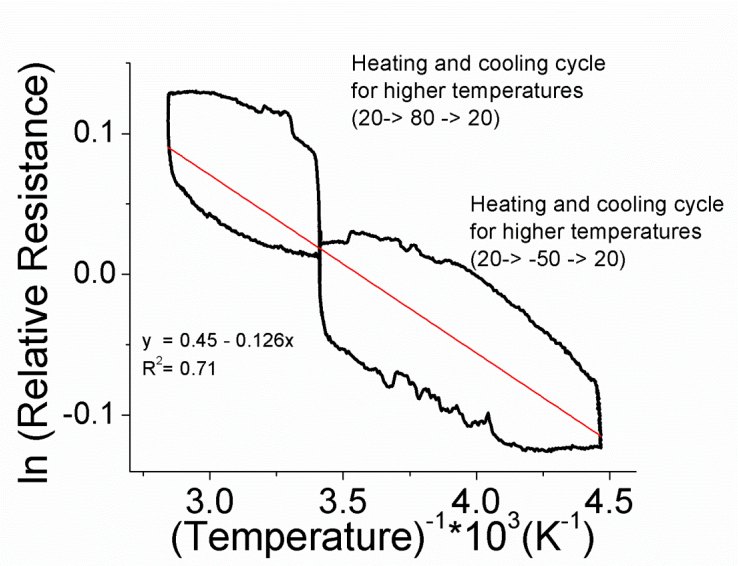

Figure 3.20. Analysis of figure 3.18 using Arhennius relationship: A hysteris loop was observed for each cooling and heating cycle varying from -50 to 80˚C. A linear line was fitted for the two hysteris loops with a R^2 value of 0.71. The slope of the line was used to calcute the activation energy of the polymer film. The calcuted activation energy was 1.076 J/mol.

Table 3.2. The activation energy values calculated from figure 3.19 and 3.20 and values obtained from the literature: The activation energy calculated using resistance changes at various temperatures was closer to the literature value than the activation energy obtained from the temperature cycle data. The activation energy value obtained from literature for the doped polymer films was much higher than the undoped polymer films.

Type of constant	**Value (kJ/mol)**
Undoped value for figure 3.15	19.197 and 2.386 J/mol for temperatures below and above 35˚C.
Undoped value for figure 3.16	1.078
Undoped value obtained from literature	3250
Doped value obtained	41 868-125604 [20]

The temperatures typically experienced in agricultural fields vary from 10 °C to 40 °C. In order to see the effect of temperature on the performance of the sensor at various temperatures, with the analyte vapor present, response of the sensors when exposed to γ-terpinene was obtained at temperatures varying from 10 to 40 °C. The results are shown in figure 3.21 below, plotted in an Arrhenius plot. The flow rate used was 0.2L/min. All other ambient conditions were kept constant. According to figure 3.21, two different mechanisms seem to control the sensor's temperature dependence. One is from 10 to 25 °C and the other is from 25 to 40 °C. To explain this effect, adsorption, desorption and the diffusion process of analyte molecules in polythiophene thin films should be considered. γ-terpinene gas molecules are absorbed by the surface of polythiophene films and then diffused into the film. At the same time, desorption occurs. The diffusion increases with increasing temperature. However the equilibrium between adsorption and desorption adjusts with temperature. At low temperature the adsorption – desorption equilibrium is in adsorption direction. At low temperatures, since there is enough gas molecules on the surface to be absorbed, diffusion governs the process. Therefore the response of the sensor increases with increasing temperature. As the temperature continues to increase above 25 °C, adsorption –desorption equilibrium of the gas molecules is in the desorption direction, and the number of gas molecules on the surface is smaller. Therefore, even though the diffusion rate increases, since the quantity of gas molecules on the surface is low, the absorption rate decreases, decreasing the sensor response. The activation energy of the diffusion governed mechanism from 25-40 °C and the absorption governed process from 10-25 °C can be calculated from the slopes of the plot. The calculated activation energy for each process was 186 kJ and -190 kJ respectively.

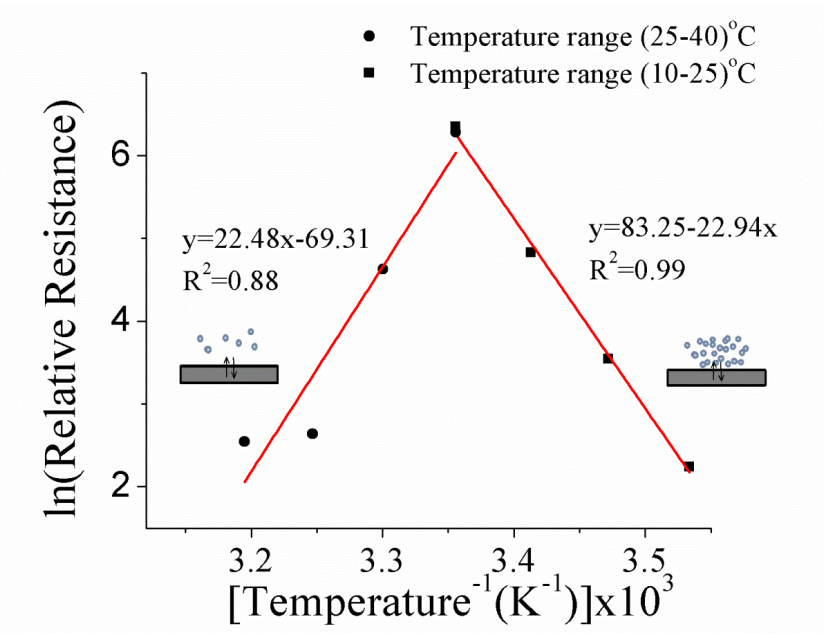

Figure 3.21. Arrhenius plot for the effect of temperature on the sensor's response at ambient pressure, 0.2L/min flow rate: Two different mechanisms seem to govern the temperature dependence; one from 10-25°C and the other from 25-40°C. The calculated activation energy for each mechanism was 186 kJ and -190 kJ respectively.

3.4.3. Effect of Humidity

Figure 3.22 shows the response of sensors to γ-terpinene vapors with varying humidities. As a control experiment the sensor was exposed to nitrogen with a specific humidity for the first 24 hours, and then exposed to γ-terpinene with the same specific humidity for the next 10 hours. The humidity of the test gas was varied by using different salt solutions. As seen in figure 3.22, there was a slight response in the control experiments in the first 24 hours which was negligible when compared to the sensor response to γ-terpinene over the next 10 hours.

3.5. Concentration Dependence of Polythiophene Films

In order to determine the concentration dependence and detection limit of the sensor, the sensor was exposed to different concentrations of the analyte vapor, γ-terpinene. The response of the sensor increased with increasing concentration as expected. The responses obtained for various concentrations are shown in figure 3.23. The sensitivity constant at each concentration was calculated using equation 3.1 illustrated in section 3.2.2. According to IUPAC standards, the detection limit is the concentration at which the extrapolated linear portion of the calibration graph intersects the baseline of the calibration curve.

In order to calculate the detection limit, the linear portions of each graph was plotted. A linear equation was obtained for each plot with a R value 0.9 or greater, as shown in figure 3.24 (a). The slope of each equation was equal to the sensitivity at each concentration. The sensitivity at each concentration was plotted as shown in figure 3.24 (b). Lower sensitivity values were used to create the baseline, and the other values were used to create the calibration graph. The value of the intersection was the detection limit of the sensor. According to 3.24 (b), the detection limit of the sensor was found to be 36 $\pm$ 2 ppm. As discussed in the introduction,

the literature shows that plants emit volatile compounds at an average concentration of 100 ppm. Therefore the poly 3-hexylthiophene sensors show adequate sensitivity to detect early stages of insect infestation.

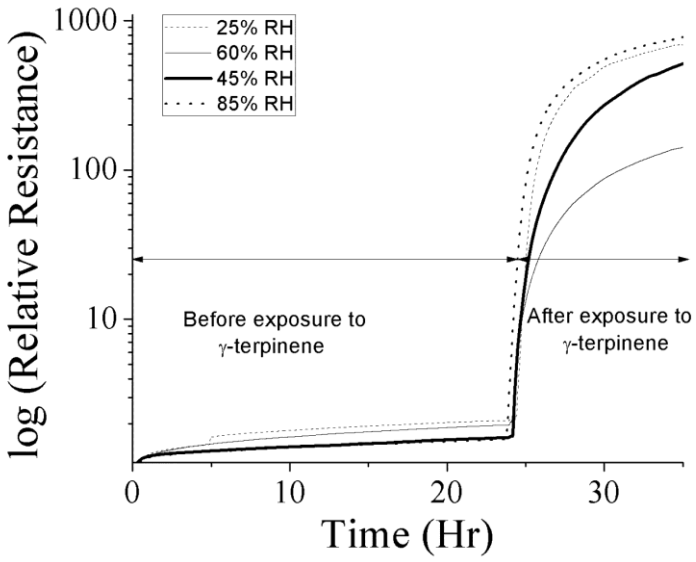

Figure 3.22. Stability and performance of P3HT sensor under different humidity conditions: When the sensor was exposed to nitrogen gas under different humidity conditions, the sensor response was almost constant, only a small difference in response to different humidities was measured (less than a factor of 2 difference). When exposed to γ-terpinene gas under different humidity conditions, the response of the sensors was again very similar.

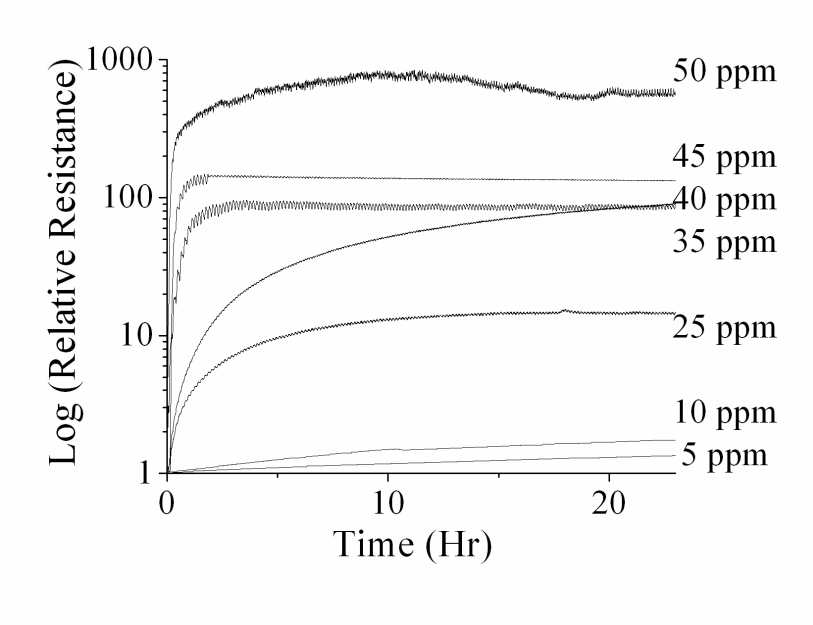

Figure 3.23. The response of P3HT sensors when exposed to different concentrations of γ-terpinene: The response of the sensor increased with increasing concentration. The curve consists of a linear portion and a dynamic portion as explained in section 3.2.2. The linear portion of the graph was used to calculate the sensitivity for each concentration value. The sensitivity values obtained at each concentration was used to calculate the detection limit of the sensor.

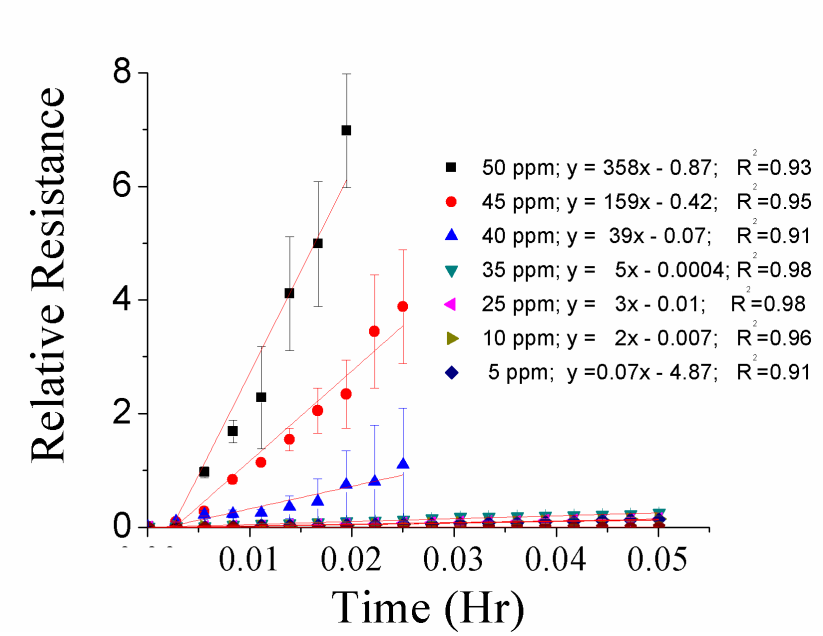

Figure 3.24 (a). Calculating the sensitivity: The linear portion of figure 3.18 was plotted and a linear line was plotted with a R^2 value of 0.9 or greater. The slope of the graph was equal to the sensitivity at each concentration.

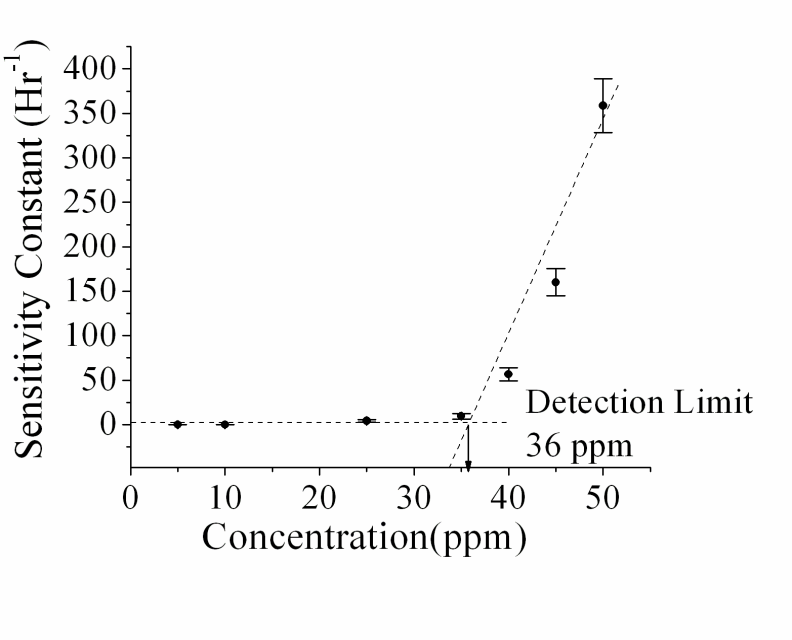

Figure 3.24 (b). Detection limit of sensor: The intersection point of the baseline and calibration graph was equal to the detection limit of the sensor. The detection limit of the polythiophene sensors was found to be 36 $\pm$ 2 ppm.

3.6. Reversibility of Polythiophene Thin Film Sensors

The reversibility of the sensor is shown in figure 3.25. In order to determine the degree of reversibility, the sensor was exposed to γ-terpinene with nitrogen as the carrier gas. Next the sensor was exposed to nitrogen without the analyte gas (γ-terpinene) and the exposure to nitrogen continued until the sensor returned to its original resistance. Like the response curve, the recovery curve had a linear part where the resistance quickly decreased and a dynamic part where the resistance slowly decreased. However the recovery curve was slower than the exposure curve. It should be noted that in figure 3.25, the time of the response and recovery were kept approximately the same and the sensor was not allowed to completely recover. The time for the sensor to recover back to its original value was about 1 week.

In order to see the effect of temperature on the sensor reversibility, the sensors were exposed to γ-terpinene at 20 $^{\circ}$C, and then allowed to return back towards its original resistance, at 20 $^{\circ}$C, the first 12 hours, and at 50 $^{\circ}$C the next 12 hours. This response is shown in figure 3.26. To calculate the rate of reversibility, the linear portion of the reversibility curve at each temperature was plotted with time. This plot is shown in figure 3.27. The slope of each curve was equivalent to the rate of reversibility at each temperature. The reference temperature used to calculate the relative resistance at each temperature was the resistance value at the start point of the reversibility curve for each temperature. According to figure 3.27, the rate of reversibility at 20 $^{\circ}$C and 50 $^{\circ}$C was equal to 0.4 Hr^{-1} and 2.3 Hr^{-1}, respectively. As seen from the values, the reversibility calculated at 50 $^{\circ}$C was nearly 6 times faster than the value calculated at 20 $^{\circ}$C. To explain this effect, the equilibrium between adsorption and desorption, and the diffusion of analyte molecules in polythiophene thin films should be considered. At higher temperatures,

without the presence of analyte gases, the equilibrium between adsorption and desorption is in the desorption direction, increasing the rate of reversibility.

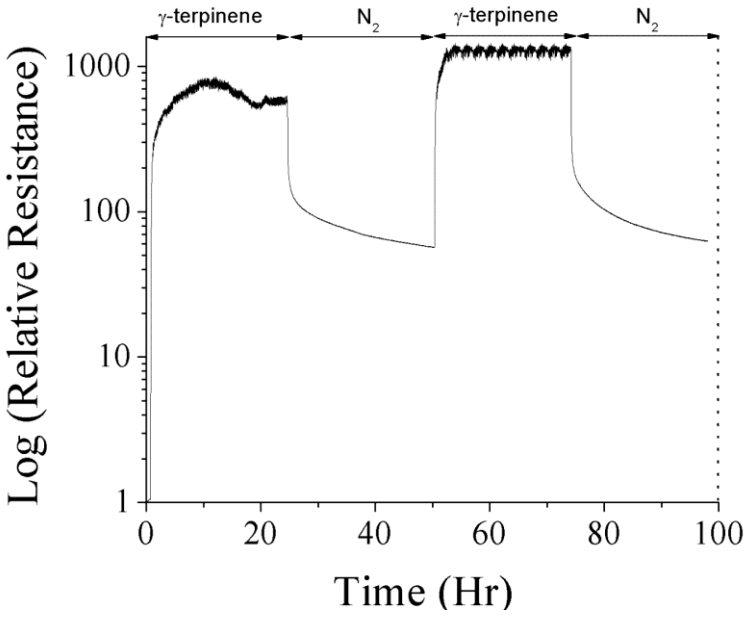

Figure 3.25. Typical response of P3HT sensor when exposed to γ-terpinene and nitrogen: the sensor had a recovery curve similar to the response curve. However the recovery curve had a shorter linear response and longer dynamic response than the exposure curve.

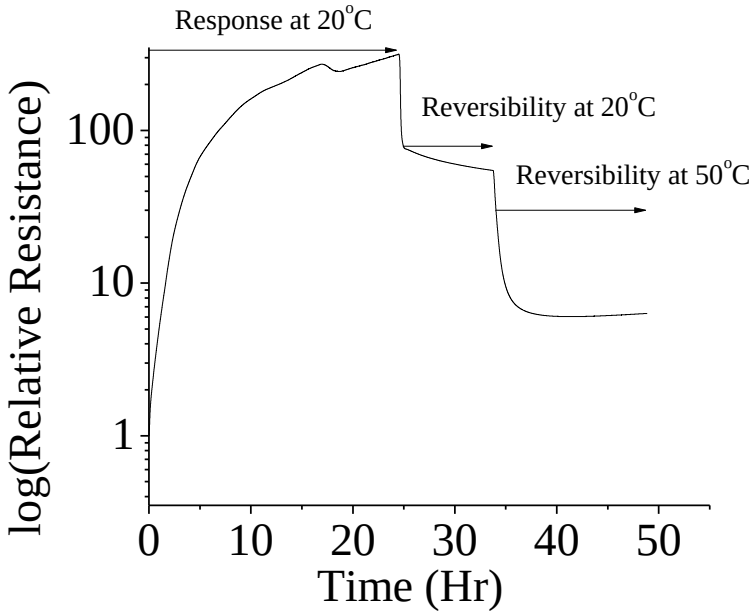

Figure 3.26. Reversibility of Polythiophene sensor films at different temperatures: The sensor was first exposed to γ-terpinene and then was allowed to return to its original resistance first at 20 and then at 50 °C. The rate of reversibility at each temperature could be calculated by plotting the linear portion of the reversibility curve.

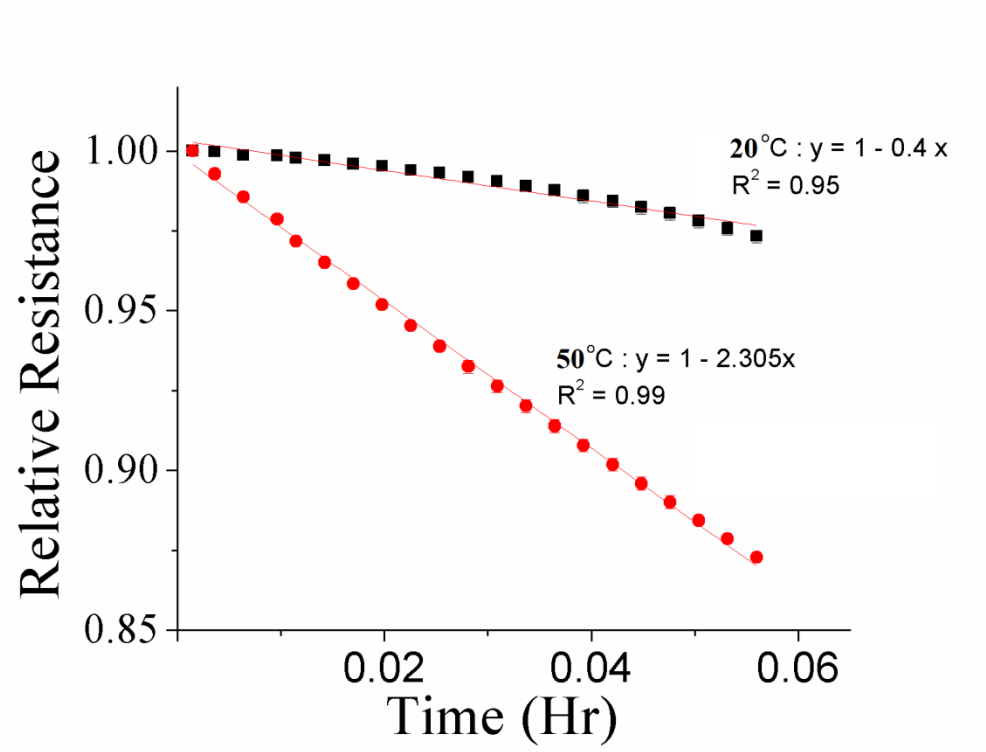

Figure 3.27. The rate of reversibility of polythiophene film at different temperatures: The rate of reversibility at 50 °C and 20 °C were calculated by plotting the linear portions of the reversibility curve at each temperature. The slopes of each curve at each temperature were equal to the rate of reversibility at each temperature. The calculated rate of reversibility at 20 °C and 50 °C was equal to 2.3 Hr^{-1} and 0.4 Hr^{-1} respectively. The reference temperature used to calculate the relative resistance at each temperature was the resistance value at the start point of the reversibility curve for each temperature.

3.7. Response of Polythiophene Sensor to Other Volatile Organic Compounds

In order to obtain the response of the sensor to other plant volatiles, sensors were exposed to 6 plant volatiles: limonene, α-pinene, farnesene, cis-hexynyl acetate, p-cymene and γ-terpinene. The flow rate was maintained at 0.2 L/min and room temperature and humidity was used in this experiment. Gas chromatography techniques as described in section 2.6.4 were used to calculate the concentration of each analyte detected. The calculated concentrations were 65, 50, 65, 45, 50 and 50 ppm for limonene, α-pinene, farnesene, cis-hexynyl acetate, p-cymene and γ-terpinene respectively. The average concentration detected was 50 ppm. As seen in figure 3.28, the sensor was more sensitive to γ-terpinene, limonene and p-cymene. It was less sensitive to farnesene, cis-hexylacetate and α-pinene. It should be noted that γ-terpinene, limonene and p-cymene have relatively similar structures to P3HT, while the structures of farnesene, cis-hexylacetate and α-pinene are not similar.

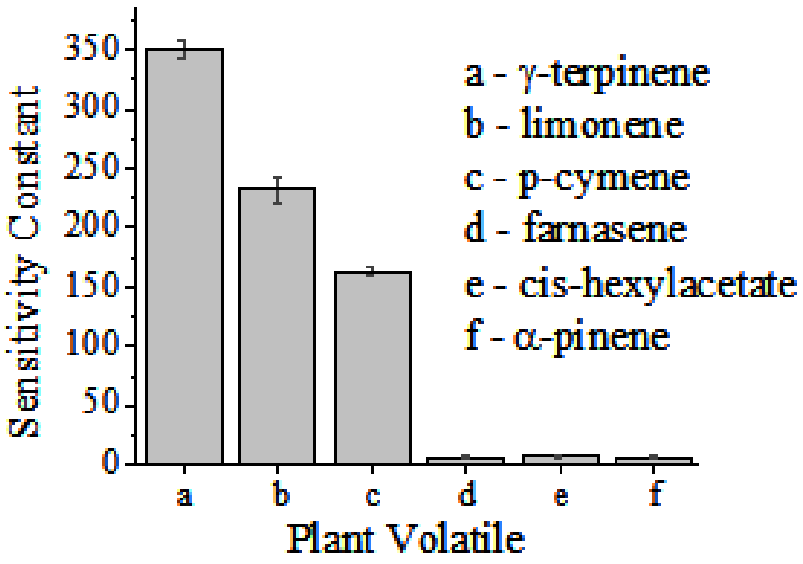

Figure 3.28. The sensitivity of polythiophene sensors to various plant volatiles: The sensor was more sensitive towards γ-terpinene, limonene and p-cymene. It was less sensitive towards farnesene, cis-hexylacetate and α-pinene. The calculated concentration for limonene, α-pinene, farnesene, cis-hexynyl acetate, p-cymene and γ-terpinene detected was 65, 50, 65, 45, 50 and 50 ppm respectively.

3.8. References

[1] B. Li and G. Sauve, "Volatile Organic Compound Detection Using Nanostructured Copolymer", *Nano Letters*, vol. 6, pp. 1598-1602, 2006.

[2] H. Bai and G. Shi, "Gas Sensors Based on Conducting Polymers". *Sensors*, vol. 7, pp. 267-307, 2007.

[3] B. Li and S. Santhanam, "Volatile Organic Compound Discrimination Using Nanostructured Polythiophene Sensors", *IEEE Sensors*, pp. 191-194, 2005

[4] J. W. Gardner and P. N. Bartlett, "Electronic Noses: Principles and Applications", Oxford University Press, New york, 1999.

[5] R. Zhang, and B. Li et. al. , "Nanostructure Dependence of Field-Effect Mobility in Regioregular Poly(3-hexylthiophene) Thin Film Field Effect Transistors", *J. Am. Chem. Soc.* , vol. 128, pp. 3480-3481, 2006.

[6] B. Li and D. N. Lambeth, "Mechanims of Polythiophene Chemical Sensors", *IEEE conference proceedings*, pp. 1330-1333, 2007.

[7] A. Keawprajak, P. Piyakulawat, U. Asawapirom, "Study of Nanostructures of Oriented Regioregular Poly(3-hexylthiophene) and PCBM by AFM and TEM", *Journal of Microscopy Society of Thailand*, vol. 23(1), pp. 138-141, 2009.

[8] H. Kajii, H. Okuya, A. Sakakibara and Y. Ohmori, "Oligothiophene Organic Transistors Using Poly(3-hexylthiophene) Fabricated by Spin Coating", *Japanese Journal of Applied Physics*, vol. 44(51), pp. 1567-1569, 2005.

[9] M. Canetti, F. Bertini, G. Scavia and W. Porzio, "Structural Investigation on Bulk poly(3-hexylthiophene): Combined SAXS, WAXD, and AFM Studies", *European Polymer Journal*, vol. 45, pp. 2572-2579, 2009.

[10] K. Weerakoon, S. Li, H. Shu and B. Chin, "Detecting Insect Infestation with Poly3-hexylthiophene Thin Film Sensor", *SPIE Advanced Environmental, Chemical and Biological Sensing Conference proceedings*, vol. 7312, April 2009.

[11] R. Osterbacka, C. P. An, X. M. Jiang, Z. V. Vardeny, "Two Dimensional Electronic Excitations in Self-assembled Conjugated Polymer Nanocrystals", *Science*, vol. 287, pp. 839-842, 2000.

[12] M. S. A. Abdou, F. P. Orfino, Y. Son, S. Holdcroft, "Interaction of Oxygen with Conjugated Polymers: Charge Transfer Complex Formation with Poly(3-alkylthiophenes)", *Journal of American Chemical Society*, vol. 119, pp. 4518, 1997.

[13] H. Sirringhaus, N. Tessler, D. S. Thomas, P. J. Brown and R. H. Friends, "Advances in Solid State Physics", ed. B. Kramer, pp. 101, Vieweg, Braunschweig, 1999.

[14] J. Ficker, H. von Seggen, H. Rost, W. Fix, W. Clemens and I. McCulloch, "Influence of Intensive Light Exposure on Polymer Field Effect Transistors", *Applied Physics Letters*, vol. 85, pp. 3378-1379, 2004.

[15] H. Shu, "Applications of Poly(3-hexyl thiophene) Thin Film as a Hydrazene Sensitive Chemiresistor", Auburn University, Auburn, Alabama, pp. 33-55, 2006.

[16] H. G. O Sandberg, G. L. Frey, M. N. Shkunov, H. Sirrinhaus and R. H. Friend, "Ultrathin Regioregular Poly(3-hexylthiophene) Field Effect Transistors", *Langmuir*, vol. 18, pp. 10176-10182, 2002.

[17] R. E. Hummel, "Electronic Properties of Materials", 3rd ed, Springer, New York, 2001.

[18] J. W. Gardner and P. N. Bartlett, "Electronic noses: Principles and applications", Oxford University Press, New york, 1999.

[19] Y. Wang and M. F. Rubner, "Stability Studies of the Electrical Conductivity of Various Poly (3-alkylthiophenes)", *Synthetic Metals*, vol. 39, pp. 153-175, 1990.

[20] G. Gustafsson et al., "Thermal Undoping in Poly(3-alkylthiophenes)", *Synthetic Metals*, vol. 26, pp. 297-309, 1988.

Chapter 4

Polymer/Carbon Sensor Optimization and Investigation Of Sensor Mechanisms

4.1. Polymer/Carbon Thin Films for Volatile Organic Compound Detection

Low mass fraction polymer/carbon composite sensors are reported to be highly responsive to a variety of organic volatile compounds. In addition they are highly stable, inexpensive and easy to fabricate [1]. The sensor element usually consists of a sensor platform which is usually chemiresistor based, and an active layer film that is made of a polymer matrix and carbon filler. Common matrix materials include polyvinylpyrrolidone (PVP), polyethyleneoxide (PEO), polyisoprene (PISO), polymethylmethacrylate (PMMA), poly(ε-caprolactone) and polyethylene-co-vinyCAl acetate (PEVA) [2-3]. When the carbon concentration of the active layer is low enough and near the percolation threshold, the sensor can be used as a "chemical switch." When the sensor is connected to an electrical circuit, it will "switch on" when exposed to analyte vapor by showing a very high resistance and switch off when analyte vapor is no longer present [1]. These sensors are stable in air, and are able to provide a fast, large signal when exposed to an analyte and return quickly to their original state when the chemical is no longer present. Eight sensors which can act as chemical switches and may be applied to early detection of insect infestations are discussed in the following section. The structures of these polymers are shown in figure 4.1.

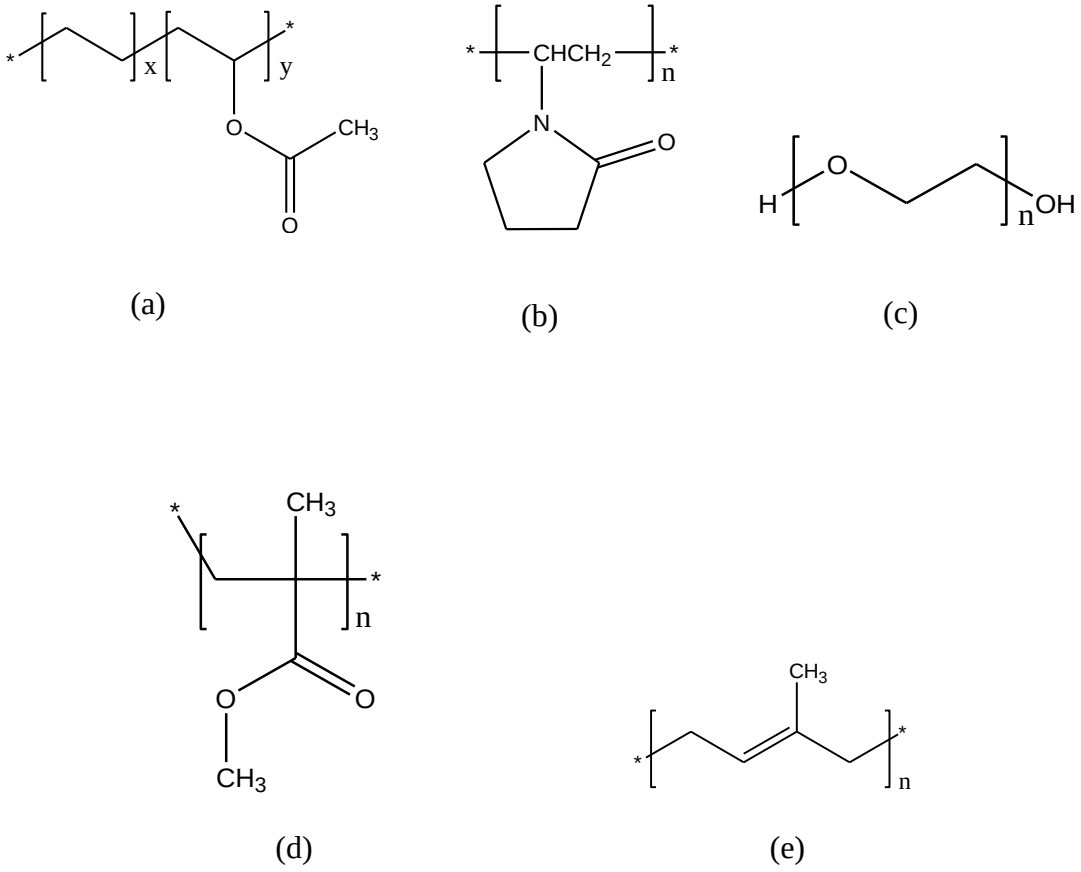

(a) (b) (c)

(d) (e)

Figure 4.1. Structures of polymers used to study the swelling ability: polyvinylpyrrolidone, polyethyleneoxide, polyisoprene, polymethacrylate and polyethylene-co-vinylacetate (40% vinyl acetate).

4.2. Polymer/ Carbon Chemiresistor Sensor, the Mechanism of Detection

The mechanism of polymer/carbon composite film sensors is understood and described in the literature [1-6]. The sensor elements include a film of swellable insulating organic polymer with conductive regions of dispersed carbon particles. The carbon makes the films conductive. Current travels along continuous pathways of carbon particles. When sorption occurs, swelling of the films results, which breaks the continuous pathways, increasing the resistance of the composite film. Removal of the analyte species or desorption causes the carbon particles to return to their original places, thus decreasing the resistance of the film. The resistance response of the polymer/carbon film can be understood by the percolation theory, which relates response of composite film to the change in carbon content (fraction of conducting filler phase) of the composite. According to the percolation theory, the transition of a bulk material from being a conductor to an insulator, can be achieved by increasing the concentration/volume content of the conducting species of an insulator-conductor composite, above a threshold value; the percolation point [4-6].

Chen et. al. found that when a crystalline polymer such as polyethylene is used as the insulating matrix, the crystallinity change caused by vapor absorption can have an effect on the resistance change of the polymer film [7]. In crystalline and semi-crystalline polymer/carbon films, carbon particles can form conducting pathways on the boundaries of crystal grains and amorphous regions between grains. Absorption of the analyte causes the crystalline polymer matrix to dissolve, and the movement of the carbon particles results in destruction of the conductive networks in the amorphous regions, which raises the electrical resistance of the film [2]. In these kinds of sensors, temperature may have an adverse effect on the sensor response,

because the crystallinity may change with temperature. Therefore the response, reversibility, reproducibility and stability of this kind of sensor depends, not only on the molecular weight of the polymer matrix and the content and the dispersivity of carbon, but also on the environmental conditions such as temperature and organic vapor concentration.

According to a study done by Kirkpatrick et.al. on percolation effects on metal semiconductor transitions in disordered systems, or in the unusually low mobilities associated with free carriers in amorphous materials, the resistivity obeys a power law in the form of:

$$\rho \sim (X-X_c)^t \quad \text{Equation 4.1}$$

Where ρ is the bulk resistivity of the composite, X is the concentration of the conductive component, X_c is the percolation threshold and t is the universal conductivity exponent. Currently accepted theoretical values for the universal conductivity exponent is t=2 for three dimensional lattices [9]. More recent studies indicate the value of the universal conductivity exponent and thus the transport behavior in continuum percolation may not be universal. These investigations calculated non-universal values for various systems. In a study done by Heanley et al. it was illustrated that equation 4.1 above could be modified to equation 4.2, for carbon black-polymer composites. Here ρ_o is the resistivity scaling factor which is 15.2 Ωcm^{-1}, for the system [9].

$$\rho = \rho_o[\frac{(X - X_c)}{(1 - X_c)}]^{-t} \quad \text{Equation 4.2}$$

This model was experimentally obtained by measuring (ρ/ρ_o) values with change of concentration of carbon black in polymer matrix [9]. The data obtained is displayed in figure 4.2. According to the data shown in figure 4.2, a value of 2.9 was obtained for the t value for the polymer/carbon composite.

Kinetics of sorption and desorption of small permanent molecules into polymers can be described by Fick's second law (equation 4.3) where c is the analyte concentration in the polymer, t is the time, D is the polymer analyte diffusion coefficient, and x is the distance.

$$\frac{\partial c}{\partial x} = D\frac{\partial^2 c}{\partial t^2} \quad \text{Equation 4.3}$$

Examples of polymer/carbon films that have been used to make sensors to detect volatile organic vapors include: poly(ε-caprolactone)/carbon, poly(ethylene adipate)/carbon and polyethylene (PE)/carbon [2]. Polyethylene-co-vinyl acetate (PEVA) is produced by copolymerizing vinyl acetate with polyethylene. Polyethylene is highly crystalline. When made into composite films with carbon and exposed to organic vapors, polyethylene changes its crystallinity, thus changing its resistance. However adding vinyl acetate groups make the polymer more polar and less crystalline. The crystalline properties of the polymer can be tuned by varying the amount of vinyl acetate used. In fact, the addition of a substantial amount of vinyl acetate reduces the crystallinity the glass transition point of the polymer. In a non crystalline PEVA copolymer (with very little polyethylene), it could be assumed that the operation mechanism of the polymer is not the common mechanism for polymer/carbon composites, i.e. not involving dissolution of the crystalline matrix.

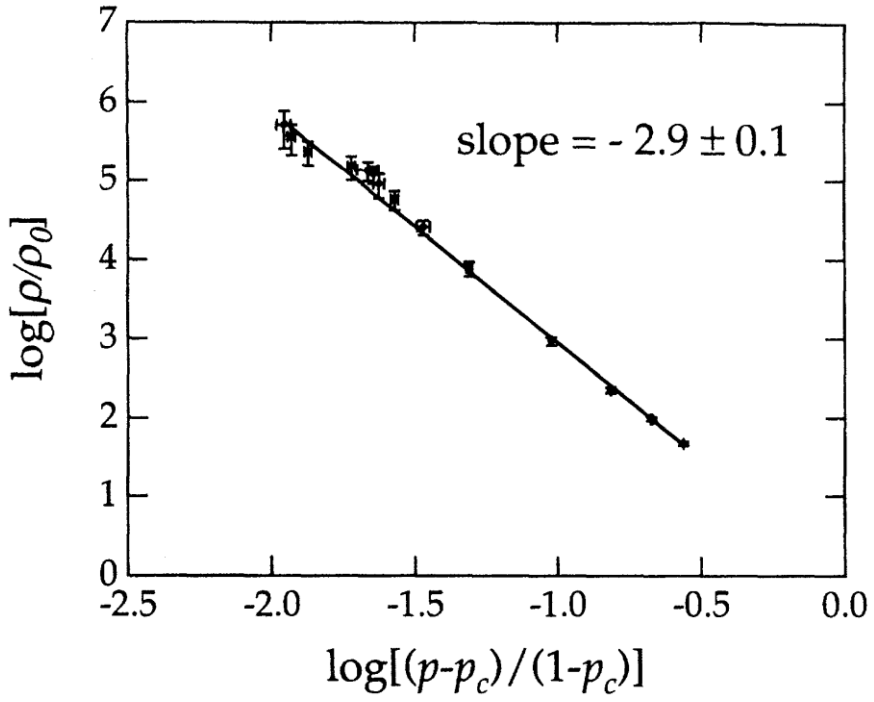

Figure 4.2. Resistivity change with respect to carbon black polymer content [9].

4.3. Degree of Swelling of Various Polymers

When a thin polymer film is exposed to a solvent, the solvent diffuses into the free volume. This phenomenon is also referred to as mass uptake. When the solvent is exposed to a polymer system that has strong interactions with the solvent, the net interactions between the polymer segments become repulsive. As a result the coiled polymer chains dissolve in the solvent and start to unravel. This results in swelling of the polymer film. In a recent study, it was demonstrated that volumetric film swelling was the key variable determining the resistance change in polymer/carbon composite film sensors when exposed to organic vapor [5-6, 9]. Therefore, in order to see whether the selected polymer candidates absorb plant volatiles, a simple experiment was carried out, where various polymers including polyvinylpyrrolidone, polyethyleneoxide, polyisoprene, polymethacrylate and polyethylene-co-vinylacetate were coated onto glass slides and were exposed to the plant volatile γ-terpinene. The weight difference of polymer coated slides was obtained before and after exposure to the volatile. This data was used to calculate the swelling ability of each polymer using the equation 4.4 below, where W_0 and W are weight of the polymer film before and after absorbance of the volatile vapor.

$$\text{Degree of Swelling} = \frac{(W - W_o)}{W_o}\% \quad \text{Equation 4.4}$$

Figure 4.3 below, shows the degree of swelling obtained for various polymers.

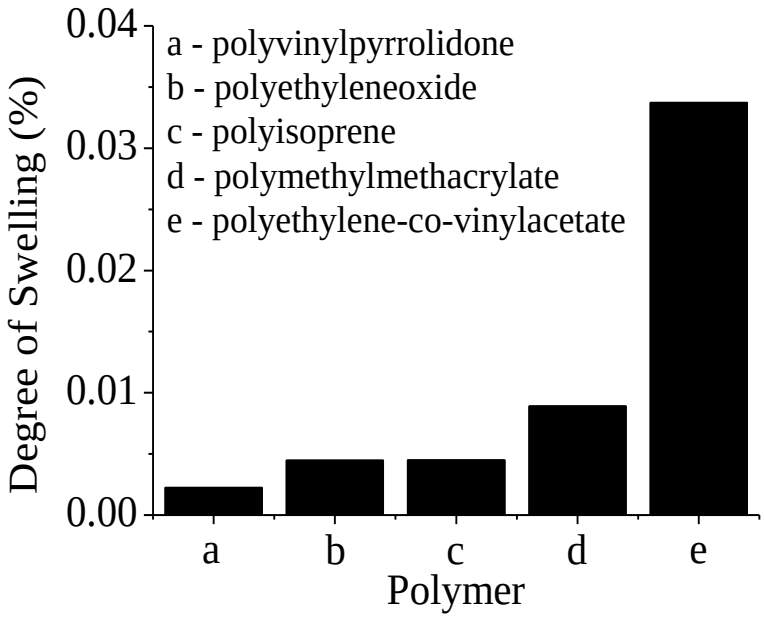

Figure 4.3. Degree of Swelling for various polymers including polyvinylpyrrolidone, polyethyleneoxide, polyisoprene, polymethacrylate and polyethylene-co-vinylacetate: Degree of swelling for polyethyele-co-vinylacetate was significantly higher than for other polymers.

According to the results, the highest degree

of swelling and the most mass uptake occurred in polyethylene-co-vinyl acetate, but the other polymers absorbed the analyte as well. Since the polymers absorbed the vapors in different amounts this suggested that the polymers show different physical interaction with the vapor, which makes them good candidates for a sensor array detecting volatile vapor compounds.

4.4. Determination of Percolation Point

Disordered conductor-insulator composites, exhibit a transition from being conductive to insulative when the composition of the conductive component is decreased below a critical threshold value. This transition is also referred to as a "continuum percolation phase transition" and is expected to be sharp. Near the transition point the composite obeys a power law as shown in equation 4.1 above [9]. When a sensor consisting of an active layer of polymer/carbon composite film, where the carbon concentration is near the threshold, the absorbance of the analyte will cause a sharp increase in the resistance. Therefore, it is important to determine the percolation point for a polymer. In order to determine the percolation point, the sensor was coated with PEVA/carbon films of different carbon black concentrations. The resistance of these sensors made with different carbon black compositions is shown in figure 4.4 below. As shown the percolation point was observed at a 1-2.5% weight percent carbon for polyethylene-co-vinylacetate. Therefore, in order to ensure that the resistance would change drastically when absorbing the analyte, the carbon composition of the sensors used in this study was kept at 4%.

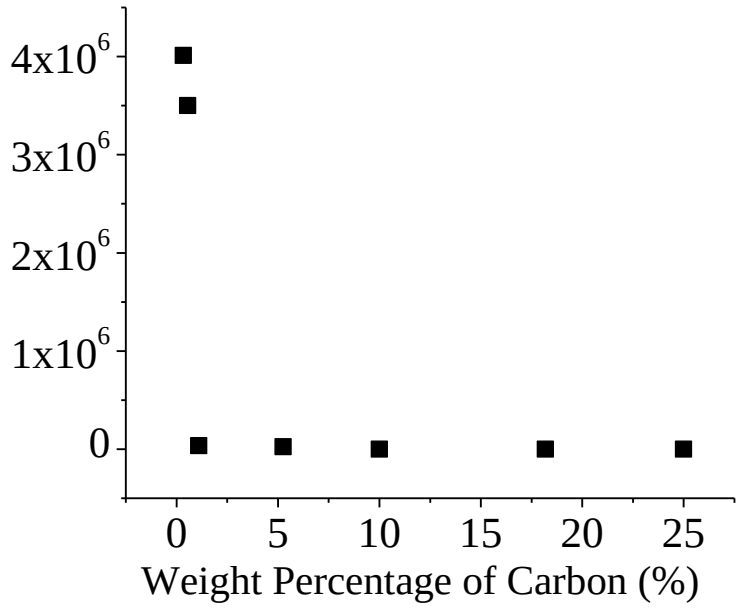

Figure 4.4. Determination of Percolation point of polyethylene-co-vinylacetate/carbon films: The percolation point was between 1-2.5% Carbon.

4.5. General Performance of Polymer/Carbon Sensors

In order to observe the sensor performance when exposed to analyte, sensors with 4% carbon in PEVA were manufactured and exposed to γ-terpinene. For the first 20 minutes the sensor was exposed to pure nitrogen to make sure the sensor does not react with oxygen or other atmospheric gases. As shown in figure 4.5 the sensor response was flat for the first twenty minutes, and then when exposed to analyte vapor γ-terpinene, the resistance increased by over two orders of magnitude. When exposed to pure nitrogen gas, the sensor returned back to its original resistance, and stayed stable, showing a "switch on-switch off" type response. This result confirms that PEVA/carbon sensors can be used as a "chemical switch" to detect plant volatile compounds.

4.6. Investigation of Sensor Mechanism

The mechanism of operation of the PEVA/carbon sensor is clearly understood in many studies [1-5]. According to these studies, the increase in resistance when an analyte is absorbed is caused by the breakage of conducting pathways between carbon particles, due to swelling of the polymer matrix. In order to prove this, silicon wafers were coated with PEVA/carbon composite, and were exposed to γ-terpinene. Optical microscope images of these samples before and after exposure were obtained, as shown in figure 4.6. The black areas in the picture are carbon particles or its aggregated carbon. There is no carbon present in the white areas. Before exposure, the carbon in the polymer is aggregated, and as seen in figure 4.6 (a), the black area is significantly more than the white areas. When exposure happens, the polymer swells and as result the distance between carbon and aggregates increase. Therefore, as seen in figure 4.6 (b), within the same area, the white area increases, with less black. Therefore, after exposure to γ-

terpinene, the distance between carbon aggregates increased, proving the mechanism hypothesized.

4.7. Environmental Stability of Polymer/Carbon Sensors

Environmental stability of the polymer/carbon sensors is of utmost importance, because these sensors are meant to be used in agricultural fields that subjected to continuously changing weather. In order to determine how the sensors may be affected by environmental changes, the sensors were tested in air, and under various temperature and humidity conditions. To investigate the effect of temperature on sensor stability, PEVA/carbon sensors were first tested under different temperatures as well as during a temperature cycle without the exposure to analyte gas. Then the sensors were tested under various temperatures with the exposure to γ-terpinene. The sensors were also tested under different humidity conditions, with and without exposure to analyte vapor. The stability of sensors was monitored over a long period in air to investigate the response to ambient gases present.

4.7.1. Effect of Ambient Gases

In order to test the stability of polymer/carbon sensors during exposure to the presence of ambient gases, the resistance of the sensors was monitored for a 72 hour period, under air. It was reported in the literature that these films exhibit some instability soon after fabrication. This instability was observed. This instability is hypothesized to be due to the slow evaporation of solvents, resulting in a constant resistance change. These sensors were fabricated by the drop casting method and hence solvents can be trapped within the polymer. However after complete evaporation of the solvent the sensors were expected to be stable. Therefore in order to

investigate the stability under air, the sensors were monitored over a 240 hr period. The results are shown in figure 4.7 below. The results show that the sensors are stable after a period of 150 hours (6 days). Therefore, for the sensor array experiments, the sensors were allowed to stabilize over a 1 week period. Faster stabilization could be obtained, by hard baking in UV light or by storing in a vacuum. After stabilization, the sensors do not change their resistance in the presence of ambient gases.

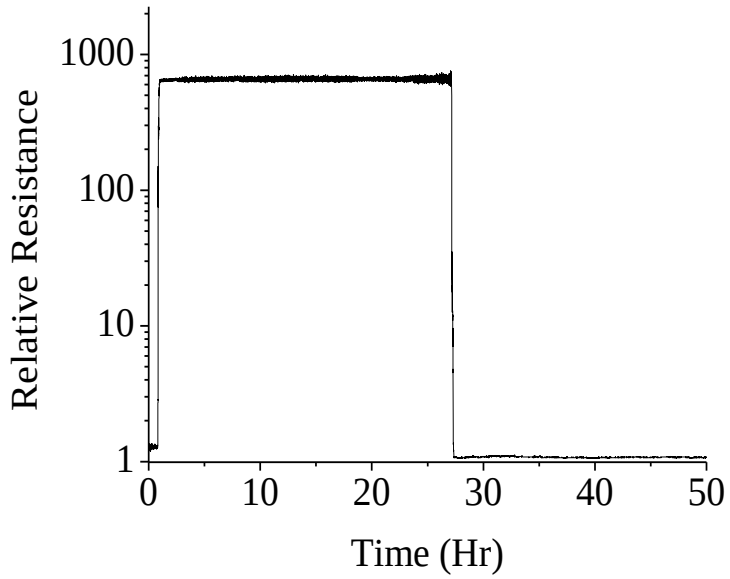

Figure 4.5. Typical response obtained when PEVA/carbon sensors containing 4% C are exposed to γ-terpinene: The resistance of the sensor increased by over three orders of magnitude and returned back to its original resistance when exposed to pure nitrogen.

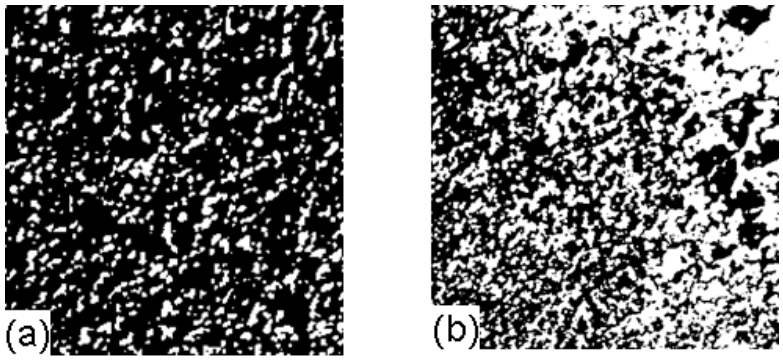

Figure 4.6. Optical microscope images of PEVA/carbon sensors (a) before and (b) after exposure to γ-terpinene: The black areas are carbon particles and its aggregates while the white areas are areas without carbon. There is significantly more black in the picture before exposure, and the white area increases after exposure. Therefore after exposure to the chemical, the distance between carbon aggregates increased, confirming hypothesized mechanism for PEVA/carbon sensors.

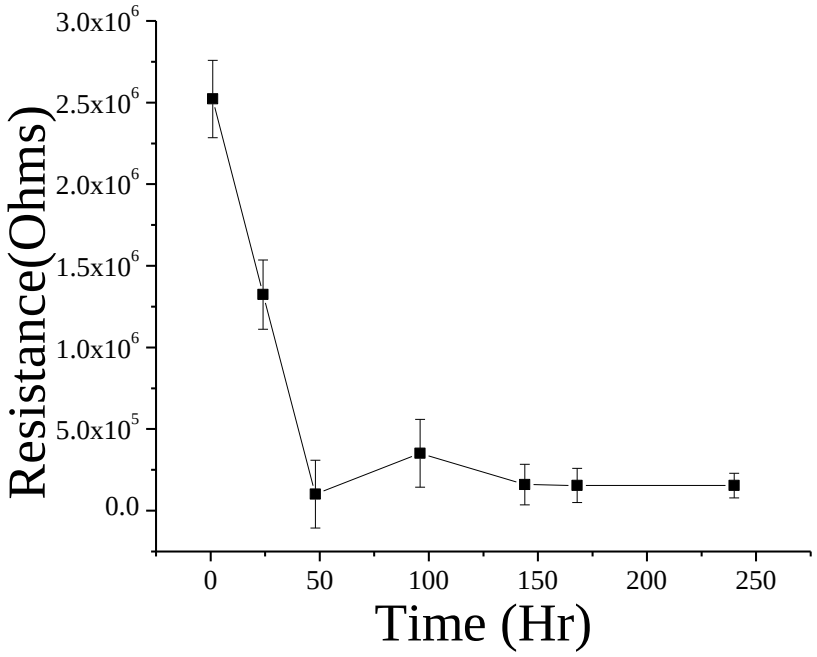

Figure 4.7. The Stability of PEVA/Carbon (18% VA) sensors over a 240 hour period: The sensors had a very high resistance soon after fabrication, and they start to stabilize after 2 days. Faster stabilization occurs if the sensors are hard baked or stored in a vacuum.

4.7.2. Effect of Temperature

In order to measure the effect of temperature on the stability of PEVA/carbon sensors (with vinyl acetate at 18%), the sensors were tested for a change in resistance at various temperatures without the presence of analyte gas. These temperatures included 0, 10, 25, 35, 40, 45 and 50 °C. The results are shown in figure 4.8 below. In order to see clearly, the maximum relative resistance change obtained at each temperature is plotted in figure 4.9. According to this plot, a slight proportional relationship was observed between resistance and temperature. For comparison, the sensors were tested during a temperature cycle, varying from -50 to 80 °C as shown in figure 4.10. The sensors showed a proportional relationship agreeing with results obtained from figure 4.9.

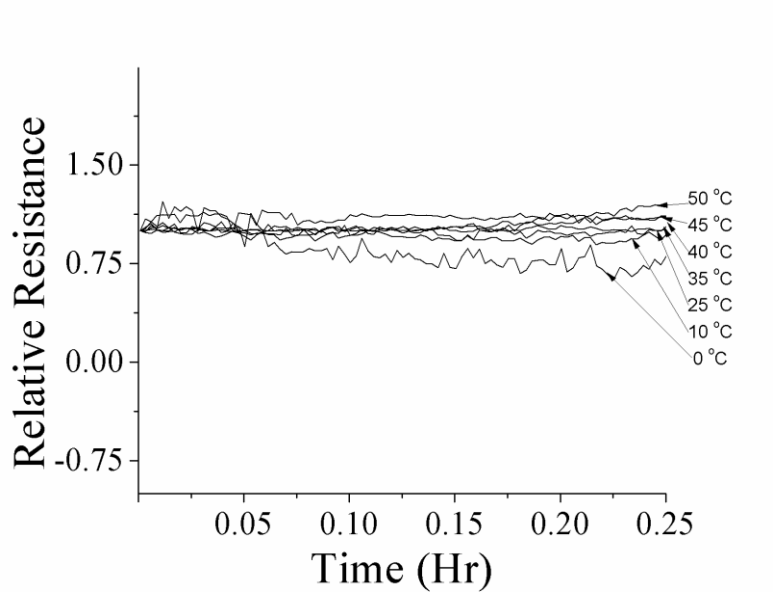

Figure 4.8. The resistance of the PEVA/Carbon Sensors at various temperatures: The resistances of the sensors were monitored at different temperatures including 50, 45, 40, 35, 25, 10 and 0°C without the presence of analyte gases, in room humidity conditions. The maximum resistance change obtained at each temperature was plotted and is displayed in figure 4.9.

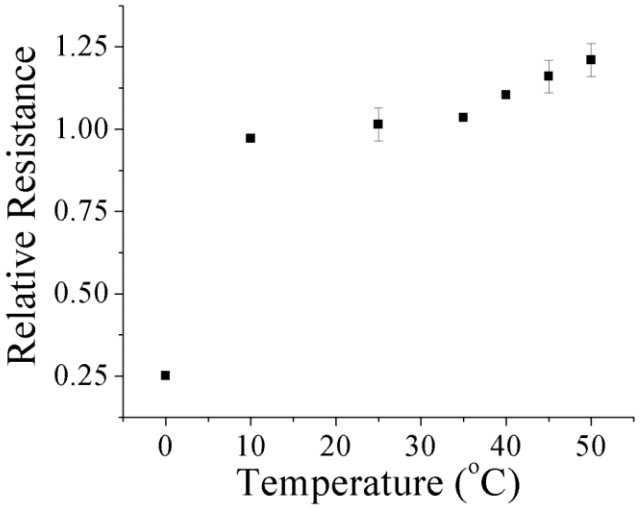

Figure 4.9. The maximum resistance changes obtained at different temperatures: The plot in figure 4.8 was reanalyzed to obtain maximum resistance changes at each temperature. The relative resistance change increased as the temperature increased.

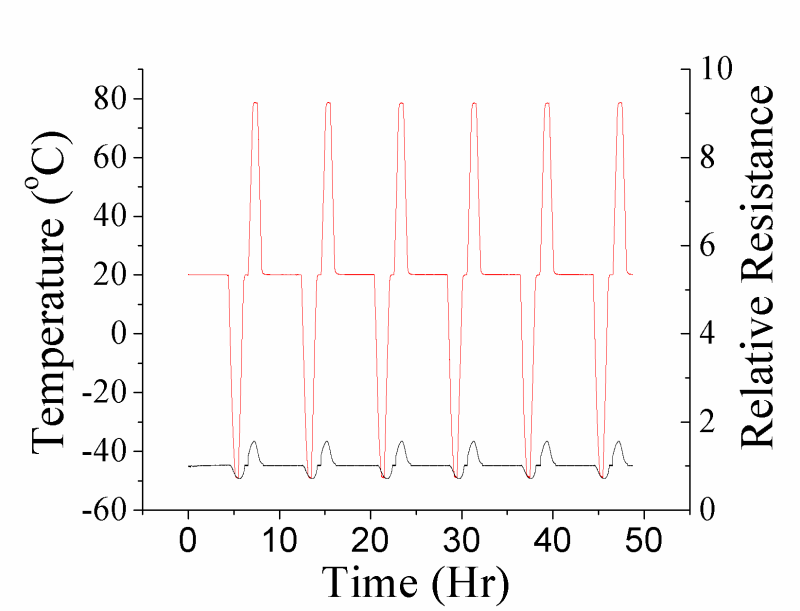

Figure 4.10. The resistance change of PEVA/carbon sensors during a temperature cycle: The resistances of PEVA/carbon sensors were measured for 5 cycles of temperatures varying from -50 to 80 °C. The resistance had a proportional change with temperature. This agrees well with the results illustrated in figure 4.7.

There are various mechanisms used to describe the dependence of temperature in polymer/carbon thin films, including tunneling, variable range hopping, thermal activation energy, and thermal expansion. The tunneling effect occurs at very low temperatures typically from 1-100K (-272 to -173 °C). The thermal activation model and variable range hopping models are effective at temperatures ranging from 80-300 K(-193 to 27 °C) and thermal expansion typically occurs for temperatures above room temperature. We are interested in the hopping mechanism, thermal activation mechanism and thermal expansion mechanism, which are applicable for the temperature range investigated in this study.

The variable hopping mechanism is often described for tunneling in granular or amorphous materials and has conductivities that fit equation 4.5 below, where ρ, ρ_o, A and T are resistivity, initial resistivity, activation energy and temperature respectively. This model was used to describe rubber/carbon composite materials in previous studies [10]. The exponent, n, can vary anywhere between 1/2, 1/3 or 1/4.

$$\frac{\rho_0}{\rho} = \exp(-\frac{A}{T^n}) \quad \text{Equation 4.5}$$

Many carbon polymer composites follow the thermal activation energy model described by previous works [11]. This model follows is essentially an arrhenius type relationship which is described by equation 4.6 below. ρ, ρ_o, A and T are resistivity, initial resistivity, activation energy and temperature respectively. The activation energy in this case is defined by equation 4.7 below. V_o is the height of the potential barrier, A the cross-sectional area of the junction, w the junction separation, and e the electron charge [10].

$$\frac{\rho_0}{\rho} = \exp(-\frac{A}{T}) \quad \text{Equation 4.6}$$

$$E = \frac{2V_{oA}}{\pi e^2 w} \quad \text{Equation 4.7}$$

The thermal activation model is used to describe the behavior of composites at higher temperatures, where an increase in resistance is caused by the separation of carbon particles due to increased flow of the polymers. This relationship would also follow an Arrhenius type relationship with temperature, where there will be a proportional relationship between resistivity and temperature.

For polymer/carbon sensors used in this application, the temperature dependence of resistance increase was expected to be a combination of the thermal activation model and the expansion model. Figures 4.9 and 4.10 were reanalyzed to create Arrhenius plots as shown in figure 4.11 and 4.12. Both plots seem to follow the Arrhenius model. The Arrhenius plot corresponding to the temperature cycle showed hysteresis similar to the Arhennius plot of polythiophene. The hysteresis was due to the change of polymer chain conformation. For the Arrhenius plot of resistance changes at different temperatures, two linear lines could be constructed below and above 20˚C. These correspond to two different activation energies for each plot. The activation energies calculated from each plot is shown in table 4.1.

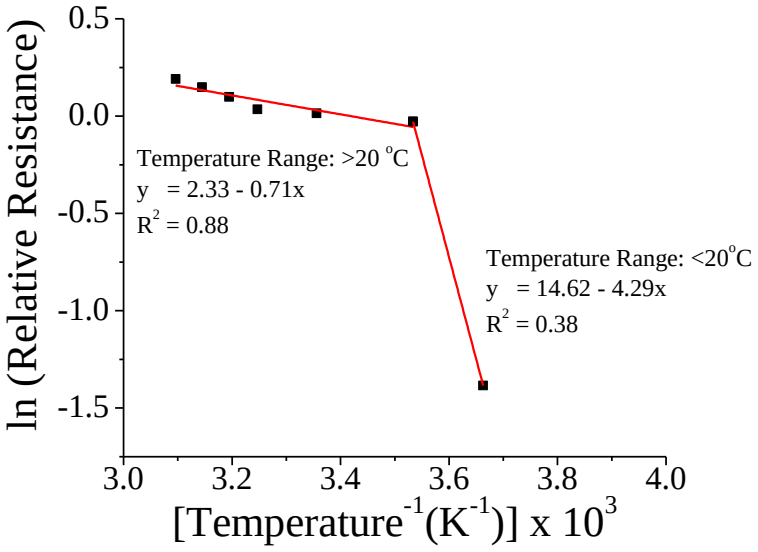

Figure 4.11. Arrhenius plot corresponding to resistance changes of PEVA/carbon sensors at different temperatures 0, 10, 25, 35, 40, 45 and 50 °C: The ln (relative resistance change) was plotted against 1/T of figure 4.9 was used to create an Arrhenius plot. There are two activation energies involved, meaning there seems to be two mechanisms responsible for the change in resistance with temperature.

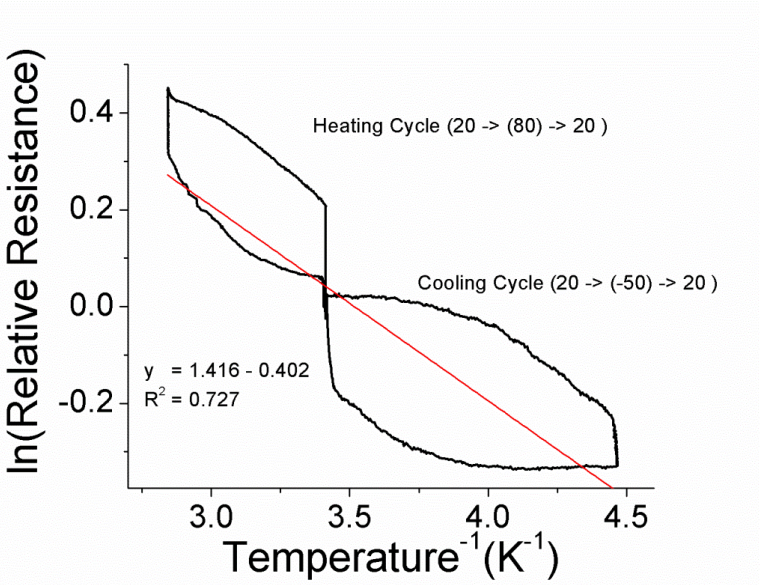

Figure 4.12. Arrhenius plot corresponding to resistance changes of PEVA/carbon sensors tested during a temperature cycle varying from -50 to 80 °C: The plot showed hystersis, corresponding to chain conformation caused by the heating and cooling cycles. The ln (relative resistance change) was plotted against 1/T of figure 4.10 was used to create an Arrhenius plot. There appears to be two activation energies, meaning there are two mechanisms responsible for the resistance as a function of temperature.

Table 4.1. Activation energy values calculated for Arrhenius plots in figure 4.10 and 4.11 at different temperature ranges: Two activation energy values were calculated from Arrhenius plots for the PEVA/carbon sensors illustrating the resistance change at different temperatures and during a temperature cycle. Two activation energies indicate that two mechanisms were responsible for the measured resistance change with temperature. The activation energy for the temperatures above 20 °C was more than the activation energy for temperatures below 20 °C.

Arrhenius Plot	Activation energy for temperatures < 20°C (kJ)	Activation energy for temperatures > 20°C(kJ)
Different temperatures: Figure 4.10	3.15	5.07
Temperature cycle: Figure 4.11	5.91	35.65

The two activation energies for each plot depicts that there are two mechanisms involved for the temperature dependence of the sensor stability. At lower, temperatures, the activation energy is low, and could be a combination of the thermal activation model and the thermal expansion model described above. At high temperatures, the activation energy is higher, and only the thermal expansion model is involved in this case. It should be noted that the resistance changes caused by temperature changes in film stability are negligible compared to resistance changes caused by γ-terpinene, i.e., the temperature changes caused by analyte vapor exposure is 3 orders of magnitude higher than the resistance changes caused by changes in temperature.

In order to investigate the effect of temperature with exposure to analyte gas, the resistance of the sensors were monitored at different temperatures including 10, 25, 30, 35 and 40 $^{\circ}$C, during exposure to γ-terpinene gas. The corresponding Arrhenius plot for maximum resistance changes at each of these temperatures is shown in figure 4.13.

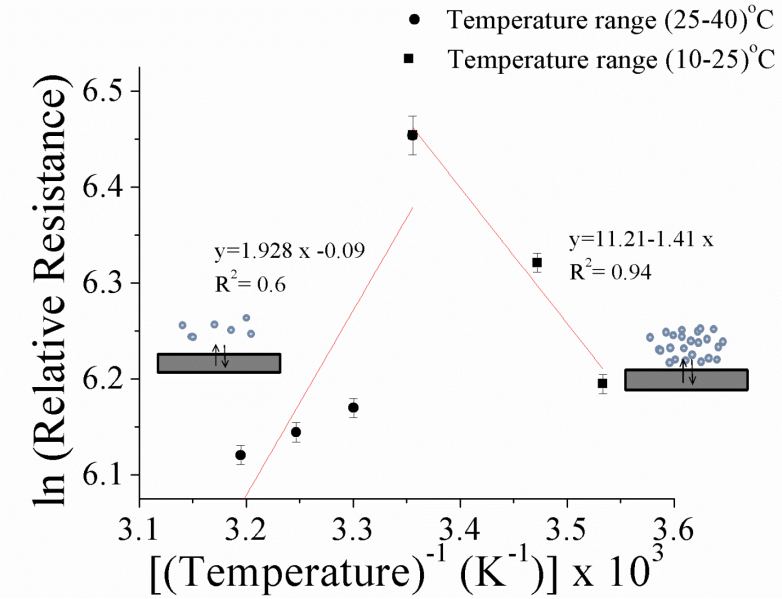

Figure 4.13. The Arrhenius plot corresponding to maximum resistance changes obtained at different temperatures with exposure to analyte gas: The maximum resistance changes were obtained at temperatures including 10, 25, 30, 35 and 40 °C. The graph can be separated into two regimes, one at the temperatures below 25 °C where the activation energy is positive and the other for temperatures above 25 °C where the activation energy is negative.

According to figure 4.13, for temperatures above 25 °C, the slope of the Arrhenius curve was negative with a positive Arrhenius energy value. For temperatures below 25 °C, the slope of the curve was positive, with a negative activation energy. The temperature dependence of the sensor while exposed to anlayte gas could be explained in terms of diffusion, absorption and desorption. γ-terpinene gas molecules are absorbed by the surface of PEVA/carbon film and then diffused into the film. At the same time, desorption occurs. The diffusion increases with increasing temperature. However the equilibrium between adsorption and desorption adjusts with temperature. At low temperature the adsorption –desorption equilibrium is in the adsorption direction. At low temperatures, since there are enough gas molecules on the surface to be absorbed, diffusion governs the process. Therefore the response of the sensor increases with increasing temperature. As the temperature continues to increase above 25 °C, adsorption – desorption equilibrium of the gas molecules is in the desorption direction, and the number of gas molecules on the surface is smaller. Therefore, even though the diffusion rate increases, since the quantity of gas molecules on the surface is low, the absorption rate decreases, decreasing the sensor response. The activation energy of the diffusion governed mechanism from 25-40 °C and the absorption governed process from 10-25 °C can be calculated from the slopes of the plot. The calculated activation energy for diffusion governed and absorption governed process was 16.03 kJ and – 11.72 kJ respectively.

4.7.3. Effect of Humidity

In order to investigate the effect of humidity on polymer/ carbon sensors, PEVA/carbon sensors with 18% VA were exposed to γ-terpinene under various humidity conditions. In the first 24 hours, the sensors were exposed to nitrogen with a specific humidity (85%, 60%, 45%,

25%), and in the next 24 hours the sensors were exposed to γ-terpinene with that specific humidity. The humidity levels were adjusted by exposing the carrier gas to various saturated salt solutions. As seen in figure 4.14, there was no significant change in resistance in the first 24 hours for all four conditions. When the sensors were exposed to γ-terpinene analyte vapor, there was a large change in the resistance due to the γ-terpinene but no apparent relationship between the sensor response and the humidity conditions. The relative resistance change due to analyte vapor exposure was nearly 2 orders of magnitudes greater than the relative resistance caused by changes in humidity.

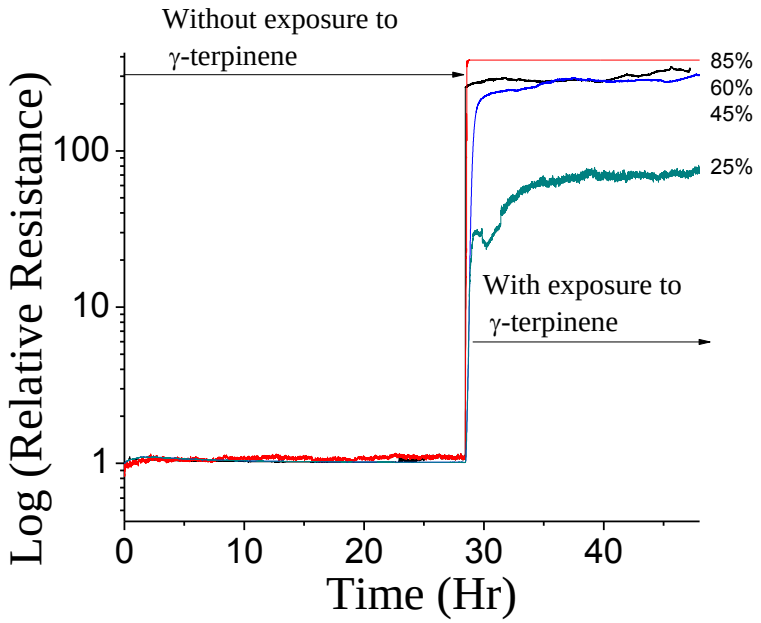

Figure 4.14. The Effect of humidity on PEVA/Carbon sensors: During the first 24 hours, the sensors were exposed to γ-terpinene vapor at different humidity conditions. The sensors were tested for different humidity conditions including 25, 45, 60 and 85 % RH. In the next 24 hours, the sensors were exposed to analyte vapor at different humidity conditions. The relative resistance change due to analyte vapor exposure was nearly 2 orders of magnitudes greater than the relative resistance caused by changes in humidity.

4.8. Effect of Concentration

In order to see the effect of γ-terpinene concentration on the sensor response and the detection limit of the sensor, the sensor was exposed to different controlled concentrations of γ-terpinene gas. The concentration was controlled by the flow rate. The vapor flow from the analyte flask was maintained at 0.2 L/min and was diluted by a second flow of pure nitrogen at flow rates of 0.85, 0.75, 0.45. 0.3, 0.15 and 0 L/min corresponding to concentrations of 1, 5, 18, 32, 42 and 50 ppm respectively. These concentrations were calculated using the methods described in section 2.8 using gas chromatography. The responses obtained at each of these concentrations are shown in figure 4.15. According to the graph, the resistance changes with increasing concentration.

The maximum resistance changes normalized with time was plotted at each concentration to obtain the detection limit. The detection limit was calculated using IUPAC standard, where the detection limit is equal to the intersection of the extrapolated linear portion of the calibration graph and baseline of the calibration curve. The maximum resistance changes at each concentration are shown in figure 4.16. The resistance changes at low concentration values were used to create the baseline. The detection limit calculated for the PEVA/Carbon sensors was equal to 25 ppm $\pm$ 0.5. The concentration of volatiles emitted by plants is 100 ppm. Therefore the detection limit of the PEVA/carbon sensor is sufficient to detect the insect infestation. The resistance change of the sensor also increased as the concentration of the analyte vapor increased.

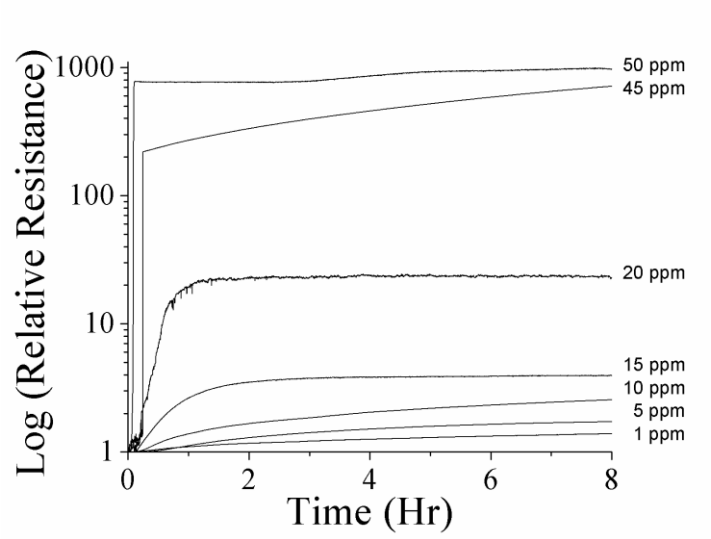

Figure 4.15. The response of PEVA/carbon sensors at different concentrations: The PEVA/carbon sensors were tested at different concentrations including 50, 45, 20, 15, 10, 5 and 1 ppm, at room temperature and humidity conditions. The response of the sensors increased with increasing concentration.

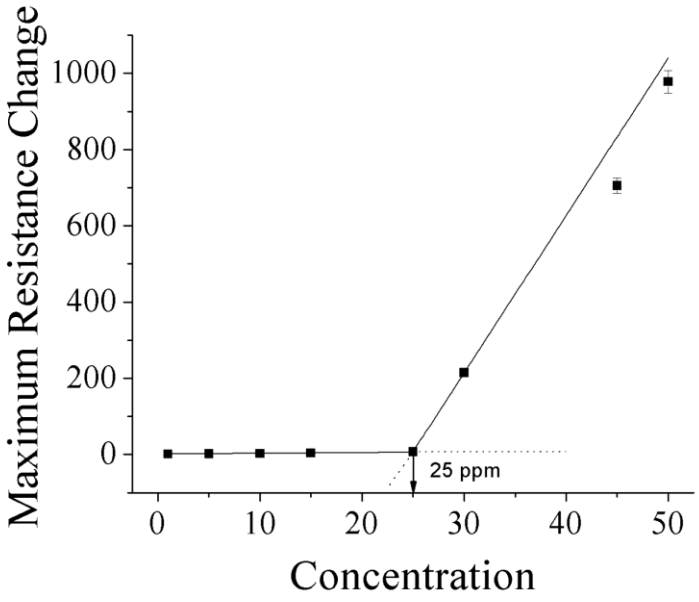

Figure 4.16. Calculating the detection limit of PEVA/carbon sensors: The maximum resistance change of each sensor was plotted with concentration. The baseline was obtained by using the maximum resistance changes obtained at lower concentration values. The detection limit using this method was 25 $\pm$ 0.5 ppm.

4.9. Response of Sensors to Various Analyte Gases

The sensor was exposed to various types of plant volatiles including γ-terpinene, α-pinene, p-cymene, farnesene, and limonene and cis-hexenyl acetate. As shown in figure 4.17, the sensor was tested and found to be sensitive to all the vapors mentioned. A flow rate of 0.2 L/min was used, which corresponded to concentrations of 50 ppm, 65 ppm, 50 ppm, 65 ppm, 64 ppm and 43 ppm of γ-terpinene, limonene, farnasene, α-pinene, p-cymene and cis-hexylacetate, respectively. These concentrations were calculated using the gas chromatography techniques described in section 2.7

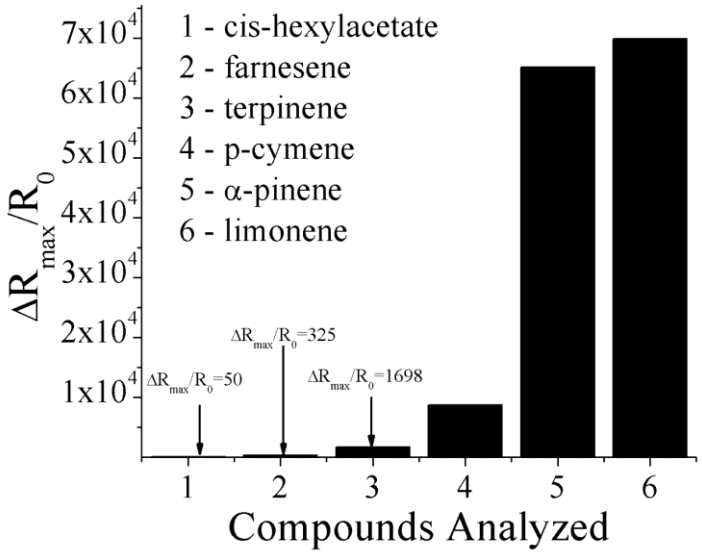

Figure 4.17. Sensitivity of PEVA sensors to various chemicals: The sensor was found to be sensitive to various compounds including γ-terpinene, α-pinene, p-cymene, farnesene, and limonene and cis-hexenyl acetate.

4.10. References

[1] B. C. Sisk and N. S. Lewis, "Vapor Sensing Using Polymer/Carbon Black Composites in the Percolative Conduction Regime", *Langimuir*, vol. 22 (18), pp. 7928-7935, 2006.

[2] N. Tsubokawa, Y. Shirai, M. Okazaki and K. Maruyama, "A Novel Gas Sensor From Crystalline Polymer-Grafted Carbon Black: Responsibility of Electric Resistance of Composite From Crystalline Polymer-Grafted Carbon Black Against Solvent Vapor", *Polymer Bulletin*, vol. 42, pp. 425-431, 1999.

[3] J. Chen, and N. Tsubokawa, "A Novel Gas Sensor from Polymer-Grafted Carbon Black: Responsiveness of Electric Resistance of Conducting Composite From LDPE and PE-b-PEO Grafted Carbon Black in Various Vapors", *Polymers for Advanced Technologies*, vol. 11, pp. 101-107, 2000.

[4] M. C. Lonergan, E. J. Severin, B. J. Doleman, S. A. Beaber, R. H. Grubbs and N. S. Lewis, "Array-Based Vapor Sensing Using Chemically Sensitive, Carbon Black-Polymer Resistors", *Chemical Materials*, vol. 8, pp. 2298-2312, 1996.

[5] E. J. Severin, N. S. and Lewis, "Relationships Among Changes on a Coated Quartz Crystal Microbalance, Thickness Changes, and Resistance Responses of Polymer-Carbon Black Composite Chemiresistors", *Analytical Chemistry*, vol. 72(9), pp. 2008-2015, 2000.

[6] A. R. Hopkins and N. S. Lewis, "Detection and Classification Characteristics of Arrays of Carbon Black/Organic Polymer Composite Chemiresistive Vapor Detectors for the Nerve Agent Stimulants Dimethylmethylphosphonate and Diisopropylmethylphosphonate", *Analytical Chemistry*, vol. 73(5), pp. 884-892, 2001.

[7] J. Chen and N. Tsubokowa, "A Novel Gas Sensor From Polymer-Grafted Carbon Black: Responsiveness of Electric Resistance of Conducting Composite from LDPE and PE-b-PEO Grafted Carbon Black in Various Vapors", *Polymers for Advanced Technologies*, vol. 11, pp. 101, 2000.

[8] X. Dong, R. W. Fu, M. Q. Zhang, B. Zhang, Z. Rhong, "Electrical Resistance Response of Carbon Black Filled Amorphous Polymer Composite Sensors to Organic Vapors at Low Vapor Concentrations", *Carbon*, vol. 42, pp. 2551, 2004.

[9] M. B. Heaney, "Measurement and Interpretation of Nonuniversal Critical Exponents in Disordered Conductor-Insulator Composites", *Physical Reviews B.* , vol. 52 (17), pp. 12477-12480, 1995.

[10] M. G. Alexander, "Anormalous Temperature Dependence of Electrical Conductivity of Carbon-poly(Methyl Methacrylate) composites", *Materials Research Bulletin*, vol. 34(4), pp. 603-611, 1999.

[11] M. L. Homer, J. R. Lim, K. Manatt, A. M. Manfreda, L. Lara, A. D. Jewell, S. P. S. Yen, H. Zhou, A. V. Shevada, M. A. Ryan, "Temperature Effects on Polymer-Carbon

Composite Sensors: Evaluating the Role of Polymer Molecular Weight and Carbon Loading", *Proceedings of IEEE*, vol. 2, pp. 877-881, 2003.

Chapter 5

Polyaniline Sensors for Plant Volatile Detection

5.1. Polyaniline Sensors for Volatile Vapor Detection

Polyaniline sensors have been used in various applications involving volatile vapor detection because of its ease of fabrication and ability to detect volatile organic compounds at room temperature. Low mass fraction polymer/carbon composite sensors are reported to be highly responsive to a variety of organic volatile compounds. In addition they are highly stable, inexpensive and easy to fabricate [1-4].

Polyaniline exists in three well defined oxidation states: leucoemaraldine, emaraldine and pernigraniline. These states are illustrated in figure 5.1. The leucoemaraldine state is the fully reduced state, where all the nitrogen atoms present are amines. The pernigraniline state is the fully oxidized state where all the nitrogen present are imines. In the emaraldine state the imine to amine ratio is 1:1. Therefore, leucoemaraldine and pernigraniline states are insulating while the emaraldine is electrically conducting. Leucoemaraldine can be converted to emaraldine chemically or electrochemically, and when emaraldine is further oxidized, the resulting product is pernigraniline. In addition, a decrease in conductivity of ten orders in magnitude can be created by treating emaraldine with alkaline media. Commercially obtained emaraldine base used in this study is such a treated material. In general, aniline monomer is electrochemically polymerized to result in polyaniline. [5]

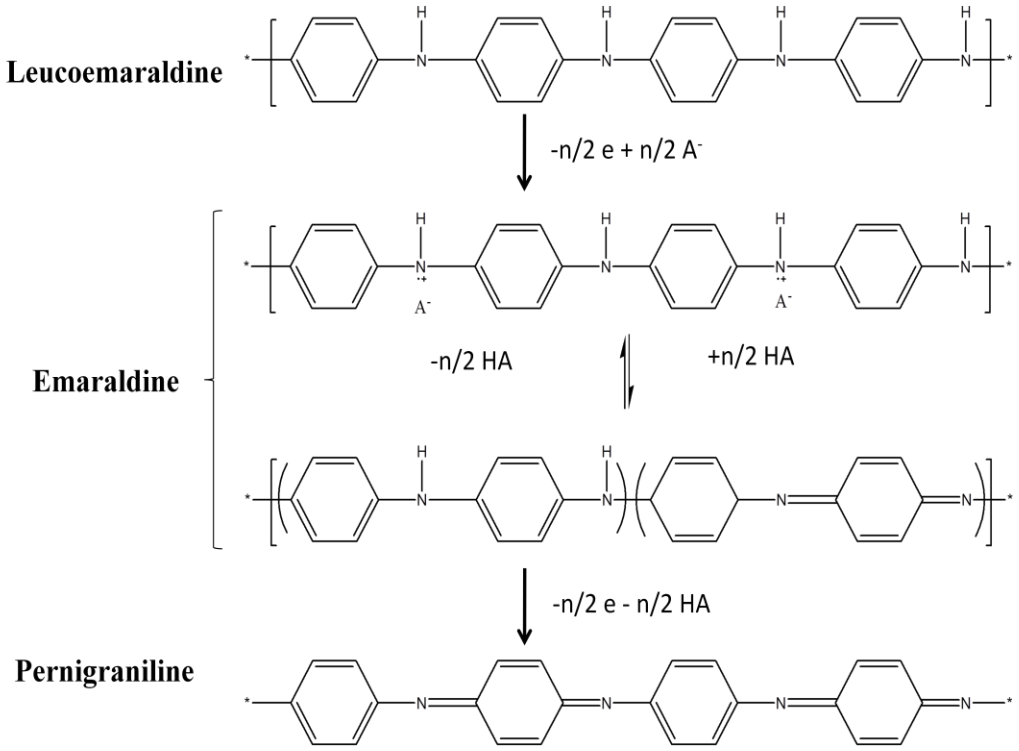

Figure 5.1. Generalized oxidative and non oxidative doping of polyaniline [5]: There are three oxidation states leucoemaraldine, emaraldine and pernigraniline. Leucoemaraldine is the fully reduced state while pernigraniline is the fully oxidized state. Emaraldine state is the in between state with a 1:1 ratio of amine to imine groups.

The main mechanism of detection of volatile organic compounds by polyaniline film sensors is redox based, where polyaniline is reduced or oxidized by partially polarized volatile organic compounds. For example, polyaniline films detecting methanol would undergo the reaction mechanism as illustrated in figure 5.2, where the polarized methanol molecule reduces the imine groups, changing the resistance of the polymer film [4-5].

Polyaniline sensors detecting volatile organic compounds would also have a secondary mechanism involving swelling. It should be noted that if both redox and swelling mechanisms are present, depending on whether the analyte vapor is reducing or oxidizing the polymer chain, the redox mechanism may or may not compete with the swelling mechanism. The main purpose of having a polyaniline sensor in this study is to increase the sensor array diversity, through having a sensor that would react differently between polar and non polar compounds. Since the swelling mechanism would be present in the sensors when exposed to all analytes, the sensor would show different responses to polar and non polar analytes. However, the degree of resistance change caused by the swelling mechanism by each analyte would differ, with the chemical structure. In this study six type of analytes were investigated: γ-terpinene, α-pinene, p-cymene, farnesene, limonene and cis-hexenyl acetate. The structures of these compounds are shown in figure 5.3 below. All the structures have double bonds, and are expected to have some amount of polarity present. However cis-hexyl acetate should be particularly polar due to the presence of an oxygen containing group.

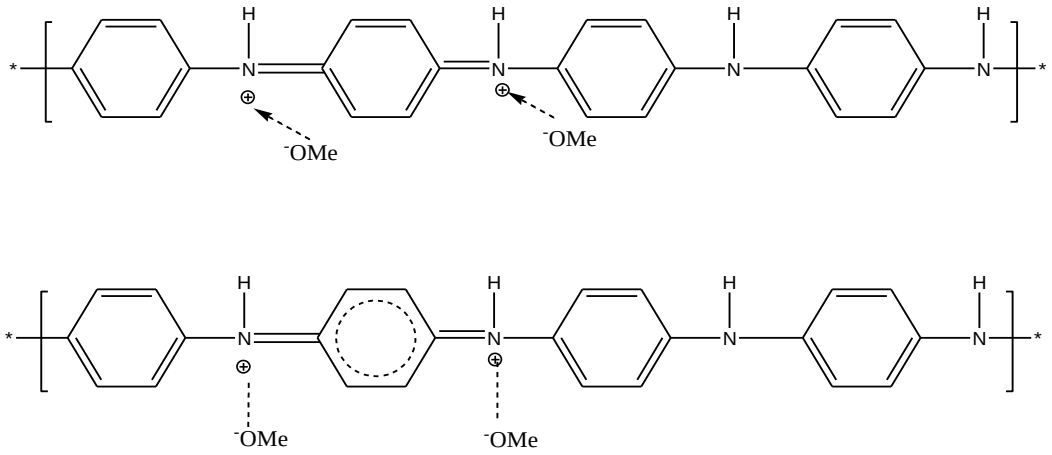

Figure 5.2. Mechanism of polyaniline detecting methanol [2]: The polarized methanol molecule reduces the imine groups, changing the resistance of the polymer film.

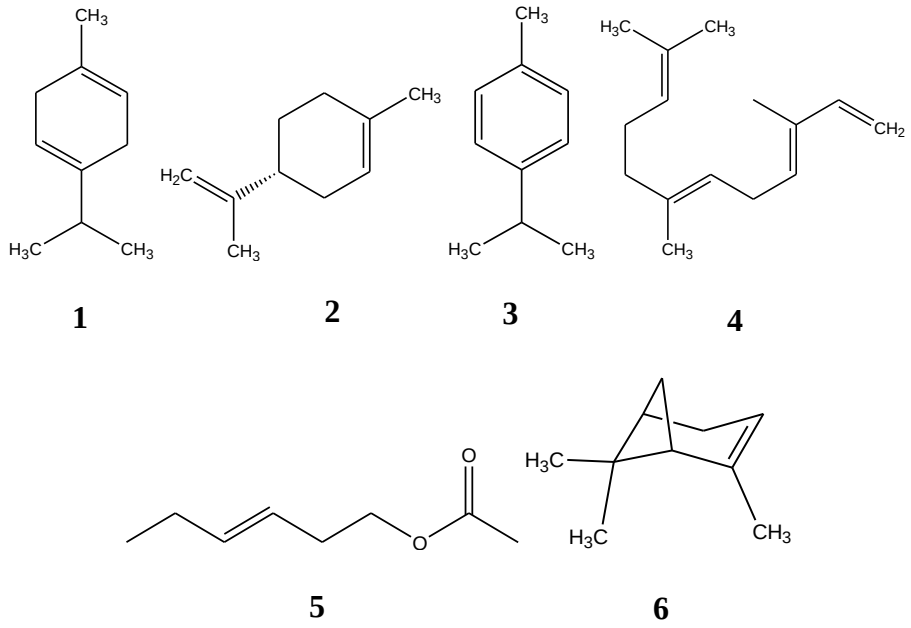

Figure 5.3. The structures of various plant volatiles 1) γ-terpinene 2) α-pinene 3) limonene 4) farnesene, 5) cis-hexenyl acetate and 6) p-cymene: All structures have a double bond which contributes towards polarity. Cis-hexyl acetate should be particularly polar due the presence of an oxygen molecule.

5.2. Response of Polyaniline Sensors Detecting Various Plant Volatiles

Polyaniline sensors that were fabricated by drop casting polyaniline emaraldine base /benzene solution onto chemiresistor sensors were exposed to various plant volatiles. The maximum resistance change (sensitivity) observed for each of the chemicals is shown in figure 5.4. The experiment was carried out using the vapor exposure and measurement system described in chapter 2, at room temperature and humidity conditions. The flow rate of nitrogen through the system was maintained at 0.2 L/min.

According to figure 5.4, the resistance change was the largest for cis-hexenyl acetate. The mechanism of the sensor detecting the above volatiles is complex, consisting of swelling and redox mechanisms, although the major mechanism involved increased the resistance of the polyaniline film.

5.3. Environmental Stability of Polyaniline Sensors

The stability of polyaniline sensors was investigated by monitoring the resistance of the sensors when exposed to various temperature and humidity conditions. The sensors were also tested in air to determine the effect of ambient gases present on the sensor performance. The temperature tests were done at various temperatures varying from 10 – 40 $^{\circ}$C. The tests were done without and with the exposure to analyte gases. The sensors were also tested during a temperature cycle varying from -50 –to 80 $^{\circ}$C. The humidity experiments were done at different humidity conditions varying from 25-85%. The sensors were first exposed to the carrier gas nitrogen and then to the analyte vapor, γ-terpinene, at various humidity conditions.

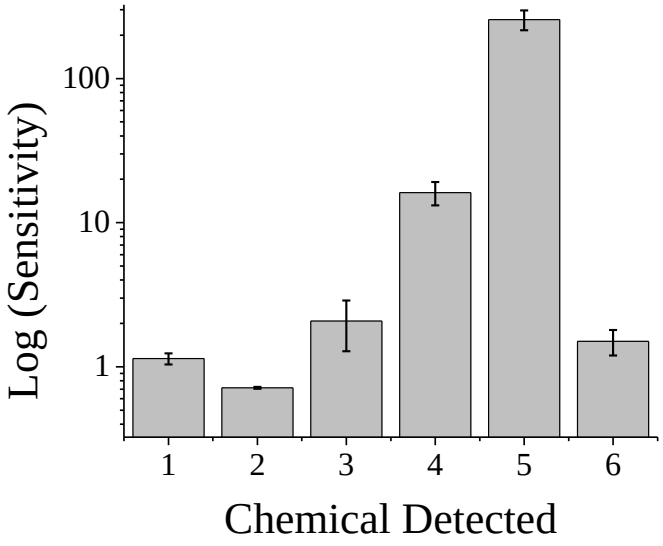

Figure 5.4. The sensitivity towards various plant volatiles: 1) γ-terpinene, 2) α-pinene, 3) limonene, 4) farnesene, 5) cis-hexenyl acetate, and 6) p-cymene: The response was greatest for cis-hexenyl acetate.

5.3.1. Effect of Temperature

In order to investigate the effect of temperature on the sensor performance, the response of the sensor was tested under a temperature cycle varying from -50 to 80 °C. The sensors were tested in air, at room humidity conditions, without the presence of analyte gas. The resistance change was observed for six cycles. The response is shown in figure 5.5 below. According to the graph, at low temperatures below 20 °C, the resistance increased as temperature decreased. However at higher temperatures above 20 °C, the resistance increased as the temperature increased. After each temperature cycle, the temperature returns to 20 °C and is maintained at 20 °C for 30 minutes. During this period, the resistance stayed constant. It was also interesting to see that the resistance change increased with each additional temperature cycle. The Arhennius plots for all temperature cycles, and the first cycle is shown in figure 5.6 and 5.7 respectively. As seen in figure 5.6, similar to PEVA and polythiophene films, polyaniline also showed hysteresis behavior. This was a result of change in polymer chain conformation. The width and values of the hysteresis loop increased with each cycle. The progressive decrease in width could be due to an increase in stability of polymer chains after each heating and cooling cycle. The increase in overall resistance could be thought to be a result of thermal fatigue. The material will fail eventually if temperature cycles are continued.

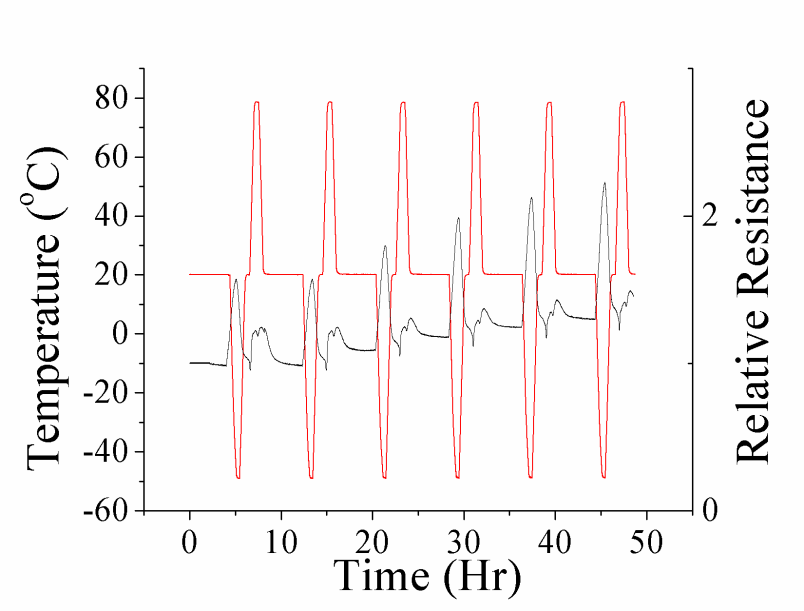

Figure 5.5. Resistance change values observed during a temperature cycle varying from -50 °C to 80 °C: At low temperatures resistivity increased with decreasing temperature, while at high temperatures the resistivity increased with increasing temperature. The resistance change also seems to increase with additional temperature cycles.

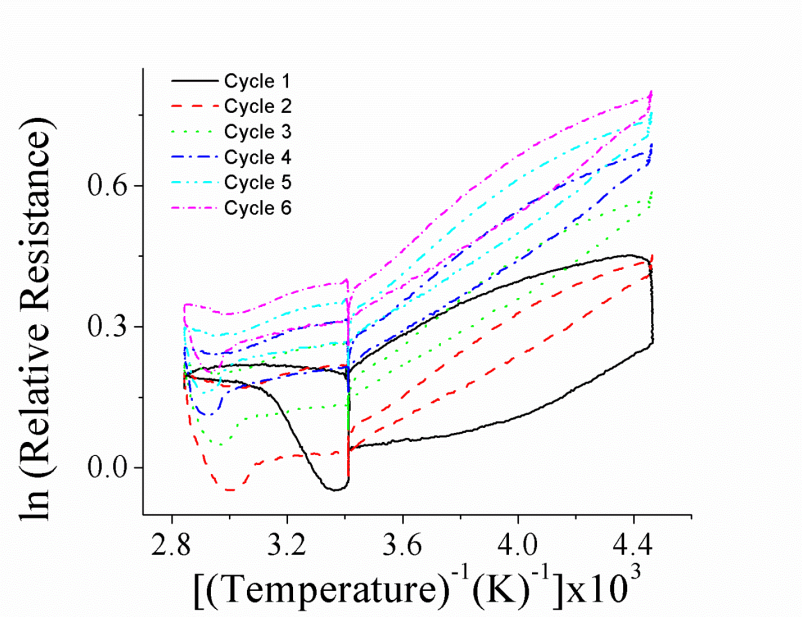

Figure 5.6. The Arrhenius plot corresponding to 5 temperature cycles: All plots corresponding to each cycle consisted of a hysteresis loop, which increased with every cycle. The Arrhenius plot was widest for the first plot. The Arrhenius plot for the first cycle is shown in figure 5.7.

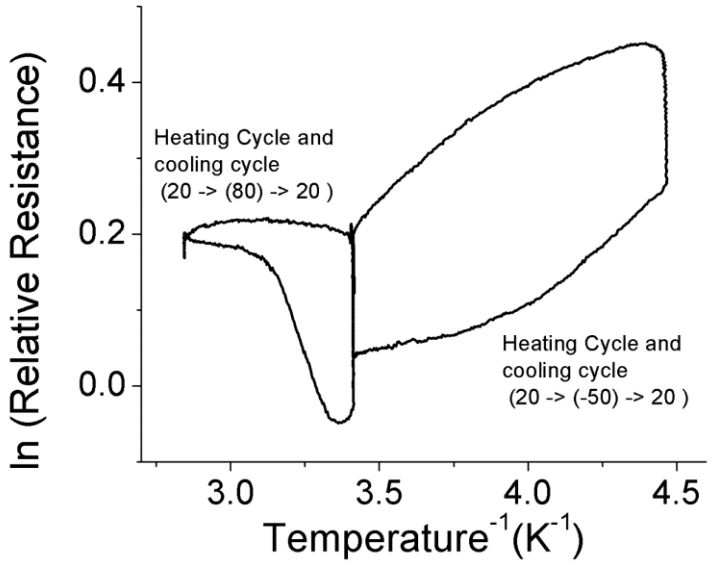

Figure 5.7. The Arrhenius plot corresponding to the first temperature cycle: The hysteresis was a result of change in polymer chain conformation. Parts of this Arrhenius plot were made to better understand the temperature dependence of polyaniline sensor films.

Polyaniline undergoes an insulator-metal transition upon oxidation or reduction, although the exact properties of the metallic state of the polymer remain a puzzle. One of these many properties that has been studied extensively is the temperature dependence. At low temperatures polyaniline has a so called "granular-metal" like behavior or a quasi 1 dimensional variable range hopping. In a granular metal, the electrons do a random walk between well distributed metallic islands. In the hopping model, the electrons hop along a line (hopping in transverse directions is very small) [7-9]. In both these cases, the resistivity, ρ, changes with temperature as illustrated by equation 5.1 below. The typical temperature range for this type of behavior is from 30 K to 280 K (-243 °C to 7 °C).

$$\frac{1}{\rho} = \frac{1}{\rho_o} \exp\left[-\left(\frac{T_o}{T}\right)^{0.5}\right] \quad \text{Equation 5.1}$$

Above 280 K or higher, the resistivity shows an Arrhenius type behavior, where resistance scales proportionally with (1/T). In order to see whether each of these relationships hold true for resistance value changes in figure 5.5, the resistance values were plotted differently for temperatures below and above 280 K (7°C). Figure 5.8 shows the ln (1/relative resistance) vs Temperature$^{-1/2}$ values for temperatures below 7°C. The plot was fitted linearly, with a R^2 value of 0.98. Therefore, in this region, the polyaniline shows a granular metal or quasi 1 dimensional hopping like behavior with temperature change. Figure 5.9 shows the Arrhenius plot for temperatures above 7°C. The Arrhenius energy can be calculated from the slope of the graphs. The plot had a positive Arrhenius energy of 2.64 kJ up to a temperature of 59°C, but a negative Arrhenius energy of 12.62 kJ for temperatures above 59 °C. This might be due to a change in

chain structure at high temperature. At high temperatures, polyaniline chains straighten out and charge conduction along the chains becomes easy, which will decrease the resistance of the film.

It was also interesting to see that the resistance changes observed seems to get greater with each cycle. Each temperature cycle seems to have a annealing effect on the polyaniline film, which will increase the crystallinity of the film. The increased crystallinity explains the observed resistance changes of the sensors.

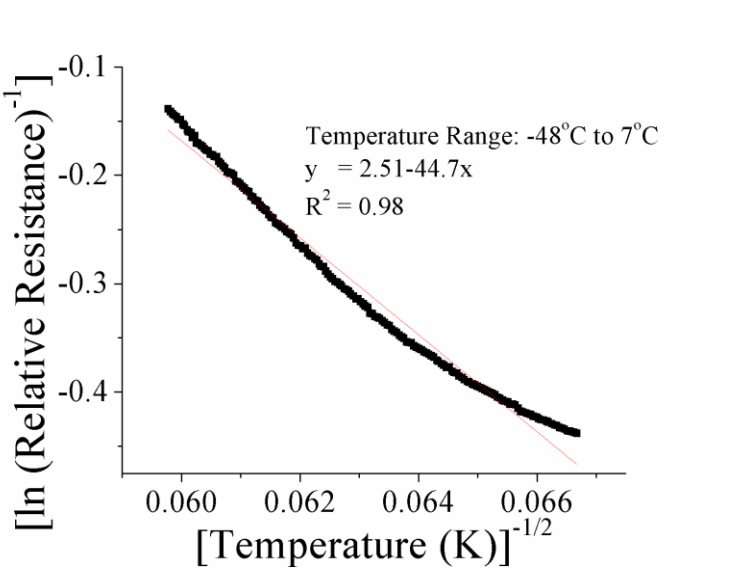

Figure 5.8. The extraction of temperature resistance change of polyaniline sensors for temperatures below 7 °C, tested in air, without the presence of analyte vapor: The resistance change showed a proportional relationship between ln (1/(relative resistance) and (temperature)$^{-1/2}$, which is consistent with the granular metal like behavior or quasi 1D hopping models illustrated in literature to describe the temperature behavior of polyaniline films at low temperatures.

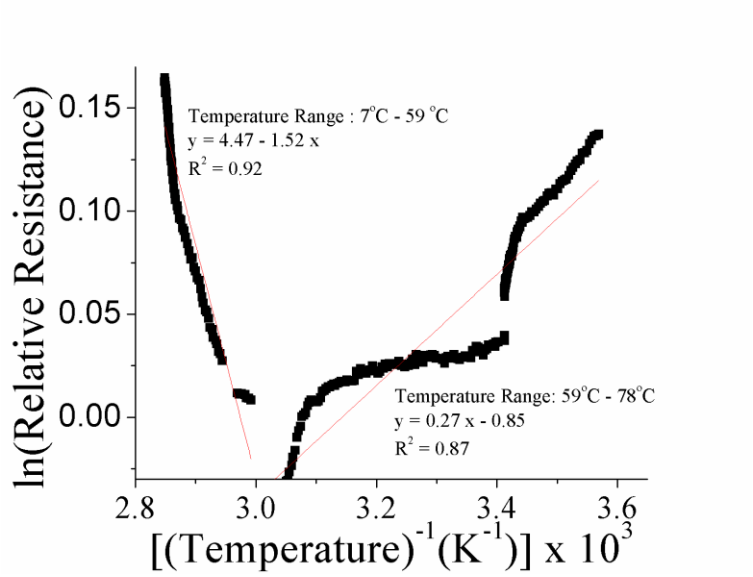

Figure 5.9. The extraction of temperature resistance change of polyaniline sensors for temperatures above 7 °C, tested in air, without the presence of analyte vapor: For temperatures up to 59 °C, The resistance change showed a proportional relationship between ln (relative resistance) and (temperature)$^{-1}$, which is consistent with the Arrhenius model. For this range the calculated Arrhenius energy was 12.62 kJ. For temperatures above 59 °C, there was a deviation from Arrhenius behavior, where a further increase in temperature causes the polymer chains to straighten, increasing the mobility of charged carriers and decreasing the resistance of the film.

Since the resistance change due to analyte vapor was comparable to the resistance change due to change in temperature, a baseline was created to extract the temperature effects, similar to baselines used to normalize data for metal oxide sensors. To obtain a baseline, resistance changes due to temperatures varying from 10-50 $^{\circ}$C was plotted for each temperature. The resistance changes were plotted for temperatures 10, 15, 35, 40 and 50 $^{\circ}$C. The resistance changes at each of these temperatures are shown in figure 5.10.

The baseline along with the sensor responses to analyte vapor at 10, 15, 25, 35 and 40 $^{\circ}$C are shown in figure 5.11 below. This temperature range was selected because the sensors will typically be used at temperatures between 10 – 40 $^{\circ}$C.

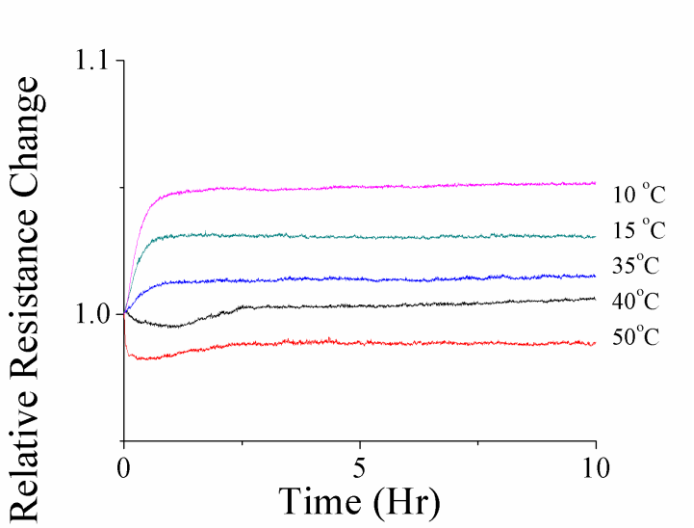

Figure 5.10. The resistance changes observed at various temperatures: The relative resistance change of sensors was observed at 10, 15, 35, 40 and 50 °C to create a baseline for polyaniline sensors. The sensors were tested without the presence of analyte gas.

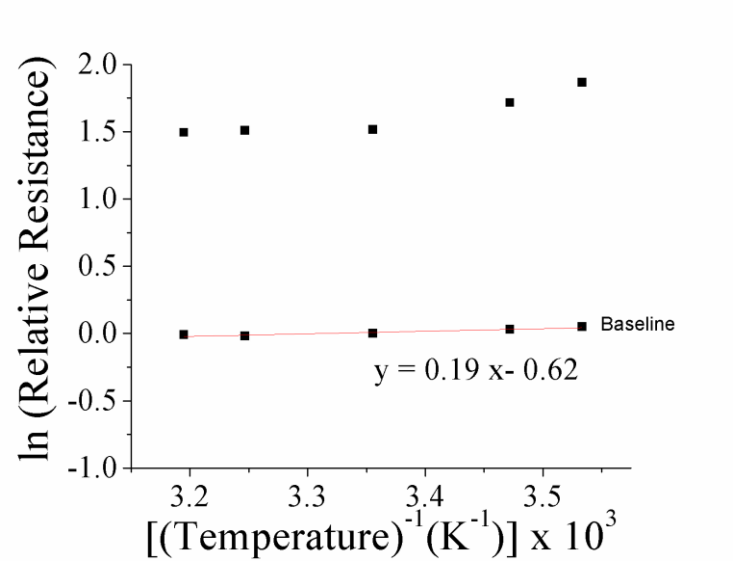

Figure 5.11. The baseline created for polyaniline sensors used to detect insect infestation: The baseline equation was y = 0.19x-0.62, and can be used to adjust the response of polyaniline sensors detecting insect infestation in fields with variable temperatures.

5.3.2. Effect of Humidity

Figure 5.12 shows the response of sensors to γ-terpinene vapor with different humidities. As a control experiment the sensor was exposed to nitrogen with a specific humidity nitrogen for the first 24 hours, and then exposed γ-terpinene with a specific humidity for the next 10 hours. The humidity of the nitrogen was varied by using different salt solutions. The sensor response when exposed to nitrogen with different humidities is identical, i.e., there is no effection humidity on the sensor itself. However the presence of humidity during exposure to the analyte, γ-terpinene, does increase the sensor's response to that analyte gas.

5.3.3. Effect of Ambient Gases

In order to test the stability of polyaniline sensors under the presence of ambient gases, the resistances of the sensors were monitored for a 72 hour period, under air. The results are shown in figure 5.13 below. According to the test results, the sensors are stable after a period of 150 hours (6 days). Therefore, for the sensor array experiments, the sensors were allowed to stabilize over a 1 week period. After stabilization, the sensors do not change their resistance in the presence of ambient gases.

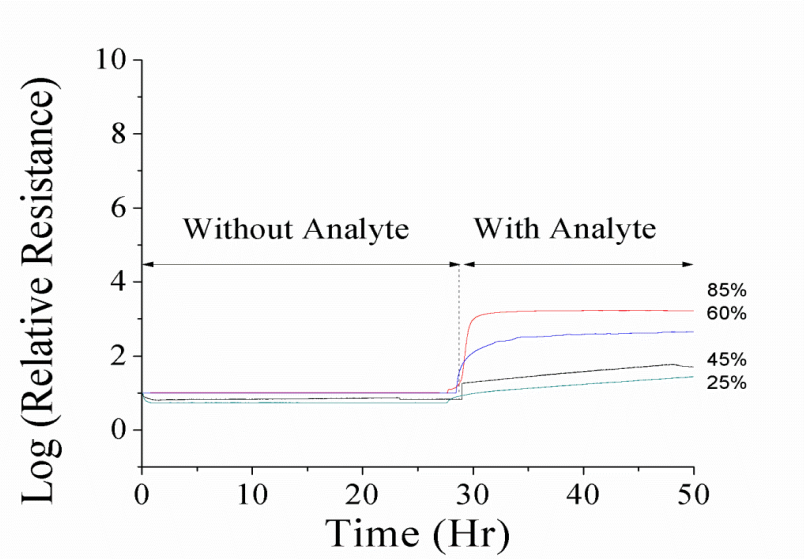

Figure 5.12. Effect of humidity on polyaniline sensors: The sensors were first exposed to nitrogen gas with variable humidity for the first 24 hours and then exposed to γ-terpinene with variable humidity. The variable humidity had nearly no effect on the sensor response to nitrogen, but increased the sensor's response to γ-terpinene.

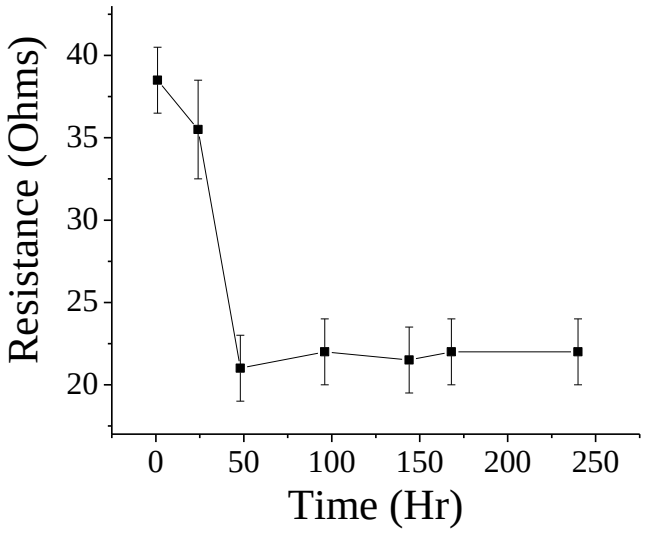

Figure 5.13. The stability of the polyaniline sensors: The sensors were tested in air for a 250 hour period. The polyaniline sensors took 50 hours to stabilize after microfabrication, and after that were ready to use for sensor applications.

5.5. Concentration Dependence of Polyaniline Films

To determine the concentration dependence and detection limit of the polyaniline sensor, the sensor was exposed to different concentrations of the analyte vapor, γ-terpinene. The response of the sensor increased with increasing concentration as expected. The responses obtained for various concentrations are shown in figure 5.14. The maximum resistance change at each concentration was calculated and is plotted in figure 5.15. According to IUPAC standards, the detection limit is the concentration at which the extrapolated linear portion of the calibration graph intersects the baseline of the calibration curve [10]. The maximum resistance values at low concentrations were used to create the baseline, and the maximum resistance changes at higher temperatures were used to create the calibration graph. The intersection point is equal to the detection limit of the sensor. According to figure 5.15, the detection limit of the sensor was 9 ± 1 ppm. This was sufficient enough to detect insect infestation in agricultural fields, because phytochemicals are emitted at an average concentration of 100 ppm.

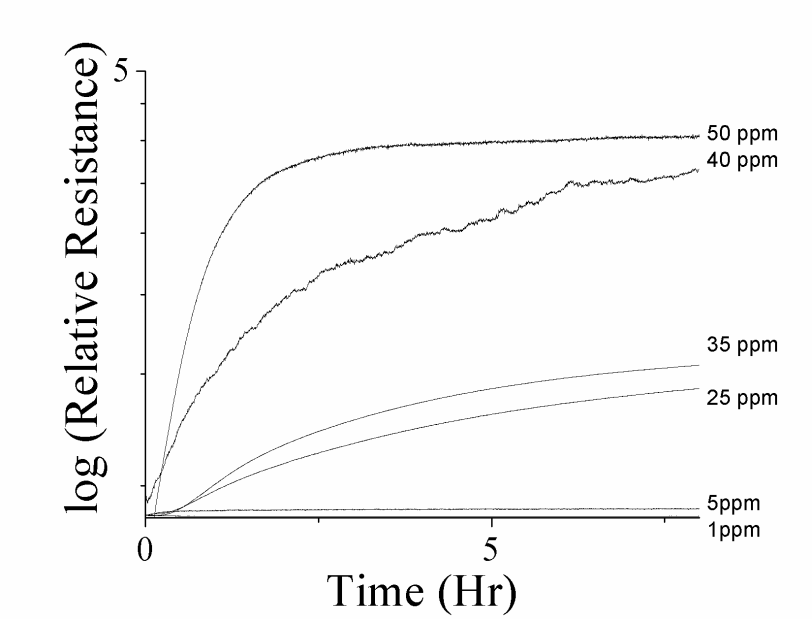

Figure 5.14. The response of polyaniline sensors when exposed to different concentrations of γ-terpinene: The response of the sensor increased with increasing concentration. The maximum resistance change at each concentration was used to calculate the detection limit of the sensor.

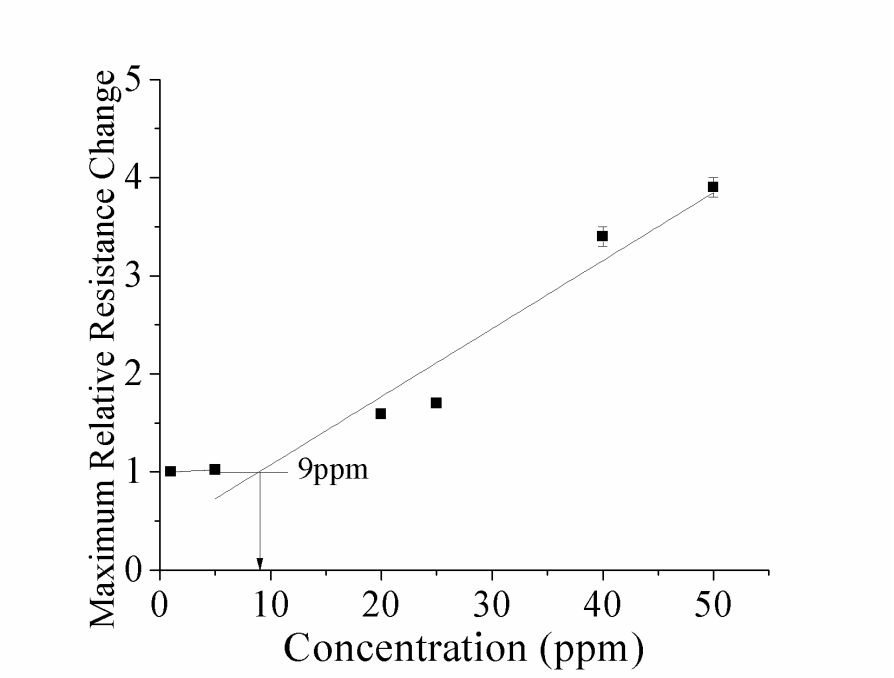

Figure 5.15. Detection limit of sensor: The intersection point of the baseline and calibration graph was equal to the detection limit of the sensor. The detection limit of polyaniline sensors was found to be 9 ± 1 ppm.

5.5. References

[1] H. R. Hwang, J. G. Roh, D. D. Lee, J. O. Lim and J. S. Huh, "Sensing Behavior of the polypyrolle and polyaniline Sensor for Several Volatile Organic Compounds", *Metals and Materials International*, vol. 9, pp. 287-291, 2003.

[2] H. Bai and G. Shi, "Gas Sensors Based on Conducting Polymers", *Sensors*, vol. 7, pp. 267-307, 2007.

[3] J. S. Kim, S. O. Sohn and J. S. Huh, "Fabrication and Sensing Behavior of PVF_2 Coated-Polyaniline Sensor for Volatile Vapor Compounds", *Sensors and Actuators B*, vol. 108, pp. 409-413, 2005.

[4] P. C. Lekha, M. Balaji, S. Subramaniam, and D. P. Padiyan, "Sensing Properties of Polyoxomolybdate Doped Polyaniline Nanomaterials for Oxidizing and Reducing Volatile Organic Compounds", *Current Applied Physics*, vol. 10(2), pp. 457-467, 2010.

[5] N. Gospodinova and L. Terlemezyan, "Conducting Polymers Prepared by Oxidative Polymerization: Polyaniline", *Progress in Polymer Science*, vol. 23, pp. 1443-1484, 1998.

[6] Q. Li, L. Cruz and P. Phillips, "Granular-Rod Model for Electronic Conduction in Polyaniline", *Physical Reviews B*, vol. 47, pp. 1840-1846, 1993.

[7] P. Rannou, B. Dufour, J. Travers, A. Pron, D. Djurado, H. Janeczek and D. Sek, "Temperature- Induced Transitions in Doped Polyaniline: Correlation Between Glass Transisition, Thermochromism and Electrical Transport", *Journal of Physical Chemistry B.*, vol. 106, pp. 10553-10559, 2002.

[8] Z. H. Wang, E. M. Scherr, A. G. MacDiarmid, and A. J. Epstein, "Transport and EPR Studies of Polyaniline: A quasi-One-Dimensional Conductor with Three-Dimensional "Metallic" States", *Physical Reviews B*, vol. 45, pp. 4190-4202, 1992.

[9] F. Zuo, M. Angelopuolos, A. G. MacDiarmid, and A. J. Epstein, "Transport Studies of Protonated Emaraldine Polymer: "A Granular Polymeric Metal System", *Physical Review B*, vol. 36, pp. 3475-3478, 1987.

Chapter 6

Performance of Sensor Array

6.1. Multi Mechanism Sensor Array for Detection of Insect Infestation

There are many sensor arrays available commercially to detect volatile organic compounds. However most of the sensor arrays that have been developed use only one sensor type. The use of one sensor type in the array has some advantages, such as simplicity in instrumentation, and sample presentation. However using a single sensor type with the same response mechanism, will restrict the sensor array's performance since the array will only respond to a limited range of molecular parameters. To overcome this restriction, it is desirable to use multiple types of sensors including different sensing principles such as metal oxide sensors, SAW devices, conducting polymers and MOSFET devices. However this increases the complexity of the sensor system and may require different measurement circuits, operating temperatures, different flow conditions, and normalization of the acquired data. Commercially available sensor arrays such as tinoxide sensors may be bulky due to individual sensor elements. This may result in slow response times, large sample volumes, and high detection limits. Therefore it is beneficial to miniaturize sensor array systems to increase sensitivity and improve detection limit.

This study presents a micro fabricated, multi-mechanism sensor array system for the detection of phytochemicals. The array consists of 8 polymer/carbon composite film sensors, 3 polythiophene sensors and a polyaniline sensor. Each of the sensors in the array produced a signal selective to a particular chemical. Using these signals, a unique finger print was

established for each of the chemicals detected. Incorporating sensors with multiple mechanisms into a single array system may be difficult, especially when integrating different measurements (i.e., resistance, capacitance, etc.). However this sensor array although consisting of multiple sensors operating with different mechanisms, uses the same measurement parameter measurement of the relative resistance over time.

The eight polymers used in the polymer/carbon composite sensor array were polystyrene (PS), polyethylenecovinylacetate (PEVA)- 12% vinyl acetate (VA), PEVA 18% VA, PEVA 25% VA, PEVA 40% VA , PEVA 0% VA (Polyethylene), polyethyleneoxide (PEO) and polyisoprene (PISO). These different polymer types (PS, PEVA, PEO and PISO) were used to optimize uniqueness of the fingerprint for each phytochemical. The analyte reacted differently with each of these polymer films due to their different chemical structures. The structures of these polymers are shown in figure 6.1.

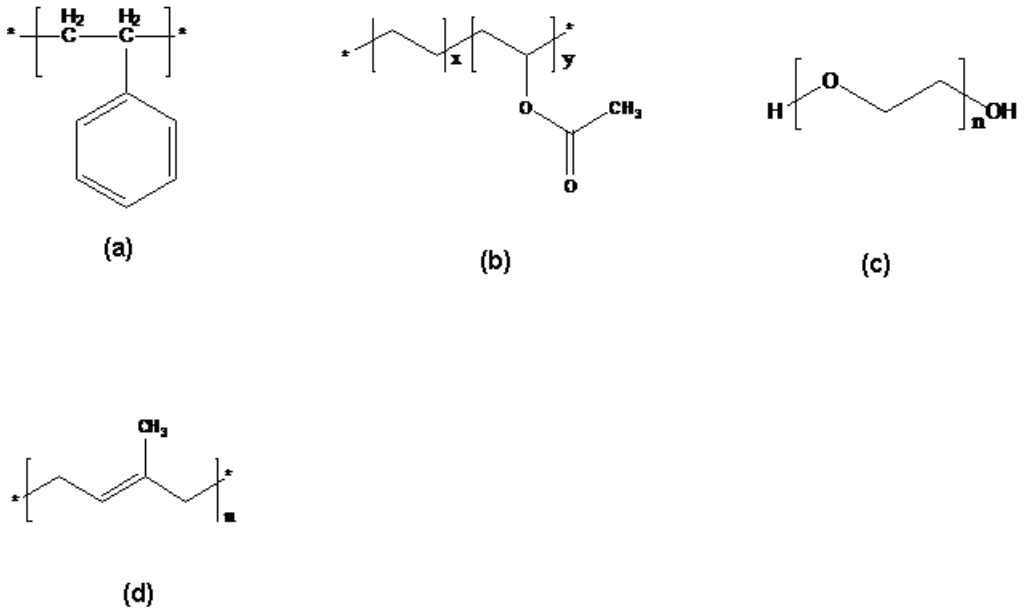

Figure 6.1. Chemical structures of different polymers used as polymer/carbon sensors: (a) polystyrene (b) polyethylenecovinylacetate (PEVA) (c) polyethyleneoxide (d) polyisoprene.

PEVA with varying constituents of VA was used to further increase the uniqueness of the fingerprint. Five films of PEVA with different VA compositions (0%, 12% 18%, 25% and 40%) were used. In crystalline polymer composite films, carbon particles can form conducting pathways on the boundaries of crystal grains and amorphous regions between grains. Absorption of the analyte causes the polymer matrix to dissolve and the carbon particles to relocate. The movement of the carbon black particles results in destruction of the conductive networks in the amorphous regions, which raises the electrical resistance of the film [1-6]. Therefore varying the crystallinity of polymer would control the movement of carbon particles and resistance change of polymer/carbon composite upon exposure to organic vapor analytes.

Polyethylene-co-vinyl acetate (PEVA) is produced by copolymerizing vinyl acetate with polyethylene. The polyethylene part in the copolymer is highly crystalline. However increasing the vinyl acetate constituent makes the polymer less crystalline. Therefore, using different VA compositions in PEVA would have an effect on the resistance change of the polymer film, further increasing uniqueness of fingerprint [3].

Three polythiophene type sensors were used, including spin coated poly3-hexylthiophene, drop casted poly 3-hexylthiophene and drop casted poly 3-dodecyl-thiophene. These polymers were chosen because the casting methods (spin coating and drop casting) and side chains (hexyl and dodecyl) had an effect on the mechanism and performance of polythiophene sensors, further increasing the uniqueness of fingerprint.

The mechanism of polyaniline sensors depend on the reducing and oxidizing of the nitrogen in aniline as well as a secondary swelling mechanism as explained in chapter 5 [7]. Therefore it would react differently according to the polarity of the organic compound to be detected. Polyaniline is expected to be particularly responsive to more polar molecules.

6.2. Sensor Array Response to Various Volatile Organic Compounds

The sensor array was exposed to 6 different analytes including γ-terpinene, α-pinene, limonene, p-cymene, farnasene and cis-hexenyl acetate, using the experimental setup illustrated in chapter 2. The responses were recorded as resistance changes through the Agilent data acquisition system. The maximum resistance recorded for each response was R_{max} and the initial resistance was R_0. For each analyte, the maximum and the initial resistance were noted for each sensor type in the array. The R_{max}/R_0 value was recorded as a function of time. These values can be either plotted in a bar plot or a polar plot to create a unique finger print pattern for each chemical as shown in figure 6.2.

Figure 6.3 below shows the unique finger print patterns obtained for each chemical γ-terpinene, α-pinene, limonene, p-cymene, farnasene and cis-hexenyl acetate using polar plots. In each polar plot there are 12 axes representing each of the different sensors: polyaniline, polystyrene, polyethylene, polyethylenecovinylacetate (PEVA) 12% vinylacetate (VA), PEVA 18% VA, PEVA 25% VA, PEVA 40% VA, polyethyleneoxide, polyisoprene, poly3-hexylthiophene spin coated, poly3-hexylthiophene drop casted, and poly3-dodecylthiophene. The ordinate of each axis is R_{max}/R_0. It should be noted that the PEVA 40% VA/carbon sensor is very sensitive to α-pinene and p-cymene while the polythiophene type sensors are sensitive to γ-terpinene. Only the PEVA 25% VA/carbon and PEVA 40% VA/carbon sensors responded to farnasene and cis-hexenyl acetate. However integrating all responses, unique fingerprints were developed successfully for each of the chemicals.

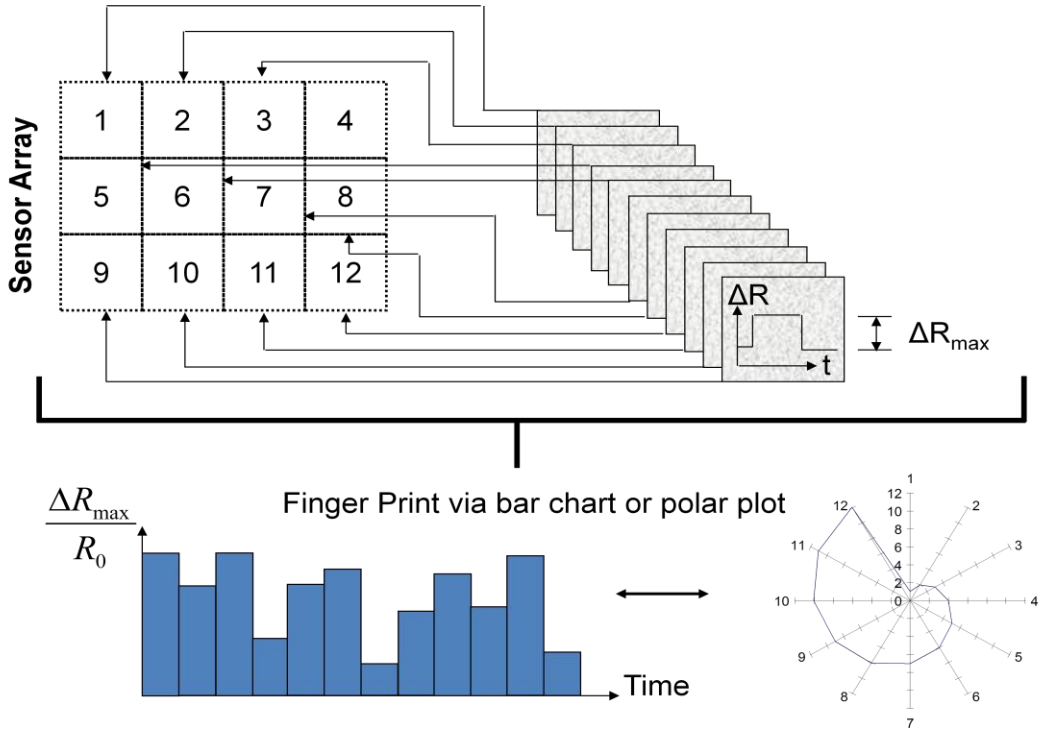

Figure 6.2. Creating finger prints for each phytochemical detected by the sensor array: The array measures a resistance change for each of the sensors in the array. The different responses are plotted as a bar chart or a polar plot to create a unique finger print for each phytochemical.

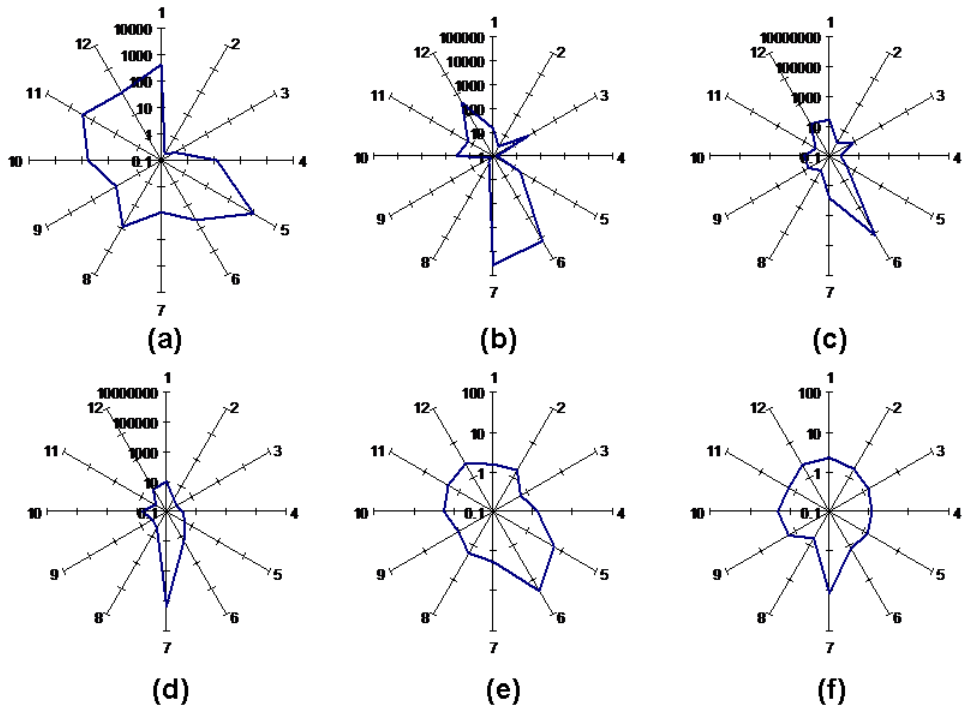

Figure 6.3. Finger print created for (a) γ-terpinene (b) α-pinene (c) limonene (d) p-cymene (e) farnasene (f) cis-hexenyl acetate, by plotting log relative resistance change for each of the eight sensors in a polar plot: Axes 1-12 in the plot represent sensors containing polystyrene, polyethylene, polyethylenecovinylacetate (PEVA) 12% vinylacetate (VA), PEVA 18% VA, PEVA 25% VA, PEVA 40% VA, polyethyleneoxide, polyisoprene, poly3-hexylthiophene spin coated, poly3-hexylthiophene drop casted, and poly3-dodecylthiophene active layers respectively.

6.3. Multivariate Analysis

When a sensor array with n number of sensors creating m number of responses, it is often beneficial to find a relationship between the sensor responses to create a more meaningful and simple output. There are several multivariate analysis methods that can be used to interpret sensor response. It may be an unsupervised analysis, where discrimination is done in an unknown set of vectors, or supervised analysis, where the unknown vectors are discriminated using previously calibrated values. The analysis method may also be statistical, where the data can be described by a probability density function. There are also multivariate methods inspired by human neural networking, such as artificial neural network algorithms [12]. Figure 6.4 below summarizes some of the multivariate analysis methods available.

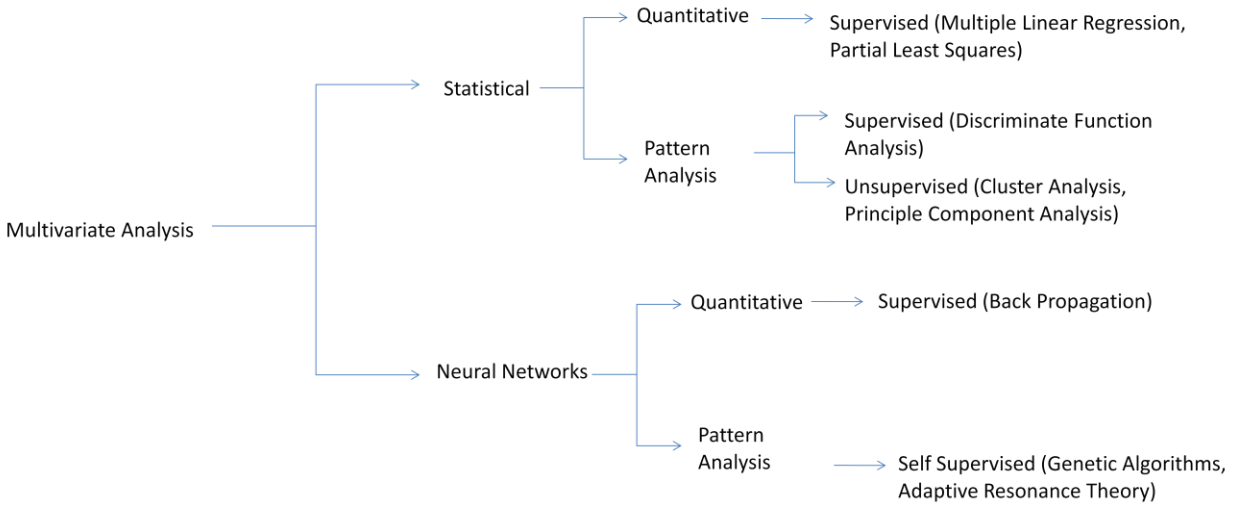

Figure 6.4. Different multivariate data processing techniques commonly employed to analyze data in sensor array systems: In this study principle component analysis which is a statistical, pattern analysis and unsupervised method was used [12].

In this study, a data set was obtained by multiple exposures, (four times) and was analyzed using principle component analysis. Principle component analysis is a powerful data analysis tool which is linear, powerful and non parametric. Principle component analysis reduces the number of variables that needs to be considered to a smaller number of indices, called principle components, PC_p, that is a linear combination of the original variables, i.e. the sensor responses. The principle components are calculated from the scalar product of the set of orthogonal (principle) vectors with the response vectors. The Principle components (PC_p) are ordered in such a way that PC_1 shows the greatest varience, and the next greatest is PC_2 and so on. The first principle component is calculated so that the variance is as large as possible and the sum of the coefficients a_{ip} of the orthogonal (eigen) vector is set to unity. The principle component PC_p can be calculated by equation 6.1.

$$PC_p = a_{1p}PC_{1j} + a_{1p}PC_{ij} + a_{2p}PC_{2j} \ldots\ldots + a_{np}PC_{nj} \quad \text{Equation 6.1}$$

If the data matrix obtained for multiple exposures produced a data matrix D, where each row is designated by j, consisting of n descriptors and each of the descriptors were normalized with the initial resistance of each sensor before the start of each experiment, then a single descriptor could be developed, d_{ij}. The coefficient required to transform the data into principle component space is done by multiplying the data matrix by its transpose D^T (i.e. diagonalizing the matrix). This produces a correlation matrix, R, whose diagonal elements are unity. The off diagonal elements become the correlation coefficients of the data. Then the corresponding eigen values a_{ip} are calculated for R. The eigen values and corresponding eigen vectors are then used to calculate the principle components using equation 6.1.

In this study, the correlation matrix, eigen values and eigen vectors were calculated using Excel, with a special add-on software "StatistiXL." The averaged, normalized data with standard deviation (for four exposures), calculated correlation matrix, and the eigen values and eigen vectors are shown in table 6.1, 6.2 and 6.3 respectively.

The first three principle components with eigen values greater than one and variance greater than 10% were used to create the principle component plot. Other principle component values were considered insignificant. Figure 6.5 shows a three dimensional principle component plot created using the first three principle components PC_1, PC_2 and PC_3. PC_1, PC_2 and PC_3 had variance values of 60%, 21% and 11% and eigen values of 7.2, 2.5 and 1.3 respectively.

The data shown in figure 6.5 demonstrates that the sensor array is capable of discriminating between the individual gases. The data was well clustered for each chemical gas. Since normalized data values were similar for each of the four data points for each chemical, they were clustered together. γ-terpinene and α-pinene were more easily discriminated from the rest of the chemicals analyzed.

Table 6.1. Average data with standard deviation used for principle component analysis: Sensors 1-12 contains polyaniline polystyrene, polyethylene, polyethylenecovinylacetate (PEVA) 12% vinylacetate (VA), PEVA 18% VA, PEVA 25% VA, PEVA 40% VA, polyethyleneoxide, polyisoprene, P3HT spin coated, P3HT drop casted, and poly3-dodecylthiophene and chemical analytes 1-6 are γ-terpinene, α-pinene, limonene, p-cymene, farnasene, cis-hexenyl acetate respectively.

Sensor Chemical	1	2	3	4	5	6	7	8	9	10	11	12
1	449.0 ±40.3	0.24 ±0.1	0.23 ±0.1	12.0 ±1.2	1182 ±118	45.3 ±4	7.4 ±1.9	70.5 ±5.8	9.5 ±0.6	61.0 ±3.1	269.9 ±14.9	90.0±1.8
2	14.6 ±1.7	2.6 ±0.7	51.2 ±1.9	1.7975 ±0.3	19.8 ±1.3	12075 ±1355.8	28700.2 ±8486.3	1.7 ±0.4	2.1 ±0.8	34.5 ±3.5	15.9 ±1.3	401.2±7.9
3	24.5 ±2.8	1.5 ±0.9	6.6 ±0.8	1.0 ±0.4	2.0 ±0.8	123024.0 ±3694.2	60.7 ±8.3	1.6 ±0.5	3.6 ±1	4.1 ±0.5	1.8 ±0.5	31.8±2.6
4	10.2 ±0.7	1.3 ±0.6	0.6 ±0.2	1.9 ±0.2	2.4 ±0.3	20.7 ±1.3	263559 ±35489.1	2.3 ±0.4	1.1 ±0.1	5.4 ±0.9	1.1 ±03	4.3±0.8
5	1.6 ±0.3	1.8 ±0.3	0.5 ±0.1	2.2 ±0.7	6.1 ±1.3	23.0 ±2.2	1.9 ±0.5	1.7 ±0.5	1.4 ±0.4	1.8 ±0.3	2.2 ±0.2	2.8±0.3
6	2.0 ±0.3	1.9 ±0.4	1.6 ±0.4	1.6 ±0.5	1.6 ±0.4	2.1 ±0.9	10.1±1.2	1.0 ±0.7	2.0 ±0.6	2.2 ±0.3	1.7 ±0.2	3.0±0.7

Table 6.1. Correlation matrix calculated for the data set used for principle component analysis: The diagonal elements are unity, while the off diagonal elements are the correlation coefficients of the data.

Column	A	B	C	D	E	F	G	H	I	J	K	L
A	1.0	-0.7	-0.2	1.0	1.0	-0.2	-0.2	1.0	0.9	0.9	1.0	0.0
B	-0.7	1.0	0.6	-0.6	-0.7	0.0	-0.1	-0.7	-0.6	-0.4	-0.7	0.4
C	-0.2	0.6	1.0	-0.2	-0.2	0.0	-0.1	-0.2	-0.2	0.3	-0.2	1.0
D	1.0	-0.6	-0.2	1.0	1.0	-0.3	-0.2	1.0	0.9	0.8	1.0	0.0
E	1.0	-0.7	-0.2	1.0	1.0	-0.2	-0.2	1.0	0.9	0.9	1.0	0.0
F	-0.2	0.0	0.0	-0.3	-0.2	1.0	-0.2	-0.2	0.0	-0.3	-0.2	-0.1
G	-0.2	-0.1	-0.1	-0.2	-0.2	-0.2	1.0	-0.2	-0.4	-0.2	-0.2	-0.2
H	1.0	-0.7	-0.2	1.0	1.0	-0.2	-0.2	1.0	0.9	0.9	1.0	0.0
I	0.9	-0.6	-0.2	0.9	0.9	0.0	-0.4	0.9	1.0	0.8	0.9	0.0
J	0.9	-0.4	0.3	0.8	0.9	-0.3	-0.2	0.9	0.8	1.0	0.9	0.5
K	1.0	-0.7	-0.2	1.0	1.0	-0.2	-0.2	1.0	0.9	0.9	1.0	0.1
L	0.0	0.4	1.0	0.0	0.0	-0.1	-0.2	0.0	0.0	0.5	0.1	1.0

Table 6.3. Eigen values and % variances calculated for the data set: The eigen values more than 1 were taken into consideration for the principle component plot. Other values were considered insignificant.

Value	PC 1	PC 2	PC 3	PC 4	PC 5	PC 6	PC 7	PC 8	PC 9	PC 10	PC 11	PC 12
Eigenvalue	7.2	2.5	1.3	0.7	0.2	0.0	0.0	0.0	0.0	0.0	0.0	0.0
% of Var.	60.1	20.6	10.8	6.0	2.0	0.2	0.2	0.1	0.0	0.0	0.0	0.0
Cum. %	60.1	80.7	91.5	97.4	99.4	99.7	99.8	99.9	100	100	100	100

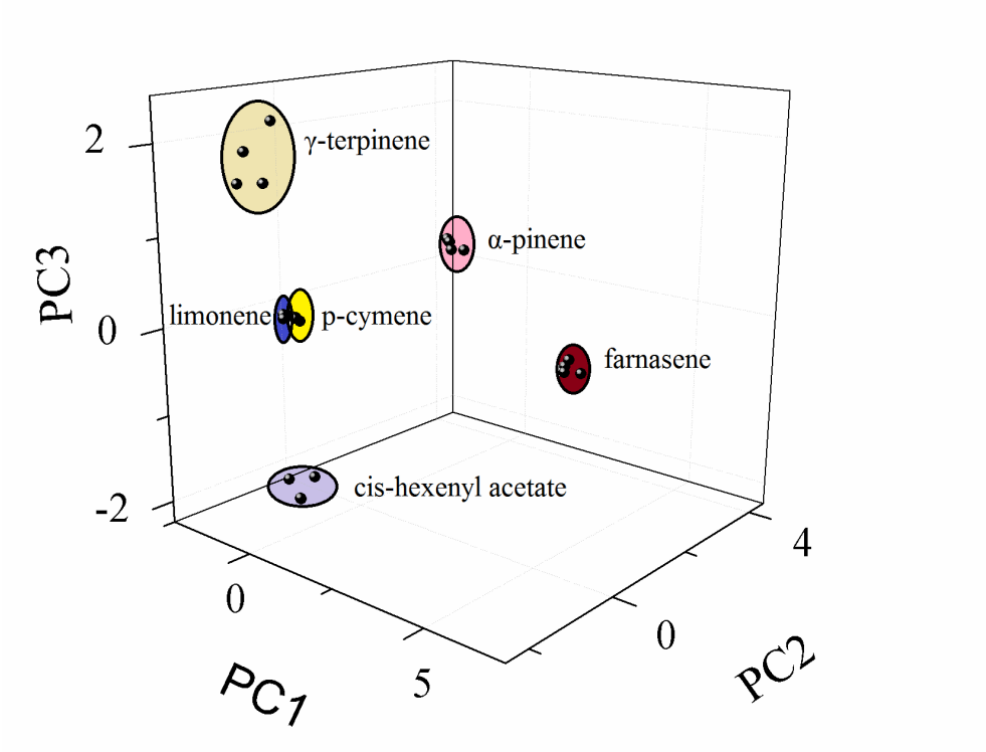

Figure 6.5. Principle component plot of different phytochemicals (a) γ-terpinene (b) α-pinene (c) limonene (d) p-cymene (e) farnasene (f) cis-hexenyl acetate: The plot shows the first, second principle and third principle components, where the eigen values were greater than 1. Clusters of data for each of the chemical type are shown, enabling discrimination among them.

6.4. References

[1] A. R. Hopkins and N. S. Lewis, "Detection and Classification Characteristics of Carbon Black/Organic Polymer Composite Chemiresistive Vapor Detectors for the Nerve Agents Simulants Dimethylphosphonate and Diisopropylmethylphosponate", *Anal. Chem.* ,vol. 73 (5), pp. 884-892, 2001.

[2] M. B. Heaney, "Measurement and Interpretation of Non Universal Critical Exponents in Disordered Conductor/Insulator Composites", *Phys. Rev. B.* , vol. 52(17), pp. 12477-12480, 1995.

[3] J. Chen and N. Tsubokawa, "A Novel Gas Sensor From Polymer-Grafted Carbon: Responsiveness of Electric Resistance of Conducting Composite from LDPE and PE-b-PEO-Grafted Carbon Black in Various Vapors", *Polym. Advan. Technol.* , vol. 11, pp. 101-107, 2000.

[4] M. C. Lonergan, E. J. Severin, B. J. Doleman, S. A. Beaber, R. H. Grubbs, and N. S. Lewis, "Array-Based Vapor Sensing Using Chemically Sensitive, Carbon-Polymer Resistors", *Chem. Mater.* , vol. 8, pp. 2298-2312, 1996.

[5] E. J. Severin and N. S. Lewis, "Relationships Among Resonant Frequency Changes on a Coated Quartz Crystal Microbalance, Thickness Changes, and Resistance Responses of Polymer-Carbon Black Composite Chemiresistors", *Anal. Chem.* , vol. 72(9), pp. 2008-2015, 2000.

[6] J. W. Gardner and P. N. Bartlett, "Electronic noses: Principles and applications", first ed. , Oxford University Press, New york, 1999.

[7] J. W. Grate and M. H. Abraham, "Solubility Interactions and the Design of Chemically Selective Sorbent Coatings for Chemical Sensors and Arrays", *Sensors and Actuators B.* , vol. 3, pp. 85-111, 1991.

Chapter 7

Conclusions

The array consisting of 8 polymer/carbon composite film sensors, 3 polythiophene sensors and a polyaniline sensor was designed, fabricated and tested to detect volatile organic compounds emitted by plants. This research study resulted in the following major conclusions.

1) The electroactive polymers were drop casted or spin coated onto gold interdigitated electrodes patterned on silicon dioxide substrates. Fabrication was performed using standard microelectronic procedures, on whole silicon wafers. The resulting sensor platform had 25 pairs of electrodes where each electrode finger was 22 microns wide and 2985 microns long. The spacing between fingers was 15 microns. Thirty three silicon wafers were fabricated at a time, where each wafer contains 360 sensors. On average, 8 out of 10 sensors were functional, resulting in an 80% yield. The cost per each sensor is about 2 dollars.

2) Thin film polythiophene chemiresistor sensors were used in the array operated by a chemical mechanism involving physical interactions between analyte vapor and the active sensing polymer layer. The polythiophene thin films physically react with organic volatile gases by absorbing the analyte gas into the grain boundaries. This absorption physically blocks charge conduction and increases the resistance of the films upon exposure to the analyte gases. For polythiophene sensors, the response of the sensors increased as the film thickness decreased. The highest response was obtained when the film thickness was maintained at 110 nm. Annealed polythiophene films showed a lower response than unannealed sensors because the

sensors had higher crystallinity. Doping increased the number of charge carriers in the polymer film, which made it difficult for analyte molecules to hinder charge motion, decreasing sensor response. The morphology of thin film P3HT varied with different casting methods (spin coating and drop casting) and with solvents (toluene and chloroform). In self organized high molecular weight polymers, such as P3HT, nodule-like structures of high crystallinity are common. The highest crystallinity was seen in the drop casted samples which used toluene as solvent. The least nodule like structures were seen in spin coated samples using chloroform. P3HT sensors, when exposed to various phytochemicals had a resistance change of over two orders in magnitude. The sensors had a long recovery curve, although recovery within 24 hours was sufficient to reproduce a response when re-introduced to analyte vapor.

3) Carbon composites including polyvinylpyrrolidone, polyethyleneoxide, polyisoprene, polymethacrylate and polyethylene-co-vinylacetate (40% vinyl acetate) were selected for the sensor array based on the mass uptake of γ-terpinene. The percolation point of the polymer/carbon films was obtained when the concentration of carbon particles was 1-2.5 (weight)% carbon. Therefore the carbon composition was maintained at 4% to obtain a drastic change in resistance when analyte vapor is absorbed. Generally, a sharp increase in resistance of over 2 orders of magnitude was obtained when the sensors were exposed to γ-terpinene. The sensors also returned quickly to their original resistance when exposed to pure nitrogen after exposure to analyte. This illustrated a switch on / switch off type behavior. A concentration as low as 1ppm was detected using PEVA/carbon sensors.

4) Polyaniline sensors used in this study were fabricated by drop casting polyaniline emaraldine base / benzene solution onto microfabricated platforms. These sensors operated by a redox reactions based mechanism and a swelling based mechanism, and were chosen for use in the sensor array because they have a higher resistance change to polar type analytes. Since polyaniline sensors had a very different mechanism from the other electroactive polymers used in this study, they provided a method of diversifying the sensor array responses.

5) The polymer sensor array in this study consisting of polyethylenecovinylacetate (PEVA) 12% vinylacetate (VA), PEVA 18% VA, PEVA 25% VA, PEVA 40% VA, polyethylene, polyethyleneoxide, polyisoprene, polystyrene, polyaniline, polythiophene (spin coated and drop casted) and polydodecylthiophene was tested and found to be sensitive to a variety of volatile organic compounds including γ-terpinene, limonene, farnasene, α-pinene, p-cymene and cis-hexenyl acetate. Unique fingerprints for each of the analytes tested was obtained from the sensor array. The sensor array was able to distinguish between each of the analytes and hence can be used to detect insect infestation effectively.

6) The sensor array was found to be stable under various environemtal conditions, including varying temperature conditions and humidity conditions. The sensors did not react with ambient gases. This made them excellent candidates as sensors for detecting insect infestation in agricultural fields that have constantly varying environmental conditions.